Seismic Tests on IBWC Levees: Weslaco, Texas

Richard D. Miller
Julian Ivanov

Kansas Geological Survey
1930 Constant Avenue
University of Kansas
Lawrence, Kansas 66047

Final Report to

Joe Dunbar
U.S. Army Engineer R&D Center
Geotechnical and Structure Laboratory
3909 Halls Ferry Road
Vicksburg, Mississippi 39180

Open-file Report No. 2005-56 October 10, 2005

Seismic Tests on IBWC Levees: Weslaco, Texas

Table of Contents

Seismic Tests on IBWC Levees: Weslaco, Texas

EXECUTIVE SUMMARY

This applied research project evaluated the potential of a variety of seismic methods to characterize the condition of levee cores constructed in the 1970s as part of the International Boundary and Water Commission (IBWC) program in south Texas. Preliminary studies of levee cores in certain areas uncovered evidence of cracking in the expansive clays locally mined and used during construction of the core. Cracking of this nature is likely the result of more than eleven years of drought in south Texas and would increase the overall permeability and leak potential of the levees. This suggestion was made based on analysis of four different data sets: abnormally low conductivity determined by both airborne and surface geophysical surveys, abnormally high levels of grout intake during borehole plugging operations, and core samples intact when first removed from the ground and placed in plastic containment vessels showing marked shrinkage and visible cracking after one year in controlled storage.

Five levee sites were selected based on airborne geophysics and physical inspection to represent the range of conditions expected in levee cores during extended periods of drought in this area of south Texas. Lithology at each of these sites varied in sand and clay concentrations and types. Core materials for each levee site were locally mined at various locations within the river valley and therefore each possessed different physical properties as evident in core drill samples and electrical properties. Miles of airborne EM and LIDAR acquired in a continuous fashion over the levees in this area were instrumental in identifying and classifying each of these five very diverse sites.

Seismic methods have proven marginally successful identifying anomalies in levees on a few occasions. Most of these studies have focused on direct wave analysis, targeting areas with reduced seismic velocities. Lower seismic velocities are usually indicative of less strength or softer materials. Therefore, anomalously low velocities for a particular levee could be an early indicator of failure potential. Testing at each of these five sites was more extensive than any earthen structure study currently available in the scientific literature. The testing included compressional and shear first-arrival analysis (classic refraction, turning-ray tomography, and through-levee tomography), multi-channel surface-wave analysis, and vibration harmonics analysis. Tests were conducted both on the levee crest and at equivalent locations along the levee toe, with expanded studies at sites identified as good candidates for ponding experiments.

Tests were designed to evaluate both body waves and surface waves using well-documented methodologies specifically adapted to the levee problem. Due to the shallow depths of investigation, reflection was not considered a viable technique and therefore tests specifically designed to evaluate reflected arrivals were not undertaken. Seismic data were recorded using both horizontally polarized source and receivers and vertical source and receivers. Shots for the 2-D surveys were recorded at stations along the lines of receivers. A 3-D tomography experiment was conducted using shots on one side of the levee face recorded by receivers on the adjacent side. Data quality was method dependent, but in general most recorded data were good, possessing excellent signal-to-noise ratios and good-to-poor signal bandwidth and range of recorded frequency. Seismic velocities (compressional and shear) were estimated from measurements of first-arrival time/offset distances and inversion of surface-wave phase velocities as a function of frequency.

These investigations targeted seismic velocities, both absolute and relative (changes). Seismic velocities of levee materials were estimated and compared both site to site and within specific sites. A unique study of surface-wave phase velocities was conducted observing phase variations in the expected (for consistent material characteristics) uniform wavetrain at and near resonance (resonance in this case is

controlled by levee height and surface-wave velocity of the materials: wavelength). This surface-wave study was conducted in hopes of identifying anomalous zones where changes in phase velocity might be indicative of reduced or increased material strength. Seismic velocities were measured based on travel time between adjacent sets of receivers.

Body-wave propagation characteristics are unique to the material through which the seismic energy is traveling. Shear velocity is generally accepted as a relative measure of material strength or stiffness. Compressional velocity is a measure of both the rock matrix and pore materials. Therefore, increases in shear velocity will generally indicate stronger materials, while increases in compressional velocity in unconsolidated materials is a good indicator of increased saturation.

Compressional-wave velocities were for the most part within a "reasonable" range for this setting; however, shear-wave velocities were estimated to be significantly higher than expected based on both levee materials and equivalent compressional-wave velocities. Shear velocities were consistently measured with a Vp/Vs ratio around 2, which is generally more characteristic of consolidated rocks. Ratios for unconsolidated fill materials such as these are generally expected to fall in the 3 to 5 range. This higher-than-expected ratio could result in measuring mode-converted shear rather than the primary direct shear arrival. It is also possible this higher-than-expected shear velocity could be real and related to these earth materials and the mechanical compaction used to construct these levees.

Estimates of shear velocity using both refraction tomography and slope intercept methods provided shear velocities that were unrealistically high and with offset-dependent arrival patterns extremely consistent with the faster compressional-wave arrivals. Calculating shear-wave velocity from inverted surface waves was strongly dependent on bandwidth and percentage of higher-mode energy recorded. During the first survey, ground conditions were not conducive to producing and/or recording broadband surface waves. Therefore, no confident shear-wave velocity sections were produced. On the second trip near-surface conditions had sufficiently changed to allow sufficient broadband surface wave that a 2-D shear wave profile could be produced for the levee core.

Velocity anomalies within the levee were detected at each of the three Retamal levee sites. Distribution and range of values for these anomalies are consistent with variations in material types used during construction and the construction process itself. It is not clear that velocity information alone will be sufficient to identify areas with a high density of cracks, which could be present as a result of the dewatering during drought of the expansive clays used in some places during core construction. However, it does seem likely that reduction in the material stiffness of the levee core could be used to identify failure risk areas with a relatively high resolution. Discontinuities in the levees associated with cracks seem to interfere with the otherwise uniform propagation of surface waves through the levee. These disturbances, once fully understood, could provide relatively accurate locations of weak zones within the core material.

Problems and pitfalls associated with using seismic techniques to estimate velocities intended to help characterize levee competence do exist and require significant attention to detail and understanding of the seismic-wavefield arrival patterns (t-x) and significance of the spectral properties of each mode. In particular, mode converted shear-wave energy can lead to completely incorrect conclusions. Interpreting the propagation irregularities in surface-wave energy is not clearly understood and, therefore, is not yet ready for use as a routine tool in interrogating levees. It must also be kept in mind that the geometry of the levee and the proximity of its basal contact with native earth can result in refracted first arrivals dominating the majority of close-offset traces where direct waves are normally expected.

Rapid, precise seismic methods for identifying areas worthy of further investigation could be developed for specific levee geometries and construction materials. Monitoring is by far the most

confident and accurate application for seismic techniques on levees. Consideration must be given for changes in skin conditions due to seasonal variations in moisture. At the five sites studied on the Retamal and Main Levees, LRGV compressional-wave velocity estimations were most accurate for all conditions using refraction tomography. Shear-wave-velocity survey data were contaminated with mode-converted energy and therefore difficult to use to estimate material characteristics. Changes in near-surface conditions between the first and second survey resulted in an increase in recorded surface-wave bandwidth and therefore reasonably confident shear-wave velocity estimations within the levee. This change in surface conditions did not seem to change the arrival patterns observed on data recorded to capture first-order shear-wave first arrivals.

Infiltration of water into the levee skin was identified on seismic data during the ponding experiment conducted during the second site visit at site 2 (oxbow lake site). Notable changes in both compressional and shear velocity can be associated with the infiltration of water dammed against the south levee face. Compressional-wave data suggest percolation of water into the native river valley sediments beneath the levee. Shear-wave velocity change was rapid, occurring at the very beginning of the simulation, and was isolated to one area within the pond. The isolated nature of the infiltration on the shear data could be related to a fracture/crack system opened as a result of the years of drought and dewatering of the core. An alternate possibility is a possible material inconsistency resulting from construction practices and locally mined core material.

Considering the observations from the ponding experiment and five-site study, it is clear that the seismic tool can be used during flood events to detect more permeable areas where infiltration is active and the potential exists for failure. The most effective use of this tool would be as a monitoring system, where a baseline survey is acquired for all suspect areas, then during a flood event repeat surveys are run using differencing techniques to detect weak points pre-failure. Complications from mode conversions and near-surface dependent propagation characteristics will limit the use of this tool in some settings until more advanced processing capabilities have been developed. Clearly, more information is present in the seismic wavefield than we currently have the capability to meaningfully extract. Optimized future use of this tool will depend to some degree on acquisition of baseline data sets that will allow full wavefield processing once the methods have been fully developed. Current research in these areas is active and incrementally moving forward with providing solution to many problems encountered on this study.

Seismic Tests on IBWC Levees: Weslaco, Texas

1–INTRODUCTION

In support of the U.S. Army Corps of Engineers' strong commitment to dam and levee safety, new and/or adaptations of existing technologies need to be identified and evaluated at sites with both physical characteristics conducive to those technologies and a history of substandard dam or levee performance. Models used to predict dam or levee performance levels during earthquakes and floods are only as realistic as the material attributes (especially rigidity) incorporated into those simulations. Proven correlation between acoustic properties and material properties (especially stiffness/rigidity) is the basis for developing and implementing field-efficient, laterally continuous, non-invasive methods to accurately measure the seismic wave field.

Characterization of levees or dams in areas with liquefaction, core failure, or leakage potential would be enhanced if Poisson's ratio were calculated based on continuous, detailed, coincident, two- and three-dimensional measurements of compressional and shear-wave velocities for cells uniformly distributed throughout the dam or levee volume. Routine non-invasive appraisal of dam/dike core integrity could prove quite valuable if lateral variability in shear-wave velocities could be accurately measured and correlated to localized anomalous material zones. This would be especially significant if these anomalous zones were indicative of dissolution activity, non-uniform compaction/settling or fracturing/cracking from dewatering of expansive clays prior to surface subsidence, the formation of vertically extensive chimney features or piping, or fracture permeability through the core. Seismic techniques hold vast potential for imaging and measuring materials in a fashion suitable for evaluating levee integrity.

This applied research project was designed to evaluate the potential of several seismic methods to characterize the condition of levee cores built in the 1970s as part of the International Boundary and Water Commission (IBWC) program in south Texas. Preliminary studies of levee cores in certain areas uncovered evidence of cracking in the expansive clays mined locally and used extensively during construction of the core. Cracking of the nature suspected here is likely the result of more than a decade of drought in south Texas and would act to increase the overall permeability and leak potential of the levees. This suggestion was made based on previous analysis of four different data sets: abnormally low conductivity determined by both airborne and surface geophysical surveys, abnormally high levels of grout intake during borehole plugging operations, and change in intact core samples (shrinkage and visible cracking after one year in controlled storage).

By isolating and measuring changes or the effects of changes to physical earth properties using seismic methods it should be possible to both reduce the inherent problem of non-uniqueness and lower the threshold of physical property change currently necessary for seismic methods to uniquely and confidently detect a change. Correlating and quantifying known changes in physical properties with observed variations in seismic data attributes should provide the basis for accurate characterization of earth materials with no *a priori* information. For that reason, comparing two data sets acquired with identical techniques and geometries—one acquired when cracks in the core are most pronounced (dewatered clay) and a second when the clay core is fully watered, allowing the cracks to heal—is the most effective approach for evaluating the various methods' ability to detect and quantify these fractures. Contrasting seismic data before and after changes in core saturation should allow differences in data characteristics related specifically to core dewatering to be identified and quantified, with a template developed for use of seismic methods as a reconnaissance tool on levees.

Program Objectives

Geophysics used during site characterization routinely involves relatively noisy measurements of earth properties, qualitatively incorporated into working subsurface models with ground truth provided by observational data sets (e.g., drilling, outcrop studies, etc.). Near-surface seismic data are no exception to this generality. The primary objective or product of most surveys of this type is the qualitative assessment of subsurface layer topography (Clement et al., 1997; Pullan and Hunter, 1990; Lankston, 1990). Travel-time structure maps or two- or three-layer velocity maps are typical interpretation products of seismic surveys. These seismic interpretation maps are routinely merged into borehole derived geologic and hydrologic models based for the most part on highly subjective and very sparse data sets. These simplistic models are then used for ground-water monitoring and remediation, geologic hazard detection, or engineering design purposes in an intuitive, experience-based manner (Steeples and Miller, 1990; Miller and Xia, 1999).

Considering the wealth of information contained in the seismic wave field, seismic measurement or imaging data are routinely underutilized for site characterization (Steeples et al., 1995). Surface seismic techniques are generally limited to routine mapping and delineation of subsurface structures, layer topography, anomalies, and stratigraphic changes (Jongerius and Helbig, 1988; Miller et al., 1989; Goforth and Hayward, 1992; Miller et al., 1995; Shtivelman et al., 1998; Guo and Liu, 1999; Stokoe et al., 1994; Michaels, 1999). In many instances, several earth properties (Vp, Vs, Qp, Qs, layer orientation, and thickness) can be estimated from the seismic wave field, for each subsurface cell. Velocity is probably the parameter most consistently measured or estimated by all the seismic methods. A single seismic shot record has the potential to be divided into multiple modes or combinations of modes and processed uniquely for each mode and wave type. One data set could be uniquely processed focusing on at least four different energy types (body waves: refraction, reflection, and tomography; surface waves: shear velocity and Q).

This applied research project evaluated the applicability of several seismic techniques to identify, delineate, and estimate the physical characteristics or properties of materials within and beneath a representative expanse of IBWC levees south of Weslaco, Texas (Figure 1). It was important that some measure be established (qualitative if necessary) of the correlation between seismic measurements, conductivity measurements, and the physical condition (increased permeability zones related to fractures, joints, dissolution, or erosion) of the levee core. Several surface seismic measurements were made and analyzed using state-of-the art methods and equipment. As part of the phase II component of this study, a repeat survey was conducted immediately before, during, and after ponding and levee saturation. Methods evaluated include: (P & S) refraction, (P & S) tomography (both 2-D turning ray and 3-D straight ray through levee), surface-wave dwell, and surface-wave dispersion curve analysis (MASW) for shear-wave velocity.

- The delayed-time method of first arrival/refraction analysis was used along the 2-D profiles at the crest and toe of the levee to look for variations in layer velocities (Vp and Vs) at the core/pervious fill contact, core/native earth interface, and any discrete velocity contrast within the first 30 ft below the base of the core along both crest and toe profile lines (Scott, 1973).

- Turning-ray tomography was used to define Vp and Vs for subsurface cells filling the space between the levee/ground surface and 30 ft below the base of the levee along the crest and toe profile lines (Lanz et al., 1998). Conventional turning-ray tomography and joint analysis of surface waves and refractions (JARS) was done to appraise their relative accuracy when appropriate (Ivanov, 2002).

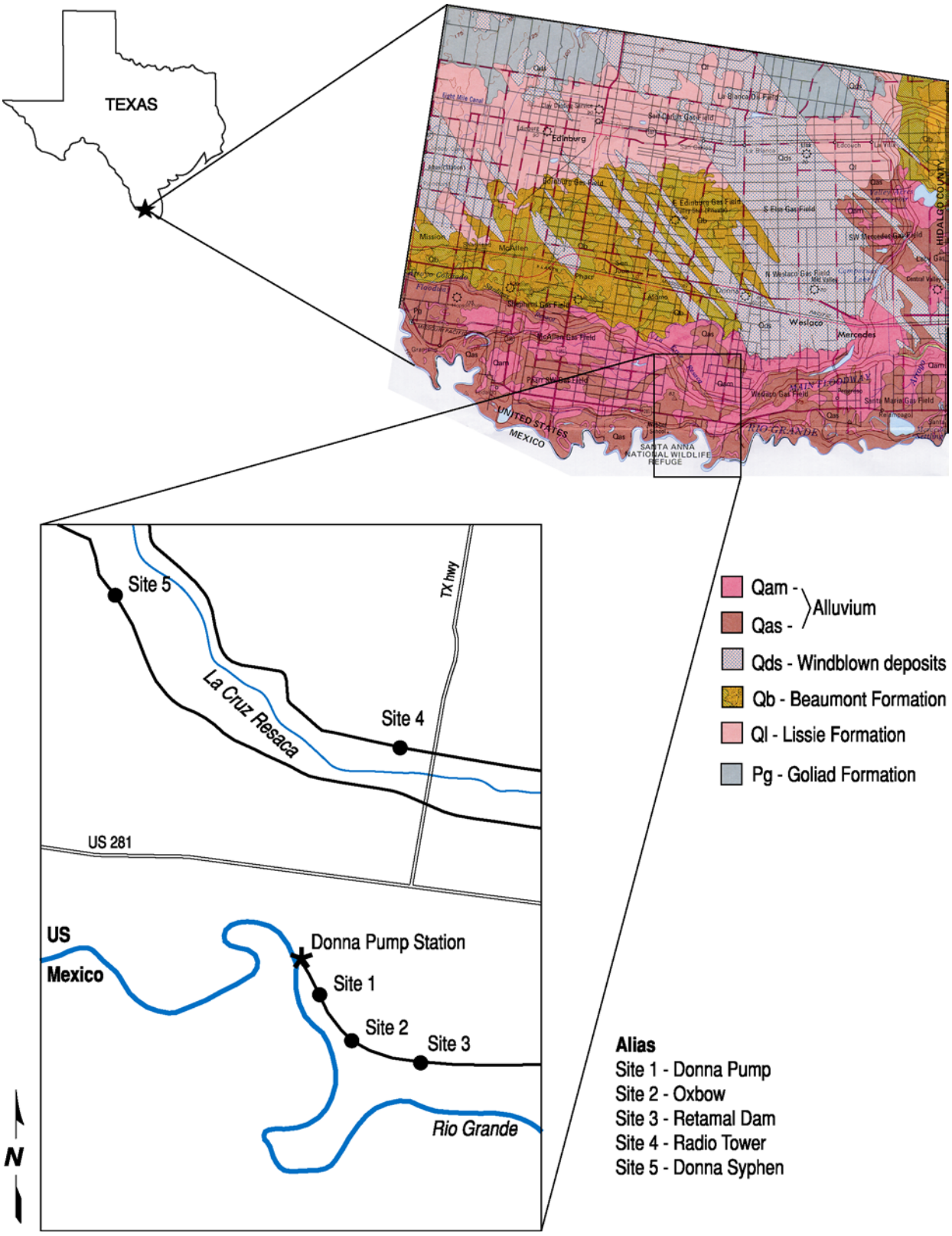

Figure 1. Maps of survey site near Weslaco, Texas (most detailed map from Texas Natural Resources Information System, www.tnris.state.tx.us).

- Through-levee tomography was completed for both compressional and shear energy along a 2-D surface grid designed with sources on one side and receivers on the other side of the levee deployed relative to the centerline road. Analysis relied on a relatively straightforward travel-time delay technique analogous to crosshole tomography (Gaffran et al., 1999).

- Multichannel surface-wave inversion techniques (MASW) have proven capable of detecting anomalous shear-wave velocity zones within and below fill materials (Miller et al., 1999). Application of this technique to differential fill and core integrity problems at levee sites with expansive clays provided key insights into and an increased awareness of areas with leak or failure potential.

- Frequency dwell experiments provided the opportunity to compare frequency-dependent changes in surface waves with physical properties and/or changes in properties. Monofrequency sweeps several seconds long were produced and recorded using the dependence of surface-wave spectra on depth of penetration and the shear-wave velocity (Xia et al., 1999).

- High-resolution seismic reflection data from the crest 2-D profiles was studied to determine the feasibility of coincidentally estimating Vp and Vs, sensitivity of reflection wavelet attributes returning from the base and/or beneath the levee to variations in core permeability (cracks), and travel time variations (static) associated with wavelet delays through cracked and/or clay core shrinkage within closely spaced subsurface cells for use in detailed mapping of levee core properties (Batzle et al., 1999; Berryman et al., 1999). Unfortunately, no usable reflection energy was recorded at any of the sites from within the levee.

Tests to determine field efficiency, resolution potential, cost effectiveness, interpretability (signal-to-noise), processing requirements, and measurement accuracy were integral to each of the individual seismic techniques studies. It was the intent of this study to acquire single-pass full-waveform compressional- and shear-wave data and to process the individual components of each mode using methodologies appropriate for the particular energy arrival. Therefore, minimal acquisition effort would yield several redundant measurements of seismic properties using different parts of the wavefield.

In summary, the primary objectives set out from the onset of this project were to determine compressional and shear velocity distribution within the body of the levee and any relationship to levee permeability. Measurements were made at several locations, each with unique physical and/or lithologic differences, while in their dry state to a depth approximately equal to the water table (geophysical tools used had at least a maximum depth of investigation extending 30 ft below the native ground surface or below the base of the levee). These measurements were followed some time later by an abbreviated comparison survey at one site after water had been introduced to the levee core/body to provide a time-lapse seismic view of the levee, studying seismic response as a function of changes in saturation. As a result, the potential of reconnaissance and high-resolution imaging using non-invasive seismic methods could be appraised.

2—SITE DESCRIPTION

Levees along significant expanses of the Rio Grande River in south Texas are currently the responsibility of the International Boundary Water Commission (IBWC). Many of these levees were designed and constructed to minimize or eliminate the threat of the statistically determined 100-year flood event. Newer (1970s era) reaches of IBWC levees were constructed, in some cases, using highly expansive clay materials. Materials used to construct the levees were generally mined from barrow pits in relative close proximity to the active construction area. Therefore, lateral variability in construction materials is common over distances of a mile or less. Average levee height in these areas is about 16 ft with slopes on the order of 1 to 3 (Figure 2).

With 11 years of prolonged drought conditions plaguing the McAllen-Brownsville corridor, soil moisture conditions reached the point that concern arose about internal levee conditions and its impact on the levees' design characteristics. It was postulated that in some areas moisture levels within the levee could have dropped to the point cracks formed in the impervious core, weakening the core to the point failure was possible under 100-year flood conditions. A series of field tests were devised to first determine if a non-invasive method existed that could measure a levee's internal strength properties sufficiently to diagnose if this problem existed, and secondly to classify levees in terms of core characteristics. These investigations included seismic, ground probing radar, resistivity, SP, drilling and sampling, and levee design-height (toe to within 3 ft of the levee crown) full-scale ponding tests. Data obtained prior to and after ponding tests were designed to assess differences at a single representative location that could be correlated to other sites with similar measured characteristics. This document is only intended to address seismic investigations undertaken by the Kansas Geological Survey.

Figure 2. Field site 1 with vibrator on south side of levee, crew working on north side, and semi parked on levee.

Preliminary studies focused on levees in south Texas between Brownsville and McAllen (Figure 1). Seismic investigations were conducted at five levee sites located in the San Juan Quadrangle (Figure 3). Three of the sites were immediately north of the Rio Grande River at low-conductivity locations along the Retamal dike and two were at levee sites on opposing sides of the La Cruz Resaca within the interior floodway. Of the two within the interior floodway, one location was at an intermediate-conductivity site and the other was at a high-conductivity site. These sites were chosen specifically based on observations from airborne and surface geophysical surveys and borehole data. To study the relationship between electrical conductivity, lithology, fracture permeability, seismic properties, and failure potential, it was necessary to study a range of sites with characteristics classified from average to extreme. Key factors in selecting these five sites were abnormally low EM conductivities determined from and consistent on both airborne and surface geophysical survey data, abnormally high grout intake while backfilling sampling boreholes, and marked shrinkage and visible cracks in year-old preserved cores.

Figure 3. Aerial photo with GPS locations of the ends of the study areas for each site.

In general, these sites are within the main floodplain of the Rio Grande River and situated on unconsolidated alluvial sediments (Figure 1). Gravels present within the alluvium at these sites included sedimentary rocks from the Cretaceous and Tertiary and a wide variety of igneous

(including some agate) and sedimentary rocks from Trans-Pecos Texas, Mexico, and New Mexico. Surface materials at sites 1, 2, and 3 are in an area classified predominantly as silt and sand, while sites 4 and 5 are in areas dominantly mud. These distinctions could be important when considering the levees are generally constructed of locally farmed earth materials. Another noteworthy distinction between these two areas is the source of the alluvium: at sites 4 and 5, several miles north of the Rio Grande River, gravels are mostly local Tertiary rocks and chert derived from Uvalde gravel.

Figure 4. Cracks/fissures evident along the flanks at site 2.

Surface investigations of the slopes and crests at all five sites revealed more evidence of differences in material characteristics. At sites 1 and 2 the conductivity was notably low, and the core samples were clearly less competent than equivalent measurements and samples from sites 4 and 5. Surface investigations at site 1 indicated a much greater concentration of sand to clay than the other sites, a characteristic also evident in cores from this site. At site 2 a higher concentration of surface cracks or fissures were observed both on the crest and along the slopes than at any of the other four sites (Figure 4). A levee core percolation test at site 2 revealed extremely rapid movement of water into/through a trench cut into the levee core. Sites 4 and 5 were in newer segments of levee with higher measured conductivity and clay cores showing little or no evidence of the dynamic properties characteristic of expansive clays (contract when dry and expand when wet) as suggested to be present at site 2.

Site 2 was selected for the percolation test based on the fairly extensive network of observed surface cracks and its relatively low conductivity. A trench was opened from the crest road down several feet into the core. The trench was then kept full of water with observations made as to the volume of water moving out of the trench and into the core. Beyond tracking the volume of water necessary to keep the trench full of water, this test was limited to surface observation of seepage along the levee sides. These surface observations were intended to determine the breadth and density of this apparent network of cracks and some qualitative idea as to flow potential within the core as a result of this likely higher than average permeability zone.

3—APPROACH (Program Components)

Refraction/Tomography

Direct and refracted P-wave and S-wave arrivals were analyzed using conventional methods (Palmer, 1981; Haeni, 1986; Lankston, 1990) and inversion techniques (Scott, 1977; Schneider et al., 1992; Ivanov et al., 2000). Use of direct and refracted arrivals for mapping distinct velocity contrasts between layers has been in routine use for everything from crustal seismic research (Steinhart and Meyer, 1961) to shallow ground-water studies (Haeni, 1978). It is an established, proven technique whose limitations are well documented (Soske, 1954; Sander, 1978). Methods to approximate solutions when physical conditions violate assumptions of the refraction method (Mooney, 1981; Redpath, 1973) are known. Recent research incorporating refraction inversion with shear-wave velocity calculations from surface-wave data has provided encouraging results that seem to be insensitive to the velocity reversal problem (Ivanov, 2002).

Tomography has a variety of applications in the subsurface, including: waste repository characterization (Peterson et al., 1985), engineering studies (Cottin et al., 1986), void detection (Lytle and Dines, 1980), and mining (Kilty and Lange, 1990). The simplicity of acquisition and lack of computational intensity makes it especially applicable for velocity estimation using data acquired for surface-wave or refraction analysis. Using this approach in conjunction with multichannel surface-wave inversion allows anomalous features within the levees to be examined from toe to toe and all along the crest using shear and compressional waves. Study of through-levee compressional waves was important if for no reason other than to provide confidence in first-arrival interpretations on shear-wave tomograms. Processing data for tomographic analysis incorporated existing algorithms and standard curved-ray methodologies (Chiu et al., 1986).

Application of refraction (tomography) methods can be inaccurate due to the problem of non-uniqueness, meaning there are many possible solutions that can generate the same first-arrival values (Ivanov et al., 2005). The Joint Analysis of Surface Wave and Refractions (JASR) method, developed at the KGS (Ivanov, 2002), offers an approach for minimizing one of the main problems in refraction tomography: nonuniqueness. A general way to overcome nonuniqueness is the use of *a priori* information. Such information generally comes from direct observations (borehole, outcrops, etc.). The JASR method obtains *a priori* information from Multichannel Analysis of Surface Waves (MASW) where a two-dimensional shear-wave velocity (Vs) section is used to construct a two-dimensional compressional-wave velocity (Vp) initial model (*a priori* information for deterministic-type refraction tomography inversion). The validity of creating a Vp model from these Vs values is based on the common elastic and density parameters on which these two types of seismic velocities depend. Qualitatively this assumption is consistent with the frequently made observation that the general trend of Vs follows to the general trend of Vp. The JASR technique significantly improves the reliability of the final refraction-tomography inversion results (Miller et al., 2001; Ivanov et al., 2000; Ivanov, 2002).

Figure 5. Shear-wave source operated along the north line at site 2 during the ponding test.

It was necessary to understand the arrival patterns of the various compressional- and shear-wave modes during through-levee tomography. At one site two-component data were recorded from a 2-D grid of sources and receivers on opposing sides of the levee (Figure 5). Three-dimensional images highlighted areas within the body of the levee with anomalous velocity characteristics. Integrating the interpretation of the crest 2-D profile and the slope through-levee tomography provided consistent images and allowed confidence in the effectiveness of these techniques. While the emphasis of this effort is on data collection and analysis, modeling is necessary to ensure a thorough understanding of the principal features of the seismograms, and to target those features that are not clearly understood for continued investigation.

Surface Wave Inversion

Surface waves traditionally have been viewed as noise in multichannel seismic data collected to image targets for shallow engineering, environmental, and ground-water purposes (Steeples and Miller, 1990). Recent advances in the use of surface waves for near-surface imaging have combined spectral analysis techniques (SASW), developed for civil engineering applications (Nazarian et al., 1983), with multi-trace reflection technologies developed for near-surface (Schepers, 1975) and petroleum

applications (Glover, 1959). The combination of these two uniquely different approaches to seismic imaging of the shallow subsurface permits non-invasive estimation of shear-wave velocities (within 10% of measured in many cases) (Xia et al., 2002) and delineation of horizontal and vertical variations in near-surface material properties based on changes in these velocities (MASW) (Park et al., 1996; Xia et al., 1999; Park et al., 1999).

Extending this imaging technology to include lateral variations in lithology as well as tunnel and fracture detection, bedrock mapping, and subsidence/karst delineation has required a unique approach that incorporates SASW, MASW, and CDP methods. By integrating these techniques, 2-D continuous shear-wave velocity profiles of the subsurface can be generated. Estimating the dispersion curve from up to 60 receiving channels, spaced every 3 ft to 6 ft along the ground surface, enhances the signal and results in a unique, relatively continuous view of shallow subsurface shear-wave velocity properties. This highly redundant surface-wave method improves the accuracy of calculated shear-wave velocities and minimizes the likelihood that irregularities resulting from erratic dispersion curves will corrupt the analysis in comparison to the more traditional SASW approach.

Surface-wave analysis was performed on data acquired on the crest and toe of the levee and on adjacent crest lines during the ponding experiment. Each of the five profiles located at different places along the levee and the two profiles used for the water flood experiment used the same spread geometry (120 stations with both compressional and shear receivers located every 3 ft) and permitted correlation between the various processed data sets for each line and between the five different lines. Even with the unique broadband requirements of surface-wave measurements it was not necessary to use an accelerated weight drop source, a hammer was sufficient (broad enough bandwidth, low enough frequency, and high enough energy), but low frequency receivers and windowed processing was necessary to produce the highest quality results. Shear-wave velocity maps generated along each profile line were optimized for resolution and signal-to-noise. Several unique approaches were used to minimize smearing resulting from variable wavelength averaging.

Reflection

High-resolution P-wave or S-wave seismic reflection surveys did not produce reflections from the basal reflector (velocity-density contrasts) of the levee or top of water table estimated to be less than 50 ft below ground surface. It was our intent to concentrate on: 1) generating high resolution (>250 Hz P-wave and >120 Hz S-wave) signals; 2) optimizing acquisition and processing for 2-D imaging along crest and toe without compromising first-arrival analysis, which was a higher priority operation; 3) establishing equipment configurations and parameter settings to maximize signal-to-noise and resolution potential considering the first-arrival acquisition deployment; 4) correlating P-wave reflections with S-wave reflections as well as with the other seismic, EM, and drill/excavation data; 5) performing attribute analysis of reflection waveforms passing through core, as well as careful study of velocity distribution calculated from NMO curves; 6) tailoring processing flows for non-optimized acquisition equipment and parameters due to full wavefield acquisition approach; 7) correlating compressional- and shear-wave NMO velocities for specific reflector(s); and 8) integrating reflection data with other seismic data. Source spacing, geophone spacing, line orientations, imaging, interpolation requirements, and fiscal constraints were to also be addressed, but due to limitations imposed as a result of coincident acquisition of first-arrival and surface-wave data, it was not possible to optimize both. Parameter and signal requirements are markedly different between the methods. Well-established shallow high-resolution data acquisition methodologies, emphasizing correlation of modal data and optimized velocity control, were adhered to as closely as possible without compromising other seismic methods (Hunter et al., 1984; Knapp and Steeples, 1986; Steeples and Miller, 1990).

4—OVERALL PROGRAM: DATA ACQUISITION

Phase I (data acquired during trip 1 from December 4 to 12, 2003)

Initial studies at the five sites were intended to identify any seismic characteristics unique to—or that could be correlated with—specific material characteristics or conductivity readings. This research program was intended to evaluate as many seismic methods as possible and appropriate, both on the crest and on the toe, to determine the range and level of sensitivity the methods have to areas identified as susceptible to core erosion and levee failure. Single data sets were acquired with the intention of separating and processing the individual components of the wavefield with appropriate methods and portion of the seismograms.

Consistency in recording equipment and parameters was critical for site-to-site comparison and especially for time-lapse studies of the kind planned here. A Geometrics 240-channel StrataView seismograph system was used to record all the seismic data for this project (Figure 6). The system is mounted in a 6-wheel John Deere Gator for added mobility and minimal environmental impact (Figure 7). This 24-bit A/D recording system used a Geometrics StrataVisor controller for basic QC and data storage. Throughout the project the same recording system was used, configured appropriately for each data set, and configured consistently for each data type.

Figure 6. Geometrics 240-channel seismograph mounted in John Deere Gator.

Figure 7. Compressional-wave hammer survey.

An important consideration when designing and acquiring these data was the need to optimize and retain the potential to compare toe and crest data at each site. Comparing and contrasting data allowed levee-specific seismic characteristics to be identified and isolated. Consistency in acquisition from site to site was also a high priority that allowed broader assertions about the significance of the observed seismic differences and their relationship to the different physical characteristics and make-up of the levees at each site. Since it was not clear from the onset which method or levee property would prove to be most sensitive to or indicative of levee degradation potential associated with expansive clays and increased permeability that resulted after over a decade of dewatering, all seismic methods and data modes had to be evaluated.

1) Initial testing at site 2 was completed first to measure some of the basic seismic characteristics and define the optimum equipment and configuration for data recorded on and at the toe of these levee structures. Analysis of test data concluded that 10-Hz single geophones, a 16-lb sledgehammer, three impacts per station, and planted geophones were optimum for both the surface-wave and

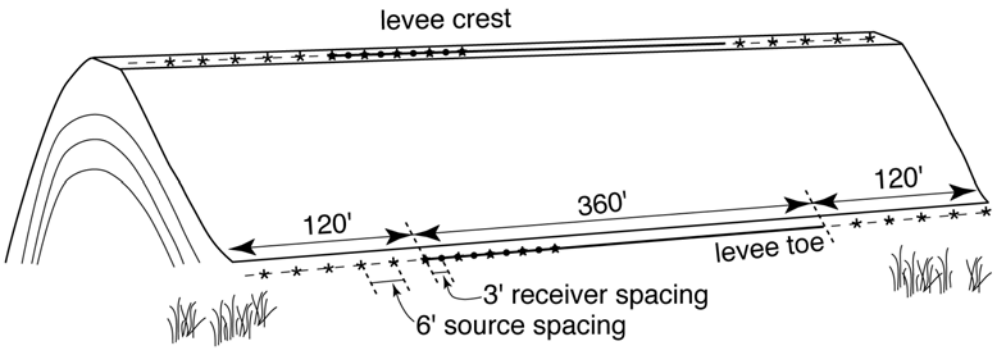

Figure 8. Crest and toe 2-D line deployments.

compressional-wave tomography. Included in the testing regimen was evaluation of land-streamer data, 12-lb and 20-lb sledgehammers, 4.5-Hz geophones, and a mechanical weight drop.

2) At each site, one 2-D, 2-C profile was acquired along the crest and at the toe of the levees (Figure 8). Receiver station spacing was 3 ft with two receivers at each location (10 Hz compressional-wave geophones and one 14 Hz shear-wave geophone) (Figure 9). Shear-wave receivers were oriented to be sensitive to motion perpendicular to the axis of the levee (transverse). A 16-lb sledgehammer impacting a striker plate of similar weight for compressional- and surface-wave data (Figure 10) and a 6" x 6" wood block outfitted with steel endplates and serrated earth-coupling teeth (Figures 11 and 12), were used for shear-wave data. The total spread length was 360 ft with 120 channels recording compressional and 120 channels recording shear signals. Source spacing through the spread varied, depending on data quality, from every 6 ft to every 24 ft. Each profile was acquired twice, once with the source in compressional-wave orientation and a second time with a shear-wave source orientation. Data were recorded from shear-wave phones when the shear-wave source was used and compressional-wave phones when the compressional-wave source was used. Stations (source and receiver) were located initially using analog measuring tapes/chain, followed by highly accurate (±1 inch) x, y, and z measurement using a Trimble DGPS surveying system (Figure 13).

Figure 9. Both compressional and shear geophones were used at each station.

Figure 10. Compressional-wave survey along levee crest road.

Figure 11. A 1-m-long wood block with steel end plates held down by standing on top of the block was used to generate shear energy.

Figure 12. Steel teeth were forced into the ground to minimize source decoupling and sliding along ground surface.

Figure 13. Differential Global Position System (DGPS) was used to accurately locate all sources and receiver stations.

3) At levee sites 1 (Figure 14) and 2 (Figure 15), a 3-D through-levee tomographic study was conducted to investigate internal variations in levee conditions (physical properties) in three dimensions (Figure 16). A 240-receiver station grid was deployed on the south side of the levee at site 1 with each receiver station separated by 4 ft both parallel and perpendicular to the levee axis (Figure 17). Two geophones (one shear and one compressional) were connected to individual recording channels at each station of the grid on the receiver side of the levee. Two shots were fired and recorded at each of the 120 source stations on the north side of the levee at site 1 (one shear and one compressional) (Figure 18). The receiver grid included eight rows parallel to the levee axis and thirty stations per row. The source grid was made up of six rows of twenty stations per row with each row parallel to the levee axis. A unique directional source was used to record the appropriate data mode. The P-wave source was the 16-lb sledge and striker plate (Figure 19) and S-wave was the 16-lb sledge and shear block (Figure 20). Receivers were three 10-Hz Mark Products U2 digital-grade vertical geophones (Figure 21) and a single GS-11 GeoSpace horizontal geophone (Figure 22). All 240 channels were live for all shots. Channel 1 was used to extract the source signature. This single source wavelet receiver was placed approximately 5 ft from the source location for each shot, allowing measurement of as pure a source wavelet as possible. The grid was initially laid out using tape measures. Once the stations were flagged, highly accurate measurements of z, y, and z were made using a Trimble DGPS surveying system (Figure 14).

Figure 14. Through-levee receiver and source grids at site 1.

Figure 15. Through-levee receiver and source grids at site 2.

Figure 16. Source grid along north side of site 1 for through-levee study.

4) A second condensed through-levee tomography experiment was completed at site 2 (Figure 17b,c). Sources and receivers were the same as site 1 (item #3), but the deployment was reduced (Figure 23). A total of 120 receivers were deployed in a grid consisting of four lines of 30 receiver stations parallel to the levee axis. The source grid included three lines of 20 source stations each. After the data were recorded, a highly accurate DGPS survey was conducted to exactly locate each station (Figure 15).

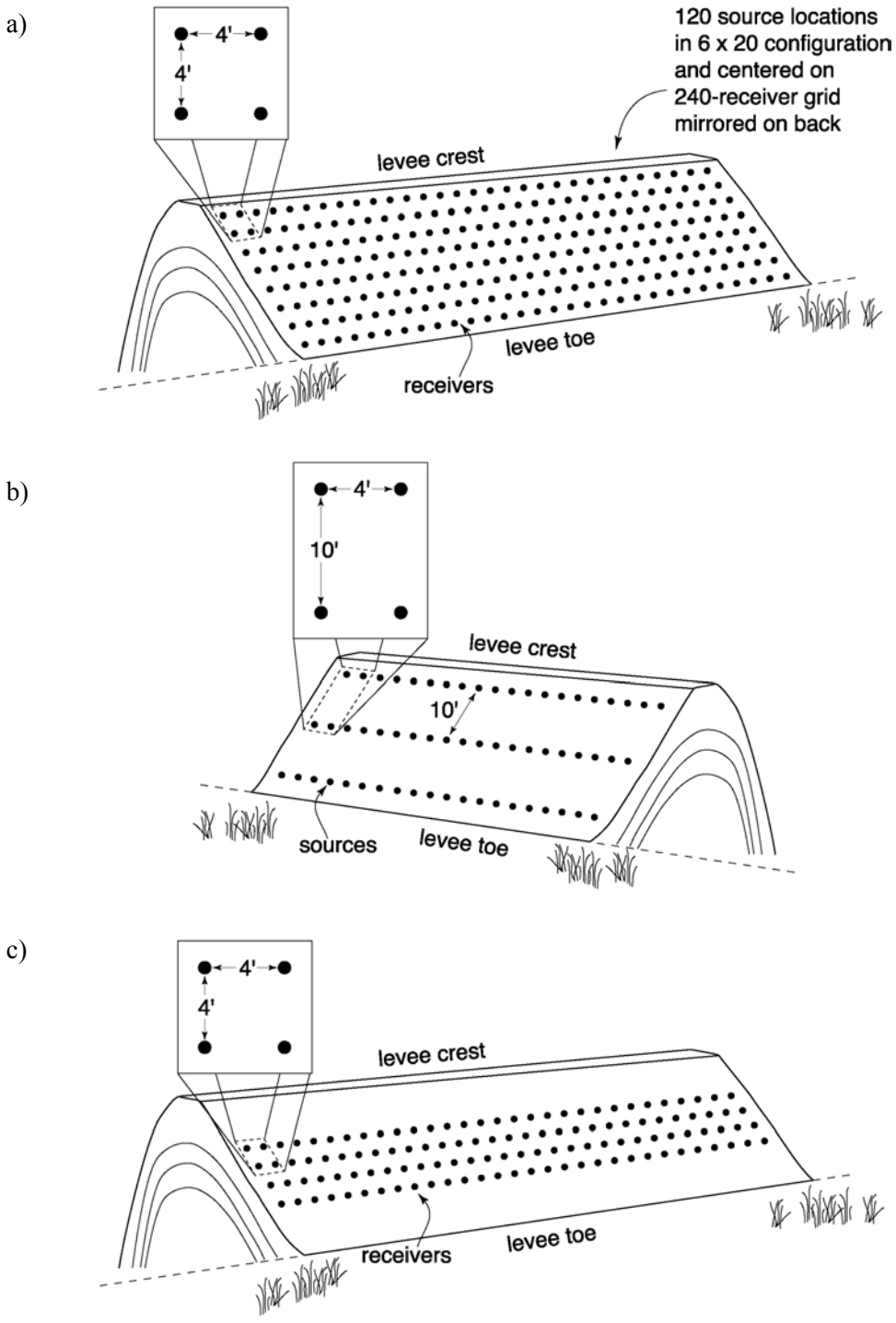

Figure 17. Deployment design for a) site 1 through-levee, b) site 2 source station design, and c) site 2 receiver location map.

Figure 18. Receiver deployment, site 1.

Figure 19. Compressional-wave data acquisition, site 1.

Figure 20. Shear-wave data acquisition, site 1.

Figure 21. Compressional-wave phones used for through-levee, site 1.

Figure 22. Shear-wave phone.

Figure 23. Compressional-wave survey, site 2.

5) Vibrator dwell experiments were run at sites 1 and 2. These experiments were designed to measure any non-uniformity in the surface-wave propagation that might relate to variable mechanical or hydrologic properties of the subsurface unique to each particular site. An IVI minivib1 was used as the source for experiments both at the crest and toe (Figure 24). Receivers used for the compressional-wave 2-D full wavefield recording (single 10-Hz GeoSpace geophones) were the same as used for the vibrator dwell experiments. Shot stations for the vibrator experiments were located immediate off each end of the 120-station receiver spread.

Phase II (data acquired during trip 2 from November 8 to 13, 2004)

6) The second trip focused on the ponding experiment carried out at site 2 (Figures 25 and 26), based on the analysis of data acquired during the first visit. A water-retention structure was built at site 2 to allow the simulation of a flood event across a portion of the levee suspected to be susceptible to internal erosion and potential failure. This experiment was intended to determine if fractures in the clay core, due to dewatering, would initiate and perpetuate piping. Site 2 was selected based on trenching, core drilling, conductivity measurements, and seismic properties. This phase of the project was designed as a time lapse experiment where differencing could be used to investigate change in seismic properties that might occur as a result of increased saturation of the permeable shell and changes in the material property as a result of piping on the core.

Figure 24. Vibrator at site 2 during dwell experiments.

7) Two survey lines were deployed along the north and south edges of the crest (Figure 27). Each receiver station has a 14-Hz shear-wave geophone (blue) and three 10-Hz compressional-wave geophones (Figure 28). Data from the appropriate receiver recorded for the source being used by physically changing the connection (Figure 29). Each mode and profile was recorded for a given survey time. A baseline survey was acquired prior to water being in contact with the levee sides (Figure 30). Surveys were acquired throughout the pool build up and retention of designed high pool (Figure 31). Day 1 baseline data included hammer compressional, transverse shear, and compressional-wave vibrator dwell on both the north and south lines (Figure 32). Day 2 water level was at 9.05 at the beginning of the data acquisition and the survey included hammer compressional (Figure 33), transverse shear (Figure 34), and vibrator dwell (Figure 35) for north and south profiles. Day 3 water was at simulated full pool (9.46) and data were recorded twice, once in the morning (hammer compressional, shear transverse, and vibrator dwell) for both lines, and compressional-wave hammer during the late evening/night. Day 4 full pool was maintained with hammer compressional, transverse shear, and vibrator dwell in the morning and hammer compressional in the late evening/night. On the morning of Day 5 the last seismic data were acquired, which included hammer compressional, transverse shear, and vibrator dwell on both the north and south lines.

Figure 25. Pond constructed to test flood simulation interrogations.

Figure 26. Water pumped into pond at rate consistent with model flood.

Figure 27. Seismic lines deployed along each side of crest road at site 2.

Figure 28. Compressional and shear phones used for monitoring experiments.

Figure 29. Receiver station spacing was 3 ft.

Figure 30. Pond was incrementally filled to simulate rising water from Rio Grande flood.

Figure 31. Pond nearing full.

Figure 32. Pool monitored with water added about once an hour.

Figure 33. Compressional-wave survey during full pool.

Figure 34. Shear-wave survey during full pool.

Figure 35. Vibrator on-line and ready to begin dwell experiment at various pool stages.

Figure 36. Night acquisition was necessary to capture water at key levels.

8) For all data acquired with the sledgehammer, each shot station and energy mode retained the field operator from beginning to completion. Three different hammer operators rotated off in a set order and at consistent shot stations. Comparison of recorded amplitudes was possible through time for a given configuration and energy mode because of this uniformity in energy provided, in part, as a result of consistency in hammer operation. Maintaining a schedule with reasonable uniform survey intervals required some night operations (Figure 36).

9) Increased seismic velocities were observed on the baseline survey at site 2, which suggested the wetter than normal summer and fall of 2004 had sufficiently altered the ground moisture conditions to affect the seismic velocities and therefore possibly the material properties, such as stiffness. If this did occur then the response of the levee to ponding would not be as expected based on the material properties measured and observed during the fall and winter of 2003. This observed increase in seismic velocity was a result of weather events and not site-specific variability or inconsistency of methodologies prompted the investigation of site 4 and site 1, allowing direct comparisons with trip 1 measured velocities. Crest profiles for sites 1 and 4 were acquired using as near identical parameters and equipment as possible (Figures 37 and 38). Stations were located as closely as possible using landmarks and GPS locations established during the winter of 2003 survey. A 120-station hammer compressional-wave survey was conducted using single 10-Hz geophones on 4-ft intervals at sites 1 and 4 during the late fall 2004 campaign.

Figure 37. Compressional-wave survey, 2003 campaign.

Figure 38. Site 1 compressional-wave survey, 2004 campaign.

Summary of Acquisition

December 2003		mode	source	receivers	method
Site 1	crest	P-wave	hammer/plate	single 10 Hz	refract/tomography & MASW
		S-wave	hammer/block	single 14 Hz	tomography
		Surface wave	vibrator	single 10 Hz	dwell mono frequencies 10-100 Hz
	toe	P-wave	hammer/plate	single 10 Hz	refract/tomography & MASW
		S-wave	hammer/block	single 14 Hz	tomography
		Surface wave	vibrator	single 10 Hz	dwell mono frequencies 10-100 Hz
	slopes	P-wave	hammer/plate	three 10 Hz	3-D tomography
		S-wave	hammer/block	single 14 Hz	3-D tomography
		Surface wave	vibrator	three 10 Hz	3-D tomography
					dwell mono frequencies 10-100 Hz
Site 2	crest	P-wave	RAWD-testing	single 10 Hz	refract/tomography & MASW
		P-wave	hammer/plate	single 10 Hz	refract/tomography & MASW
		S-wave	hammer/block	single 14 Hz	tomography
		Surface wave	vibrator	single 10 Hz	dwell mono frequencies 20-300, 12-100
	toe	P-wave	hammer/plate	single 10 Hz	refract/tomography & MASW
		S-wave	hammer/block	single 14 Hz	tomography
	slopes	P-wave	hammer/plate	three 10 Hz	3-D tomography
		S-wave	hammer/block	single 14 Hz	3-D tomography
		Surface wave	vibrator	three 10 Hz	3-D tomography
					dwell mono frequencies 10-100 Hz
Site 3	crest	P-wave	hammer/plate	single 10 Hz	refract/tomography & MASW
		S-wave	hammer/block	single 14 Hz	tomography
		Surface wave	vibrator	single 10 Hz	dwell mono frequencies 10-100 Hz
	toe	P-wave	hammer/plate	single 10 Hz	refract/tomography & MASW
		S-wave	hammer/block	single 14 Hz	tomography
Site 4	crest	P-wave	hammer/plate	single 10 Hz	refract/tomography & MASW
		S-wave	hammer/block	single 14 Hz	tomography
		Surface wave	vibrator	single 10 Hz	dwell mono frequencies 10-100 Hz
	toe	P-wave	hammer/plate	single 10 Hz	refract/tomography & MASW
		S-wave	hammer/block	single 14 Hz	tomography

December 2003 (continued)

Site 5	crest	P-wave	hammer/plate	single 10 Hz	refract/tomography & MASW
		S-wave	hammer/block	single 14 Hz	tomography
		Surface wave	vibrator	single 10 Hz	dwell mono frequencies 10-100 Hz
	toe	P-wave	hammer/plate	single 10 Hz	refract/tomography & MASW
		S-wave	hammer/block	single 14 Hz	tomography

November 2004		mode	line/source	receivers	method
Site 1	crest	P-wave	S hammer/plate	single 10 Hz	refract/tomography & MASW
Site 2	crest				
	Time 1	P-wave	S hammer/plate	single 10 Hz	refract/tomography & MASW
		P-wave	N hammer/plate	single 10 Hz	refract/tomography & MASW
		Sh-wave	S hammer/block	single 14 Hz	refract/tomography & MASW
	Time 2	Sh-wave	S hammer/ block	single 14 Hz	refract/tomography & MASW
		Sh-wave	N hammer/ block	single 14 Hz	refract/tomography & MASW
		Sh-wave	Center vibrator	single 14 Hz	refract/tomography & MASW sweep 10-100 Hz
		Sv-wave	S hammer/ block	single 14 Hz	refract/tomography & MASW
		Sv-wave	Center vibrator	single 14 Hz	refract/tomography & MASW sweep 10-100 Hz
		P-wave	S hammer/plate	single 10 Hz	refract/tomography & MASW
		P-wave	N hammer/plate	single 10 Hz	refract/tomography & MASW
	Time 3	P-wave	S hammer/plate	single 10 Hz	refract/tomography & MASW
		P-wave	N hammer/plate	single 10 Hz	refract/tomography & MASW
		Sv-wave	Center vibrator	single 10 Hz	refract/tomography & MASW mono 10-50 Hz
		Sh-wave	S hammer/block	single 14 Hz	refract/tomography & MASW
		Sh-wave	N hammer/block	single 14 Hz	refract/tomography & MASW
	Time 4	P-wave	S hammer/plate	single 10 Hz	refract/tomography & MASW
		P-wave	N hammer/plate	single 10 Hz	refract/tomography & MASW
	Time 5	P-wave	S hammer/plate	single 10 Hz	refract/tomography & MASW
		P-wave	N hammer/plate	single 10 Hz	refract/tomography & MASW
		Sv-wave	Center vibrator	single 10 Hz	refract/tomography & MASW mono 10-50 Hz
		Sh-wave	S hammer/block	single 14 Hz	refract/tomography & MASW
		Sh-wave	N hammer/block	single 14 Hz	refract/tomography & MASW
	Time 6	P-wave	S hammer/plate	single 10 Hz	refract/tomography & MASW
		P-wave	N hammer/plate	single 10 Hz	refract/tomography & MASW
	Time 7	P-wave	S hammer/plate	single 10 Hz	refract/tomography & MASW
		P-wave	N hammer/plate	single 10 Hz	refract/tomography & MASW
		Sv-wave	Center vibrator	single 10 Hz	refract/tomography & MASW mono 10-50 Hz
		Sh-wave	S hammer/block	single 14 Hz	refract/tomography & MASW
		Sh-wave	N hammer/block	single 14 Hz	refract/tomography & MASW
Site 4	crest	P-wave	S hammer/plate	single 10 Hz	refract/tomography & MASW

QA/QC

The data acquired and processed on this survey were managed to ensure the highest quality and most accurate acoustic representation possible at this geologic setting. Current state-of-the-art techniques were used in a fashion that was appropriate and verified with step-by-step QA/QC. The most important (possibly even essential) QC information are samples of shot gathers. Raw and processed shot gathers allow the geophysicist and geologist to make determinations as to the authenticity of processed seismic sections. Seismic processing software and techniques are very powerful tools that, if not used properly, can and most likely will result in unrealistic interpretations.

The equipment and recorded data were continuously monitored during acquisition to ensure the highest quality sections. Receiver response and sensitivity were monitored using a modified tap test performed after the planting of each geophone or group of geophones. The continuity and leakage of each active station was monitored prior to each shot. The system was subjected to a series of pre-acquisition tests designed to ensure consistency in system noise and precision in digitally stored data. Visual analysis of general signal-to-noise ratio, environmental noise, DC bias, and variations in the optimum recording window were performed on at least every fifth field plot. Preliminary in-field processing provided excellent insights into data quality and need for real-time parameter adjustments as well.

Data Storage

Data were recorded and stored initially on the seismograph controller hard drive in SEG2 format. At the conclusion of each day's work the data were downloaded via Ethernet to computer hard drives located in the Mobile Processing Center (MPC). Once on computers in the MPC at the field site, the data were converted and viewed to verify data were fully readable and error free, archived in SEG2 format on DVD media (media was read verified with two copies burned), and processed for preliminary infield analysis. Long term these DVD media are archived at the KGS in the seismic data library. Processing of the data required reformatting into a fixed modified SEGY format.

5–DATA PROCESSING

Overview of Processing Objectives

Trip 1 — December 4 to 12, 2003

Each data set was acquired with the intent of capturing a specific mode (compressional or shear) and positioned to target certain types of energy (Rayleigh wave, reflections, refraction, first arrivals, etc.) while focusing on a particular distribution of seismic characteristics (time-offset [t-x], frequency-wave number [f-k], frequency-phase velocity [f-v], frequency-amplitude [f-a], etc.). For each site there are two unique data sets for crest and two for the toe; there is a compressional-wave survey and coincident shear-wave survey following the same line. Unique to sites 1 and 2 are the through-levee tomography. Several experiments were run using cross-modal data sets. These include acquisition using shear-wave receivers and a compressional-wave source and vice versa. Some of these more obscure data sets were not processed during this initial round of processing but were scheduled for later, more advanced processing runs.

Through-levee tomography data were processed using a crosshole 3-D tomography approach. Delay times were the focus during the first processing pass. Wavelet extraction analysis would be possible in the future using the source signature recorded on channel 1. Methods such as deconvolution and cross correlation could be used on the recorded first arrivals looking for variations in wavelet attributes that might be indicative of lithology or compaction. More than 50,000 raypaths were processed for

each mode of seismic energy (P-wave and S-wave). Throughout the processing of the through-dam tomography data, reciprocity was assumed. It was also assumed that there would be no advantage to reverse shooting or processing reverse shots at either through-levee test site.

Trip 2 — November 8 to 13, 2004

Design and construction of the water retention pond used for the flood simulation experiments was physically located directly over the through-levee tomography receiver locations at the oxbow lake site (Figure 39). The location of the pond meant no through-levee tomography was possible to observe the seismic changes due to increased saturation. However, with the crest relatively clear, baseline and monitor surface seismic experiments were acquired and processed to distinguish changes in the velocity indicative of increase saturation. If piping did occur, the experiments were set up to study the seismic changes and characteristics immediately prior to failure of the levee. Failure never occurred, so it is not clear how significant the seismic changes observed were in terms of extrapolating changes to the point of failure and, therefore, it is not clear how good an indicator or early warning potential seismic data might be in this situation.

Figure 39. Key stations occupied during 2003 seismic investigation at site 2 with location of pond superimposed.

Data acquired along the south and north sides of the crest road were processed to enhance changes in seismic velocities that could be correlated to changes in saturation. If effective, this approach could provide a method of tracking zones of increased saturation and/or leakage through the levee as water pressures increase with increasing pool height. Processing flows for tomography and MASW were maintained as close to identical as possible from one time lapse to the next to ensure changes observed were from velocity and not processing parameter variations.

Processing Software

Several processing packages were used to analyze these data, each with an emphasis on a specific energy type or travel path. For surface-wave analysis a commercial program called *SurfSeis* developed at the Kansas Geological Survey for Multichannel Analysis of Surface Wave (MASW) processing was used. Turning-ray tomography data were analyzed and displayed using *TomoSeis*, a collection of algorithms under development at the Kansas Geological Survey for Joint Analysis of Surface Waves and Refraction (JARS) processing. Seismic reflection data processing was undertaken with *WinSeis*, also a commercial processing package developed by the Kansas Geological Survey. Through-levee tomography processing was accomplished using 3-D borehole tomography and defining all the source and receiver locations in 3-D, allowing *GeoTomCG* to analyze first arrivals based on 3-D rays. Both compressional- and shear-wave data for each method were processed following the same approach and using the same software.

Data Processing Methods

Surface Wave

The surface-wave component of the seismic data was processed to estimate shear-wave velocity using the MASW method. By analyzing the fundamental-mode Rayleigh waves, a shear-wave velocity profile (1-D and 2-D) is produced that can be used to evaluate material stiffness or anomaly detection of ground materials usually shallower than 30 m, both applicable for either engineering or geophysical projects.

The *SurfSeis* processing procedure consists of three steps:

1. Field setup—This encodes the surface location of seismic source and receivers into the field data.
2. Extraction of dispersion curves—Dispersion of the fundamental-mode Rayleigh wave is extracted from the seismic data.
3. Inversion for shear-wave velocity (Vs) profiles—Extracted dispersion curves are inverted for the Vs profiles, each of which depicts the Vs variation with depth at a particular surface location.

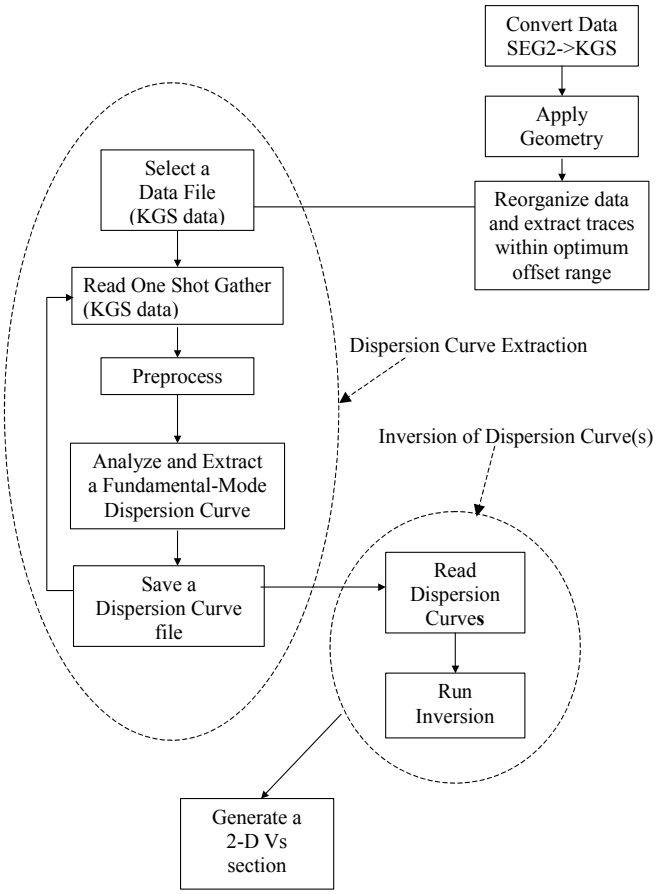

Figure 40. Processing flow for MASW data.

Processing surface-wave data for this project involved extraction of the optimum 30 or fewer traces from each 120-channel shot record, transformation to phase velocity-frequency domain, and inversion of the fundamental-mode dispersion curve to produce an estimate of the shear-wave velocity function relative to depth (Figure 40). These 30-or-fewer-trace gathers were analyzed using *SurfSeis*. Each shot gather generates one dispersion curve that is assigned a surface location corresponding to the middle point of the analyzed spread. Care was taken to ensure that the spectral properties of the t-x data (shot gathers) were consistent with the maximum and minimum f-v_c values (v_c is the phase velocity of surface waves) contained in the dispersion curve. Shear-wave velocity maps generated along each profile line were optimized for resolution using several approaches, including deblurring and slope filtering. Wavefield maps have been generated based on optimized receiver-spread offset for depths of interest and data characteristics.

2-D First-arrival Analysis

First-arrivals were processed using the turning-ray tomography approach. This method uses continuous raypath reconstruction and inversion to define the optimum velocity field beneath and between the source and receiver locations. Each subsurface cell has an optimum compressional-wave velocity assigned such that when all the cells a ray penetrates between source and receiver are summed, the travel time is consistent with the time of the observed first arriving energy. For the work we present here a method called JARS was used to help eliminate problems of nonuniqueness inherent in most

geophysical inversion problems. Incorporating the results of the surface-wave analysis permits *a priori* information to be included for construction of an initial model.

TomoSeis (under development at the KGS) analyzes first arrivals picked from seismic data that are collected along a single line and recorded by a single shot gather. First arrivals can be either direct or refracted seismic energy. Since propagation of seismic energy through the earth can be approximated by a ray traveling through multiple cells, each with unique velocity characteristics, each specific velocity set (all cells along a travel path) represent the geologic model consistent with the observed seismic shot gather. The inverse refraction traveltime problem can be solved by finding a velocity model whose first arrivals best match the observed first arrivals. However, the inverse refraction-tomography problem is nonunique and therefore many different velocity models can be valid solutions to the observed first-arrivals.

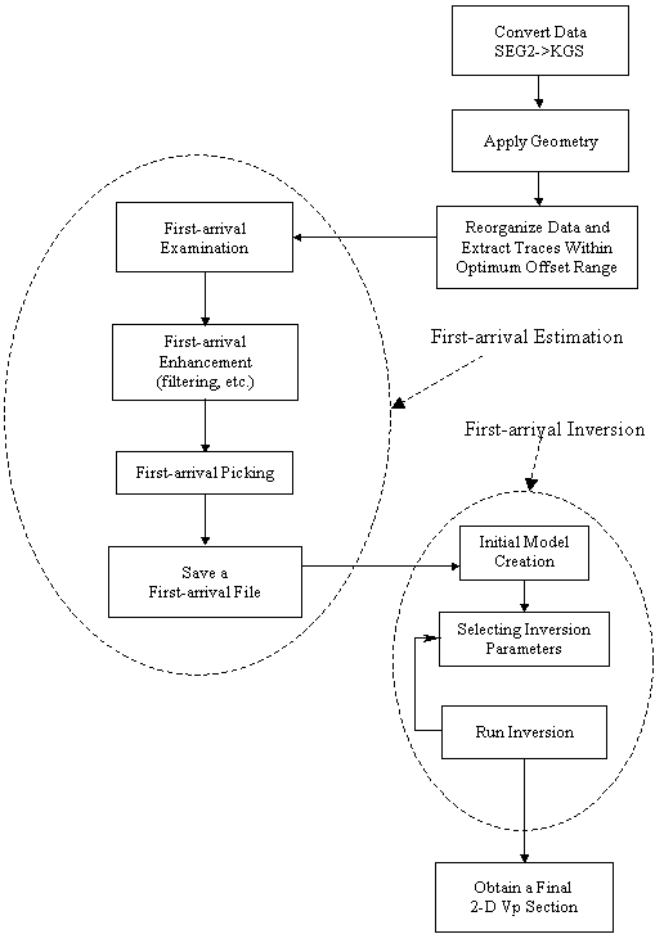

Figure 41. Processing flow for 2-D first-arrival analysis.

Two-dimensional Vs cross sections obtained from MASW analysis were used to generate an initial model for the tomographic inversion to Vp (Ivanov et al., 2000). Initial model optimization involves iterating an estimate of Poisson's ratio until model-predicted first arrivals correlate with those on actual shot records. Convergence of inversion runs required several iterations of the initial model, each time modifying conditioning parameters in a fashion appropriate for this data set (Figures 41 and 42). Optimization of the initial model was most efficient when best-fit conditioning parameters were used during preliminary analyses. Considering the resolution requirements and redundancy in rays penetrating each subsurface cell within the depth interval of interest, it was necessary for first arrivals to be picked for all traces on every shot gather.

By analyzing the correlation between model and observed data, it was possible to use final inversion results for quality control of the first-arrival picking routines. In some instances, secondary first arrival analysis was necessary for convergence to a "good" solution. Additional quality control was achieved by verifying that the 2-D Vp/Vs data were reasonable. *TomoSeis* was used to provide both traditional and JARS solutions to the 2-D refraction-tomography problem.

3-D First-arrival Analysis

First-arrival analysis of through-levee seismic energy focused on discriminating intra-levee velocity anomalies, specifically, low-velocity zones potentially indicative of areas of structural weakness or unusual material properties. Processing the source/ receiver traveltime picks was undertaken using *GeoTomCG*, a commercial software package that was designed and written to perform 3-D tomographic analyses. Because of the universal design of *GeoTomCG* and the unique geometries associated with shooting on the levee slopes, it was possible to "fool" this borehole analysis software by using high-

resolution land surveying to locate the shot and receiver lines, effectively making the lines simulate horizontal boreholes.

Key to any tomographic analysis is accurate and consistent first-arrival picking. First arrivals were picked using *TomoSeis* (the same software used for the turning-ray tomography). A total of 50,000 traces were analyzed with first arrivals automatically picked and manually inspected. From the first arrival pick a travel time between source and receiver is established and included in a grid to be inverted, iterating the inversion until convergence.

Source-to-receiver travel times can be analyzed to calculate velocities, or amplitudes can be analyzed to calculate attenuation coefficients. This method of through-levee tomography is extremely flexible, allowing source and receiver positions to be located anywhere around the study area in any configuration within a 3-D grid. The tomographic analysis calculates velocity and/or attenuation at points within the grid. Any point within the grid can be classified as having anisotropic characteristics. Raypaths between source and receiver can be straight or curved. The ability to perform 3-D analyses on data such as these is an important advantage in minimizing the problem of nonuniqueness prevalent in standard crosshole data.

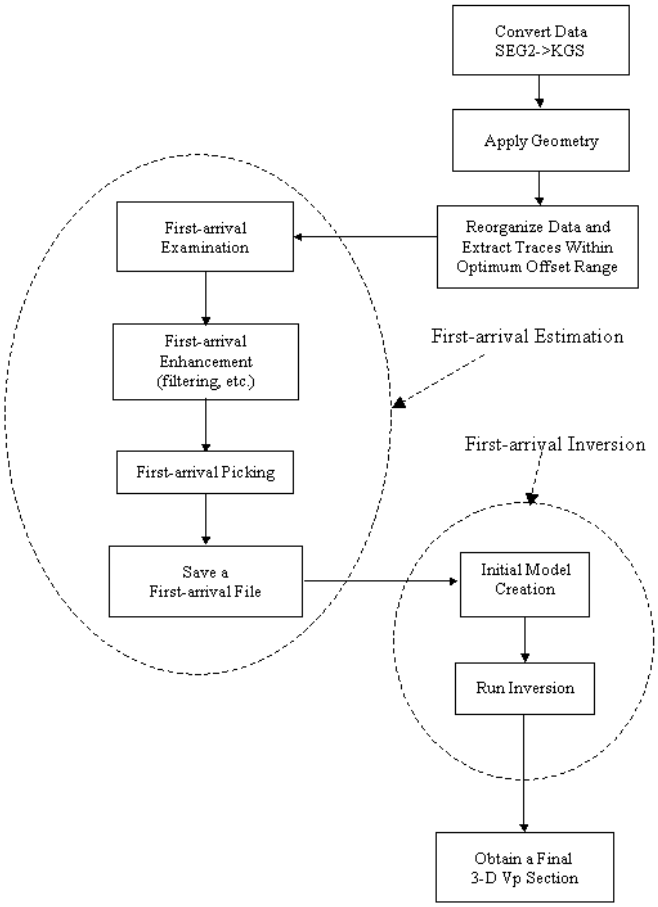

Figure 42. Processing flow for 3-D first-arrival analysis.

Reflection

Reflections from within and immediately below the basal levee contact were of interest and were the focus of reflection processing. High-resolution seismic reflection data, by its very nature, lends itself to over-processing, inappropriate processing, and minimal involvement processing. Interpretations of high-resolution shallow reflection data must take into consideration not only the geologic information available, but also each step of the processing flow and the presence of reflection events on raw unprocessed data. Processing for the reflection portion of this study included only operations or processes that by their nature would enhance signal-to-noise-ratio and/or resolution as determined by evaluation of high confidence reflections interpreted directly on shot gathers.

Unfortunately, no primary reflection energy could be extracted from these data. With the focus of the acquisition more on first arrivals and surface waves, a very reflection-conducive setting would have been necessary for reflection returns from within the levee to be observed or enhanced through processing. For the most part, processing of high-resolution shallow reflection data is a matter of scaling down conventional processing techniques and methods; however, without extreme attention to details, conventional processing approaches will produce undesirable artifacts.

The basic architecture and sequence of processing steps followed during attempts to identify and enhance reflections was similar to conventional petroleum exploration flows (Yilmaz, 1987). The primary exceptions related to the step-by-step QC necessary for the highest confidence interpretations of shallow features and realization of full resolution potential (Miller et al., 1989; Miller et al., 1990; Miller and Steeples, 1991) (Figure 43). Specific distinctions related to the emphasis placed on avoiding processing techniques that through mixing, stacking, or filtering could either alias noise to appear as reflections or actually create artificial coherency. Data were processed using *WinSeis2* beta (next generation of *WinSeis*).

Figure 43. Processing flow for reflection data.

Display Formats and Presentation

Data are displayed in this report in a variety of formats, using several different scales and color schemes. Each of the various seismic methods has a preferred or "normal" display format. The use of color and scales is generally a data-specific designation. Color is used throughout this report to enhance the dimensionality of the numerical data sets and to improve the apparent resolution of the data by focusing on the signal portion of the data.

Seismic data are recorded as digital words (representing amplitude of deflection or velocity) stored in a time-sequential order with uniform sampling rates. Sound waves are only useful for imaging if they are recorded over a finite time duration (also know as record length or recoding time). Considering that the velocity of sound in rock is generally several times to an order of magnitude or more greater than the velocity of sound in air, recording or listening times of fractions of a second are all that is necessary to fully capture the seismic wavefield from start (source impact/energy release) to finish (wavefield past the listening array). Analog display of seismic data is most commonly seen in what is referred to as wiggle-trace. In wiggle-trace format each sample is plotted as a function of time with a curve drawn through each sample forming a wiggle with the amount of deflection from the zero line equal to the amplitude of recorded signal.

Different components of the seismic wavefield are processed using very specific methods focusing on the particular characteristics of each different component. Initial surface-wave processing produces what is referred to as a dispersion curve. This curve is actually a trend in the data when displayed in frequency-phase-velocity space. A color scale indicative of degree of intensity or highest sample density is generally used to represent this pre-inversion data. Color contouring is a common display format for data that have gone through inversion. In this type of display, different colors represent different ranges of values; therefore, all areas with the same value will also have the same color. Velocity, as well, is generally represented using different colors for different ranges of values.

For most geologic applications, earth materials are generally considered to continuously change from one location to the next in a uniform and/or predictable manner. Since most seismic data are processed in a cell-by-cell or discrete fashion, to represent earth materials as realistically as possible it is necessary to interpolate between discrete sample points or cells. This process basically makes the assumption that the values between sample points transition between those points in a predictable fashion. This process of interpolation results in a smooth curve or transition across a digital data set. In its most basic form, a digital data field or plot can be contoured such that all points of equal value are connected with curves. This process allows areas with a collection of highs or lows to be easily identified and some degree of continuity in data trends established.

Merging of colors through the spectrum is a way of indicating gradational changes or transitioning of certain earth properties across a survey area. Trends associated with inferred material properties can be established and equated to known values or ground truth. Color contoured (each color representing the same value or level for the mapped property) data provide an image sensitive to changes in the displayed property and therefore allow a greater awareness of difference across a site and from survey to survey (assuming each color is assigned a fixed value that is consistent for all data sets displaying a particular property).

Discussion of Data and Processing at Each Site: Trip 1

A generally consistent set of data was recorded for each site with data processing also following a flow that was relatively consistent for each site. However, each site did have slight differences in acquisition parameters and/or methods evaluated. As previously indicated, all sites had compressional and shear data acquired at the crest and toe; what was not mentioned is that source station spacing changed slightly for sites 3, 4, and 5 based on the findings at sites 1 and 2. Also, the low conductivity at sites 1 and 2 provided opportunities for testing not available at the other sites. For example, site 2 was the site of the percolation experiment with the dug trench.

Seismic-data processing was intended to provide accurate and precise Vp and Vs earth models for the crest and toe. These key seismic properties were used to search for anomalous zones within the levee core that might be indicative of weakening to a point the levee would not perform to construction specifications under the designed water load. As well, a Vp/Vs ratio map (reasonably consistent with a version of Poisson's ratio map) could be derived and used as an additional tool to look for areas of reduced strength within the levees. The larger the Vp/Vs, generally the weaker the material from a ripability or shear strength perspective. By comparing the crest data with the toe data from each site, contributions of native materials below the levee can be accurately characterized and allow separation of the energy traveling only in the levee. A second benefit to recording and processing data from both crest and toe is the potential to verify consistency in the measured native material values.

Site 1

Estimates of cross sectional Vs were obtained for both crest and toe using tomography and surface-wave inversion techniques. Vp information was extracted from P-wave data using first-arrival analysis (tomography) of seismic data collected along both toe and crest lines. Frequency dwell data were analyzed for amplitude variations as a function of frequency, specifically looking for changes in phase that could be related to changes in material seismic velocity. A full 240-channel through-levee traveltime study was undertaken for both P- and S-wave energy. Data were acquired to allow the use of 3-D borehole tomography software to analyze first arrivals and generate a traveltime delay volume focused within the core of the levee.

P-wave First Arrivals (foundation material vs. crest/levee material)

P-wave first-arrivals were picked from data acquired along the crest. In general, shot records possessed impulsive, relatively high signal-to-noise first breaks that were picked automatically with a small percentage requiring manual adjustments (Figures 44 and 45). There are two distinctively different apparent first-arrival velocity trends from trace to trace on the P-wave data (Figures 44 and 45). From a basic refraction analysis overview perspective, the two distinctly different phase velocities observed in these data are likely from the material within the levee and the shallowest portion of the native earth (possibly the near-surface material [upper few feet of native sediments]). After selecting the first-arrival time for each trace on the P-wave data shot gathers from along the crest of the levee, a 2-D refraction-tomography Vp solution was obtained (Figure 46). In this case a 2-D solution represents a cross sectional slice of the levee, physically equivalent to cutting a trench parallel to the centerline (axis) of the levee and observing the material from some distance away either north or south (Figure 47). This solution was obtained with minimal model iterations and without any major discrepancies between the modeled and real first arrivals.

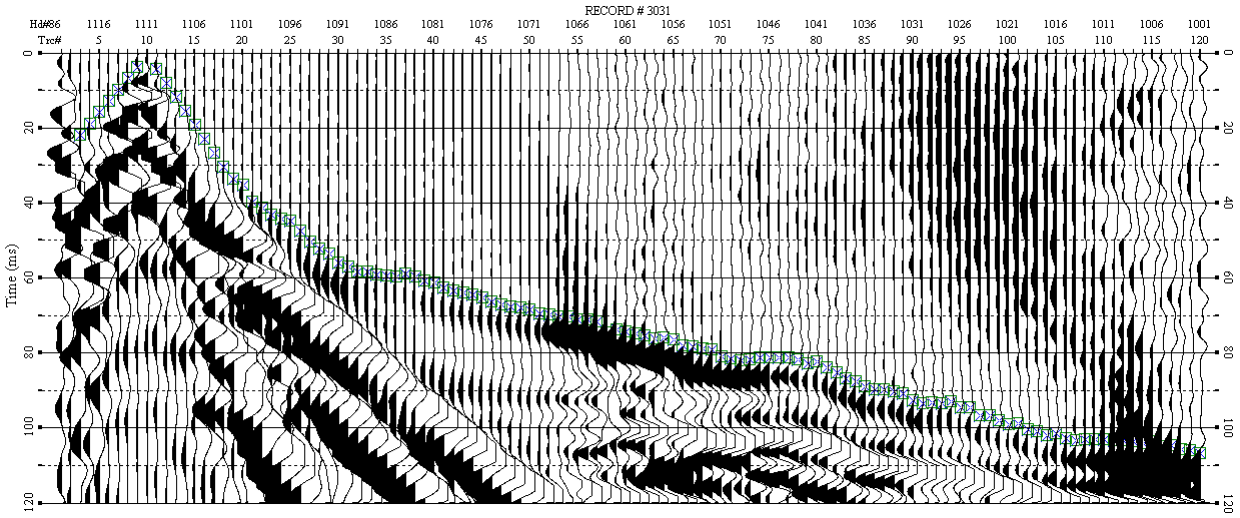

Figure 44. Estimation of first-arrivals times on a P-wave seismic data with source located at station 1111 (horizontal coordinate at 3333 ft).

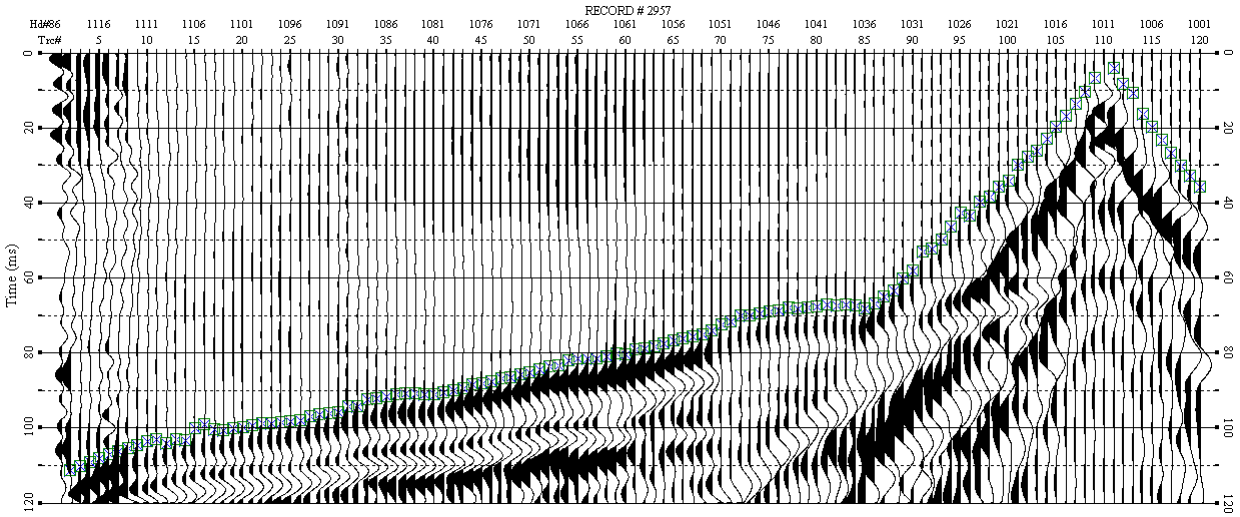

Figure 45. Estimation of first-arrivals times on a P-wave seismic data with source located at station 1011 (horizontal coordinate at 3033 ft).

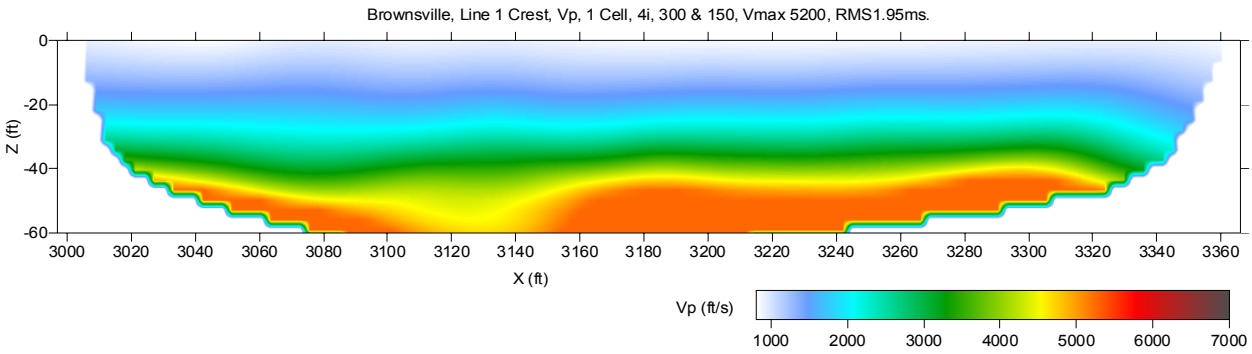

Figure 46. P-wave velocity model estimated for line 1 by analyzing P-wave-data first-arrival times using refraction-tomography software.

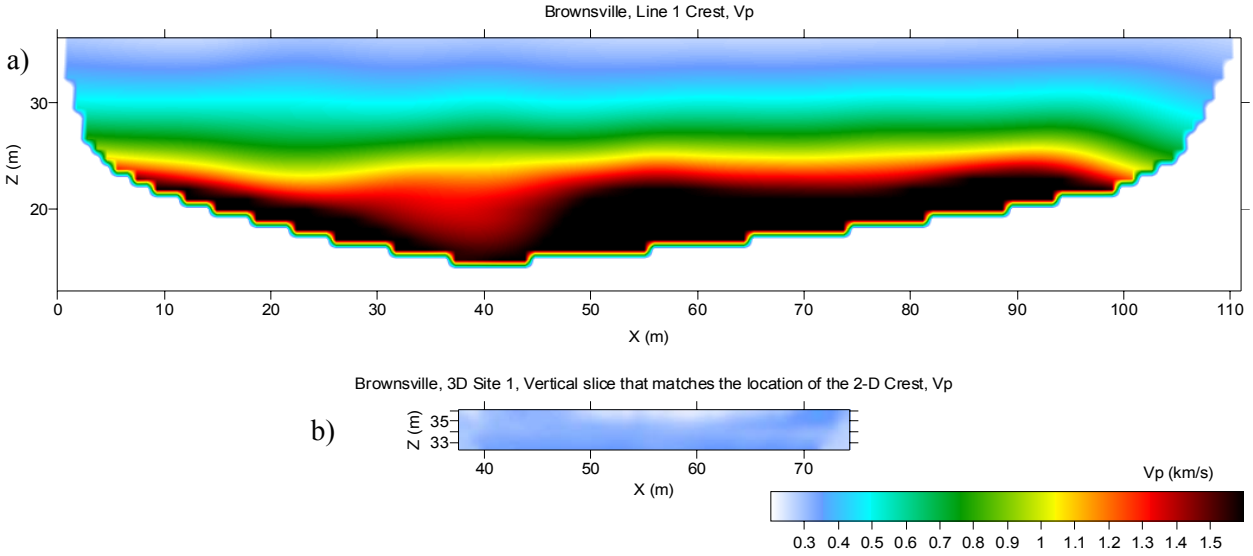

Figure 47. a) P-wave velocity model estimated for line 1 by analyzing P-wave-data first-arrival times using refraction-tomography software compared to b) a vertical slice from a 3-D P-wave velocity model estimated by analyzing 3-D through-levee P-wave-data first-arrival times using tomography software.

S-wave First Arrivals

S-wave first-arrivals were picked from data acquired along the crest site. Overall the first arrivals appeared a bit more irregular in wavelet character than observed on equivalent compressional-wave energy (Figure 48). As with the P-wave first-arrival pattern, when viewed as a function of source offset, the S-wave velocity structure appears to also support the interpretation that there are two unique velocity layers in the upper 10s of feet at site 1. However, unlike the equivalent compressional-wave data, the two different first-arrival slopes interpreted on the shear-wave data are not as pronounced with respect to consistent slope, clear cross-over, and trace-to-trace uniformity in arrivals. As expected with the slower shear velocities in the levee, the apparent shallower velocity is present on and interpreted from fewer traces within the near-offset range. As well, the velocity contrast between the two layers is relatively small so the change in slope representative of each layer's phase velocity is very subtle (Figure 48). Considering the apparent difference in the P- and S-wave first-arrival velocity trends, it would not be unexpected to have solutions for the two types of waves that were significantly different.

After picking the first-arrival times from the S-wave data shot gathers collected along the crest of the levee, a 2-D refraction-tomography Vs solution was obtained (Figure 49). In general, there is a wide range of equally possible solutions to the inverse refraction/tomography problem due to the

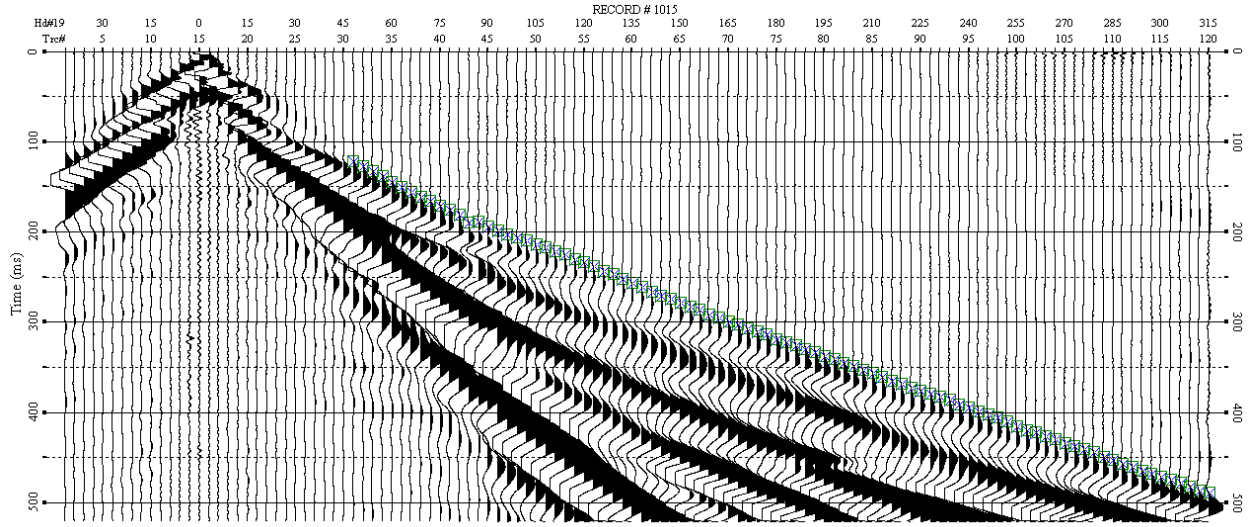

Figure 48. Estimation of first-arrivals times on an S-wave seismic data with source located at station 1111 (horizontal coordinate at 3333 ft).

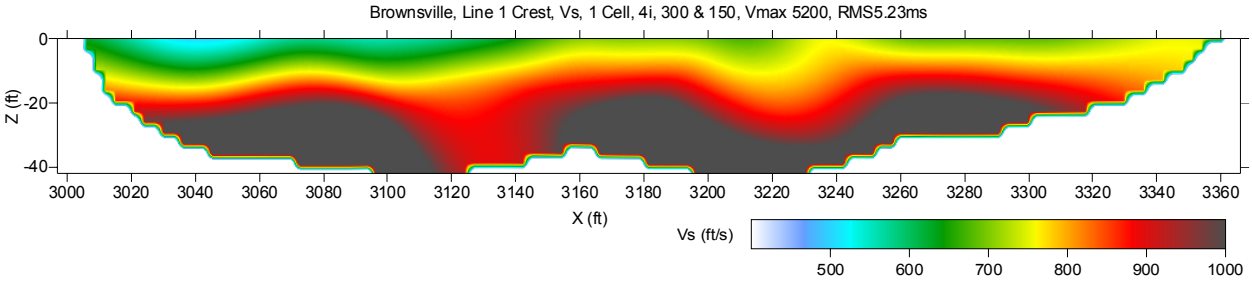

Figure 49. S-wave velocity model estimated for line 1 by analyzing S-wave-data first-arrival times using refraction-tomography software.

nonuniqueness of geophysical analysis. In addition, for the case of S-wave data, the nonuniqueness problem can be exacerbated due to the possibility of P-S wave conversions. In light of this mode conversion problem, the MASW method was preferred over the S-wave refraction/tomography analysis for estimating the Vs structure within the levee.

Rayleigh Wave

Two different methods were used to acquire and process Rayleigh-wave energy. Impulsive data were used for MASW analysis and sweep or variable frequency data were used for phase analysis. Comparisons of land-streamer data with traditional geophone coupling included comparisons of both body waves and surface waves. Surface-wave analysis of these comparative data sets was focused on dispersive data characteristics. Rayleigh-wave MASW analysis included two steps: estimation of dispersion curve, and inversion to shear velocity profile. The shear-wave velocity profile represents the geologically useful component of this analysis and therefore it was the primary emphasis of the processing and interpretations.

MASW Method Optimization at the Levee Crest

Dispersion-curve overtone analysis was used to optimize the picking of receiver-spread parameters that provide the best opportunity for recording the maximum frequency range of the surface-wave fundamental mode. Initially, all recorded traces from a fixed-spread shot gather were used to calculate the dispersion curve, thereby allowing a general idea of the dispersive character of the surface wave at this

particular site (Figure 50). The fundamental-mode energy ranges from 5 to 15 Hz at associated phase velocities from 650 to 500 ft/s. These surface-wave fundamental-mode energy characteristics were used to design the acquisition parameters and refine the dispersion-curve selection process. Two higher mode events were observed in the frequency range from 13 to 35 Hz and at velocities between 1300 to 600 ft/s (lower frequencies are sampling greater depths and therefore have higher velocities associated with them). Lower-amplitude higher-mode energy can be interpreted beyond 30 Hz and at phase velocities around 1000 ft/s. All higher-mode energy is considered noise for MASW analysis, which is designed to process fundamental-mode energy only.

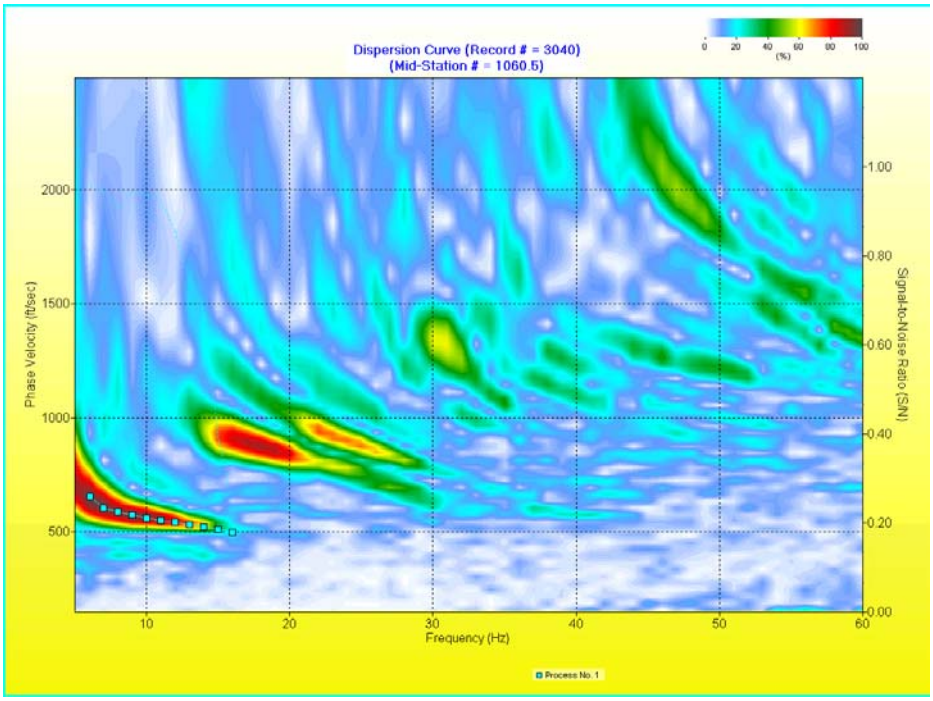

Figure 50. Dispersion-curve analysis of P-wave-data surface-wave using all 120 traces from shot record 3040.

To maximize the lateral resolution of the processed data the recording spread needs to be as short as possible and still provide adequate quality of the fundamental-mode dispersion-curve picking. Analysis of the first ten traces (Figure 51) demonstrates how a lack of far-offset traces does not allow the separation of fundamental and higher modes. This shorter spread also inhibits confident picking of fundamental-mode energy in the low-frequency range because these lower frequencies will not fully develop within the very near-offset ranges. With this short spread, close-offset data set, the fundamental and higher modes all interfere to form one dispersion curve that appears to possess a reverse trend (velocities increase with frequency).

Improvement in the separation between fundamental and higher modes is evident and identification of fundamental-mode dispersion properties at frequencies as low as about 7 Hz is possible when analysis includes the first twenty traces of the fixed spread (Figure 52). When analysis included the first forty traces (Figure 53), the high quality data were sufficient for fundamental-mode analysis of frequency as low as 4 Hz. Still troubling is the apparent lack of high frequencies in the fundamental-mode dispersion curve. The highest possible fundamental-mode frequencies identifiable on dispersion curves are between 13 and 18 Hz.

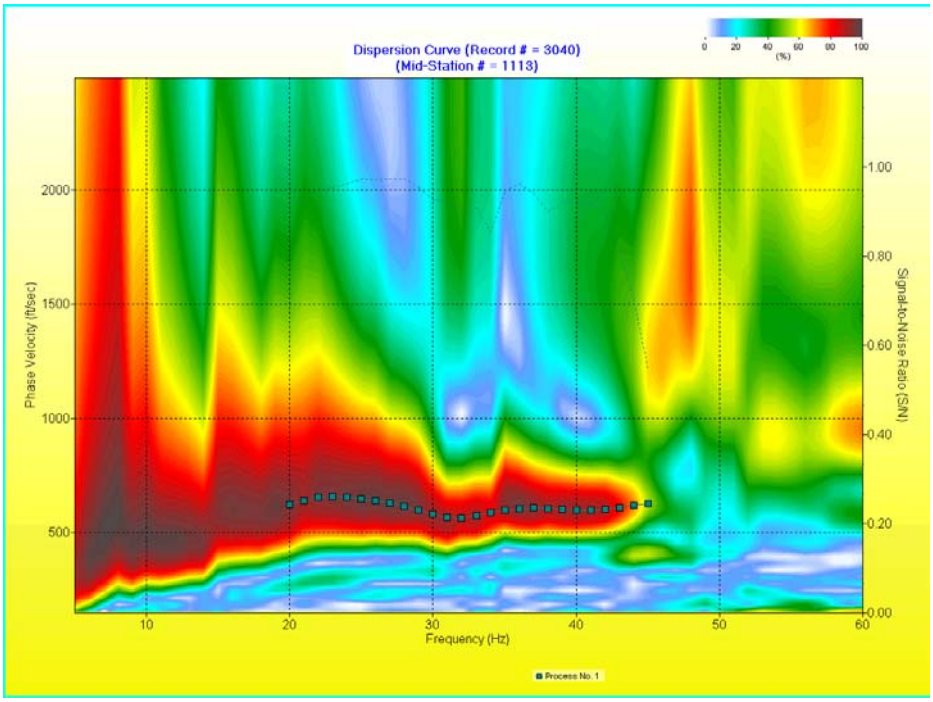

Figure 51. Dispersion-curve analysis of P-wave-data surface-wave using the first 10 traces from shot record 3040.

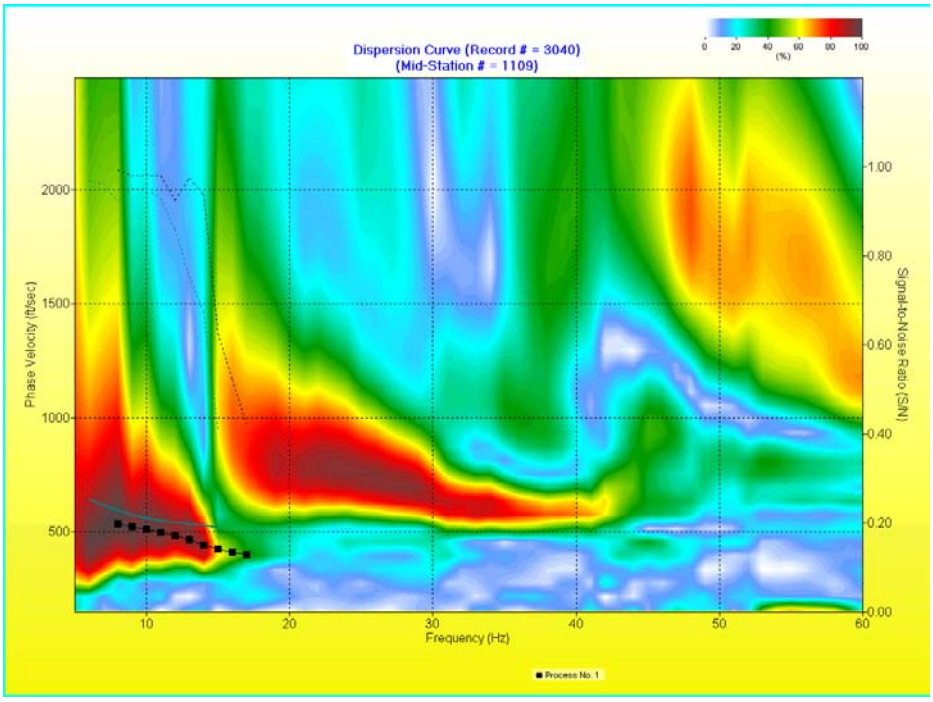

Figure 52. Dispersion-curve analysis of P-wave-data surface-wave using the first 20 traces from shot record 3040.

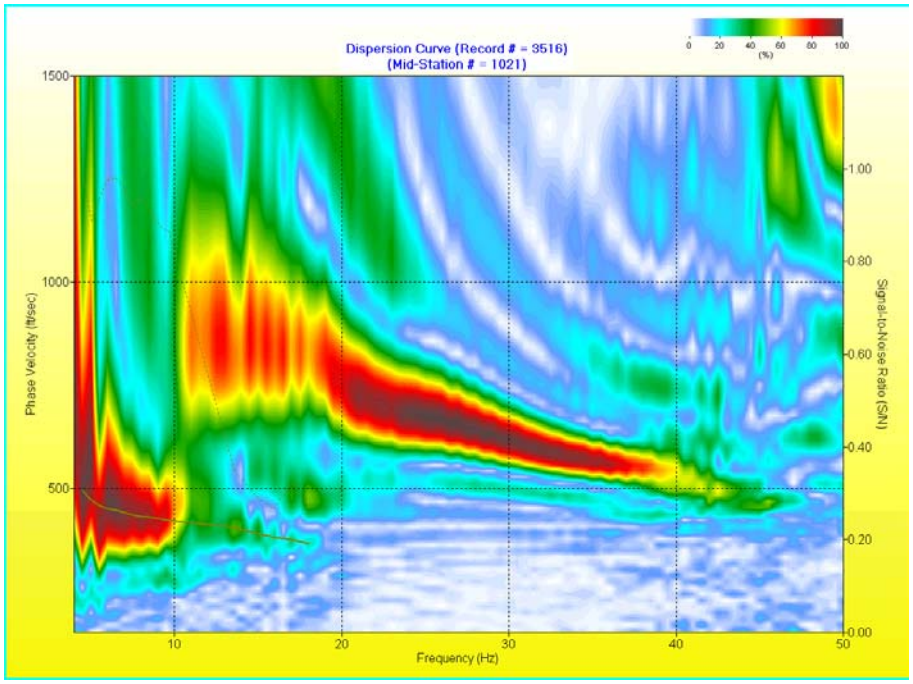

Figure 53. Dispersion-curve analysis of P-wave-data surface-wave using the first 40 traces from shot record 3040.

Using the first 40 traces and focusing spectral improvement on processing provided little in the way of significant improvements to the fundamental-mode dispersion events. Two different types of higher-mode filters were applied in an attempt to isolate any fundamental mode energy above 20 Hz (Figures 54 and 55). There appears to be no fundamental-mode energy propagating in the levee itself above 20 Hz. Energy observed on dwell experiments using the vibrator is all higher-mode energy.

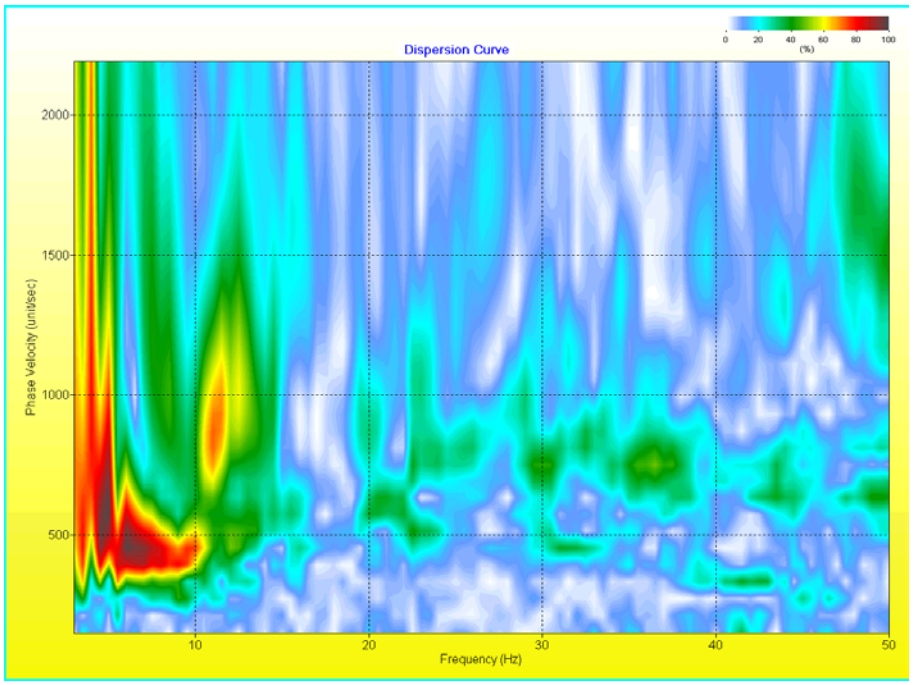

Figure 54. Dispersion-curve analysis of P-wave-data surface-wave using the first 40 traces from shot record 3040 after filtering the first higher mode (with interpolation).

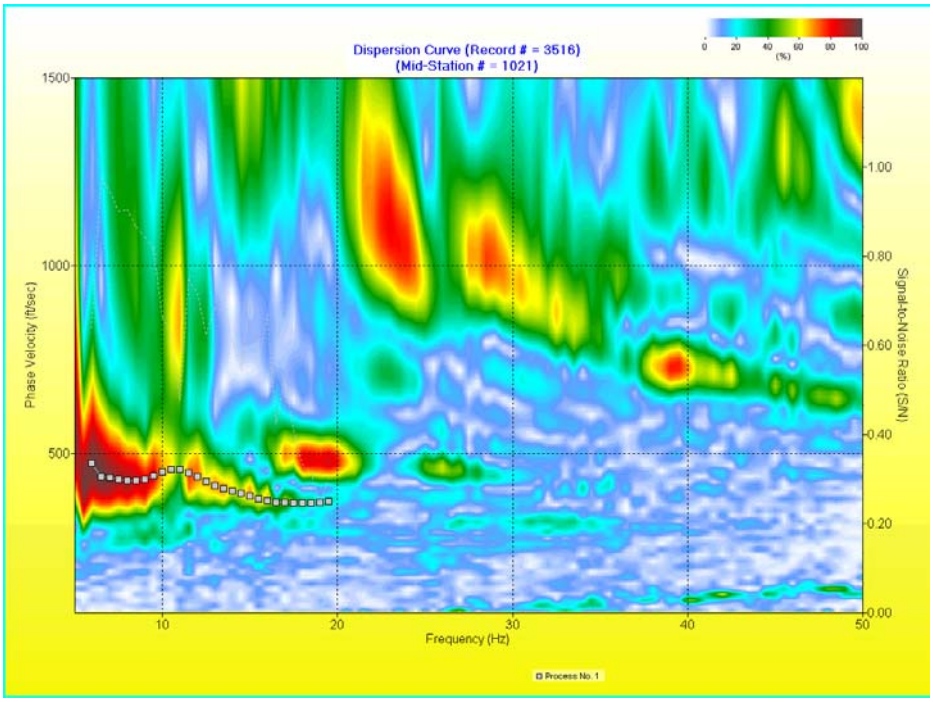

Figure 55. Dispersion-curve analysis of P-wave-data surface-wave using the first 40 traces from shot record 3040 after filtering the first higher mode (with no interpolation).

Too many traces included in fundamental-mode surface-wave analysis can result in frequency degradation and increased sample smearing of higher-frequency components of the surface-wave energy packet. An optimum number of traces should be determined based on uniformity of spectral properties across the entire proposed spread. A shot gather spectra from this site demonstrates the offset dependent nature of these seismic data (Figure 56). It is obvious that no significant energy exists above 20 Hz beyond trace 60. Thus, the largest usable spread to consider including in an image of the levee from the crest would include traces from 1 to 60.

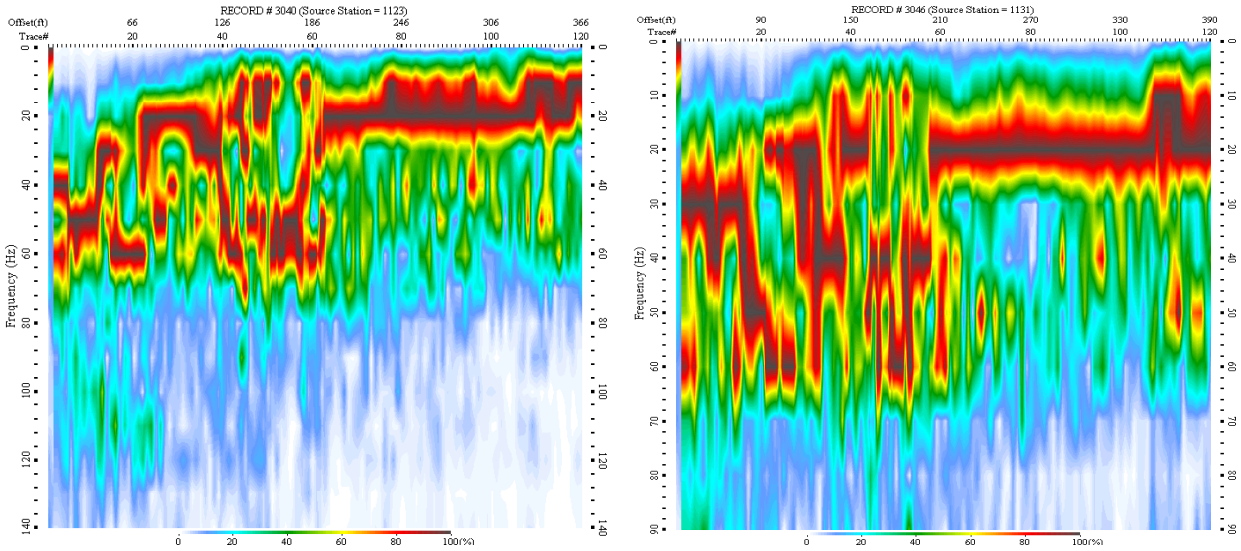

Figure 56. Amplitude spectral display of shot records 3040 and 3048.

MASW Vs Results

Even though no surface-wave fundamental mode energy above 20 Hz was recorded (and therefore no shallow Vs information, specifically no shear-wave velocity information was obtained that was isolated to the levee itself), the MASW method still provided an accurate overall estimation of the Vs from the crest to depths of between 25 ft and 70 ft below the crest of the levee (Figure 57). Even though changes in materials properties affecting velocity within the levee are not specifically sampled, lateral changes observed in lower frequency and therefore deeper penetrating energy could have remnant contributions from intra-levee properties.

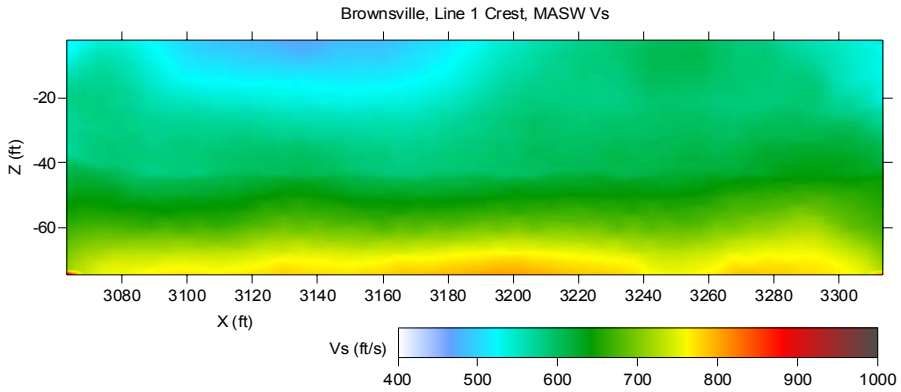

Figure 57. S-wave velocity model estimated for line 1 by analyzing P-wave-data surface-wave using MASW method.

Vibrator Dwell from Levee Crest

Frequency dwell experiments were run using a seismic vibrator to study resonance or phase abnormalities within the levees, possibly indicative of material property changes. Constant-frequency sweeps were recorded using the entire spread, allowing changes in phase velocity of the surface wave as a function of location to be studied. In particular, observations concerning interference and changes in phase velocity for the fixed-frequency energy were the primary target. Since surface-wave phase velocity is frequency dependent, any change in phase velocity for the selected frequency can be related to changes in material properties within an estimated depth range (which is dependent on the wavelength of the particular frequency of surface wave being produced). A combination of t-x and f-x analysis allowed any variations in the key seismic attributes of the surface waves to be identified.

More than 70% of all seismic energy is surface waves, therefore driving the ground with seismic energy at specific frequencies is an easy way to estimate sections of levee with laterally, and to a lesser degree vertically, inconsistent material composition. Unfortunately, in order to correlate surface-wave frequency with depth the surface-wave energy must be fundamental mode. Even using the high-energy vibrator, no fundamental-mode surface-wave energy above 20 Hz was observed on raw or processed shot gathers (Figure 58). This lack in higher frequency fundamental-mode surface-waves was a characteristic of all these sites. Of some interest was the much more chaotic and discontinuous nature observed on frequency dwell data at site 2 relative to the other sites. This phenomenon will be discussed in the section for site 2.

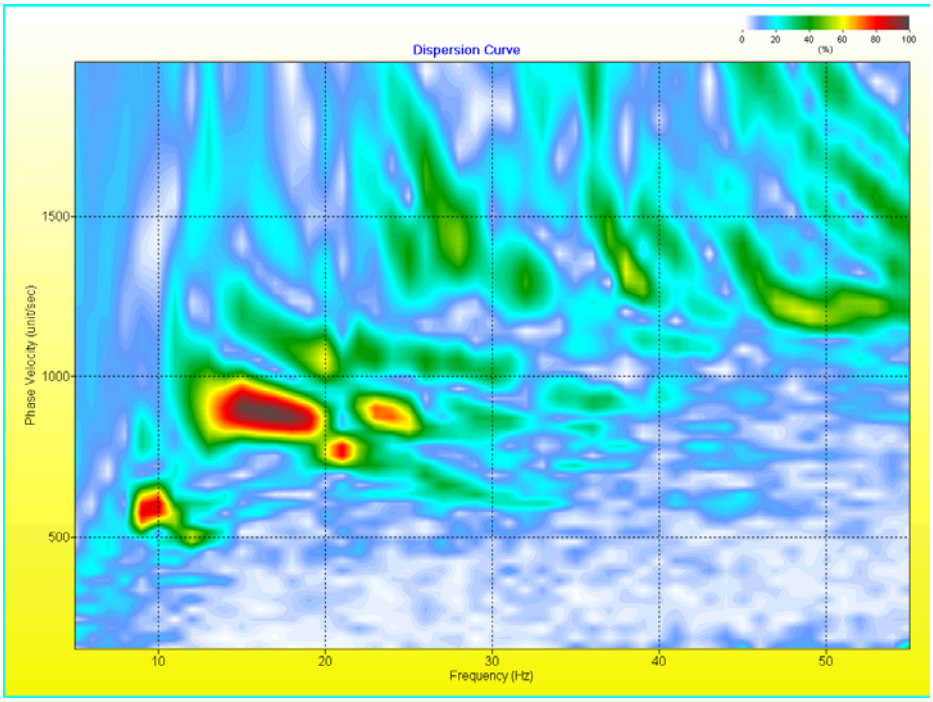

Figure 58. Dispersion-curve analysis of P-wave 10-100 Hz sweep vibrator-data surface wave using all traces from a shot.

Through-levee Tomography

First-arrival processing and analysis relies heavily on direct ray propagation paths between source and receiver and that the first-arriving energy at a receiver is primary, first order, non-mode-converted energy clearly distinguishable from any later arriving modes. For the 3-D through-levee tomography, at some stations refracted or mode-converted energy appears as the first arrival on a seismic trace. In these cases, the direct energy trails the refracted or mode-converted first arrival and with careful wavelet matching can be identified and selected for travel time analysis. This kind of meticulous and detailed trace-by-trace processing requires exorbitant amounts of time**.**

For the 3-D tomography, the geometry and overall dimensions of the levees significantly complicate event identification and analysis. With a low-velocity shell, medium-velocity core, and high-velocity base, a refracted source-receiver travel path was many times faster than direct or curved ray paths. As well, each of these interfaces represent an ideal source of mode-converted energy, and for shear through-levee tomography this becomes a significant hindrance to confident direct-ray identification. This complication is significant enough that several of the tomography analysis techniques will not provide accurate subsurface models or reliably converge on a high-confidence subsurface velocity model for levees of this type.

Visualization of tomographic images is best viewed in 3-D; however, with the source and receiver geometry deployed along the levees the most meaningful images come from 2-D slices, both longitudinal and transverse to the levee axis. Comparisons between through-levee 3-D velocity volumes and 2-D slices along the crest provide independent cross-checking of the general range of values and some level of precision possible with seismic type techniques. Considering the extreme geometry and potential for out-of-the-plane arrivals, some meaningful results can be deduced based purely on data quality.

P-wave 3-D Through-levee Tomography

Identification of P-wave Direct Arrivals

Most of the actual first-arrivals did not appear to have traveled a direct path through the levee. For example, first-arrival times for shots along the lowest-shot line on the levee face (closest to the toe of the levee) all had arrival times at the 120 lowest receivers in the spread (120 closest to the toe) within 6 ms of each other and a short travel time of 60 ms (Figure 59). Considering that the source-to-receiver-offset distance range was 22 to 38 m, if a straight line raypath was followed these first arrivals suggest a 40% change in velocity from one end of the spread to the other. This becomes even more unrealistic when the reverse shot depicts the same change in velocity with offset when assuming a straight-ray propagation path through the levee. All things considered, first arrivals from source and receiver locations near the toe are likely refractions from the basal contact. The velocity vs. offset trend is consistent with the suggestion that the first arrivals are refracted arrivals (Figure 60). The standard deviation of this data set is 52.23 m/s, reflecting the wide range of velocity values. The travel-time velocity is proportionally linearly dependent on the distance from the source, which is unlikely due to geology for a straight raypath model. More likely the first-arrivals are refracted energy.

Moving to greater time, the next set of arrivals have a time-offset relationship that is much more consistent with what would be considered a realistic direct-travelpath scenario for this site (Figure 59). Travel-time curvature of the second coherent event is consistent with the variable offset between the source and receivers. A travel-time velocity vs. distance relationship for the second coherent event contains velocity values that span a significantly smaller range, making them much more realistic candidates for direct waves (Figure 61). The standard deviation of this data set is 11.23 m/s and the velocity appears much less offset dependent. However, consistently picking the same wavelet and phase arrivals for an event from within the wavefield (that is, not the first arrival) is extremely difficult due to interference from all the other modes and coherent energy arriving at a receiver from a variety different travel paths.

Reversing the polarity of the data set greatly increases the confidence in picks of the initial onset of the direct traveling wave (Figure 62). Because the polarity is reversed, some adjustment was necessary to compensate for picks that were now being made on the second lobe of the direct-arriving wavelet.

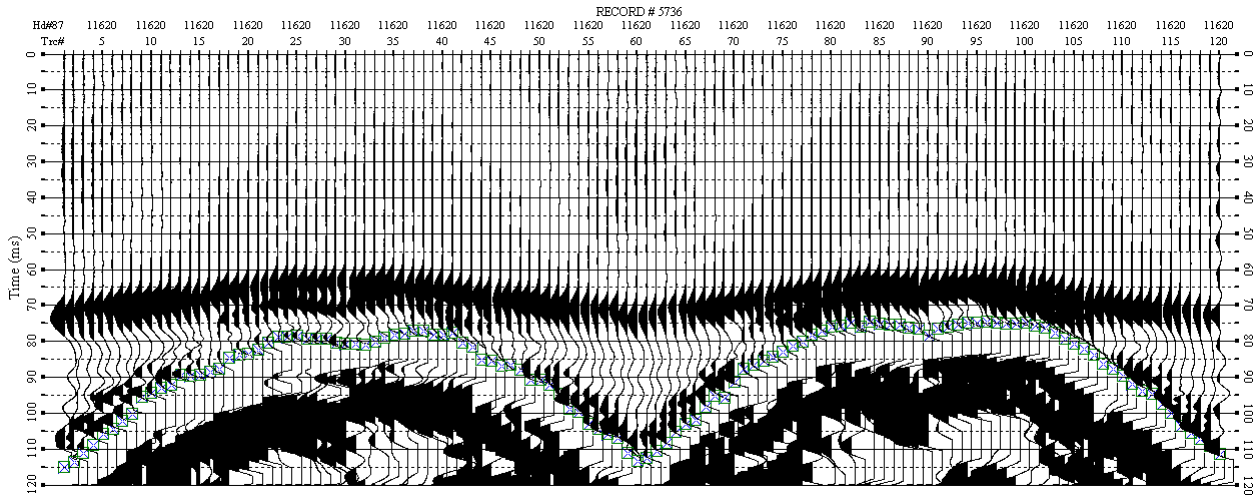

Figure 59. Estimation of first-arrival and secondary-arrival times on 3-D P-wave through-levee seismic data with source and receivers located at lowest altitude (closest to the toe), shot record 5736.

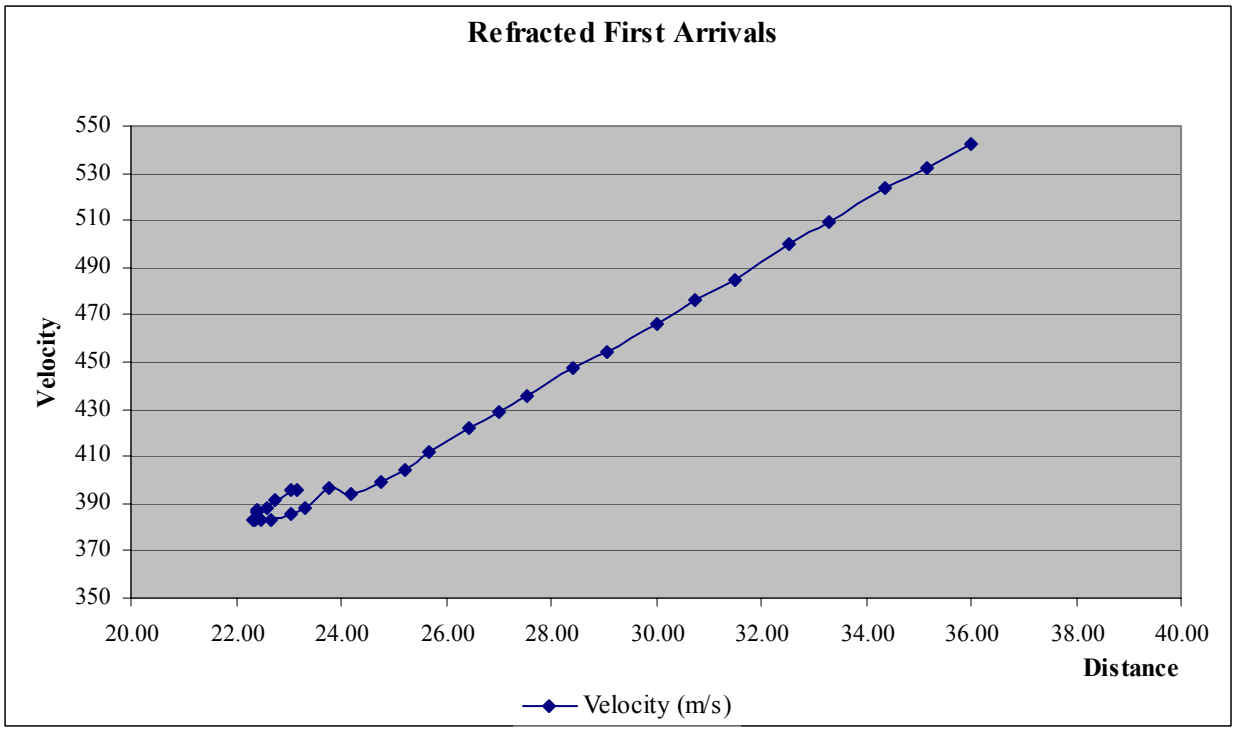

Figure 60. Through-levee first-arrival average velocity analysis versus distance.

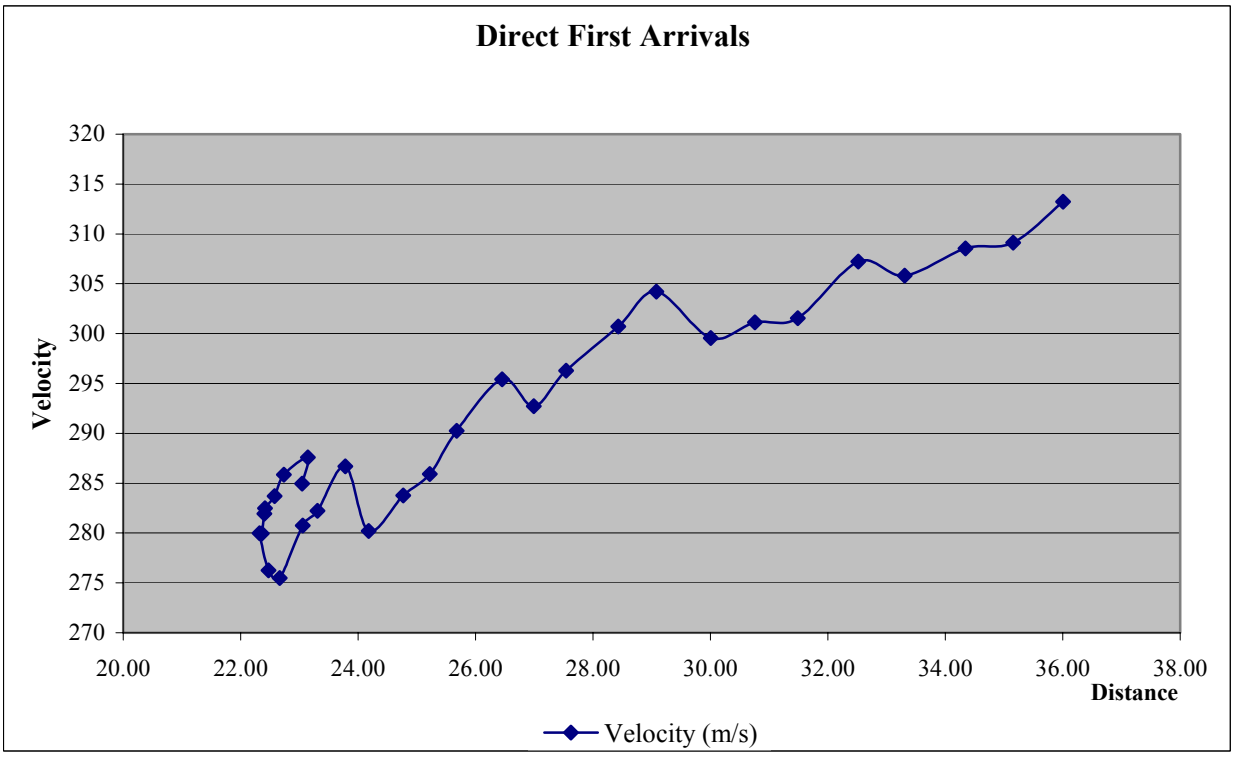

Figure 61. Through-levee secondary-arrival average velocity analysis versus distance.

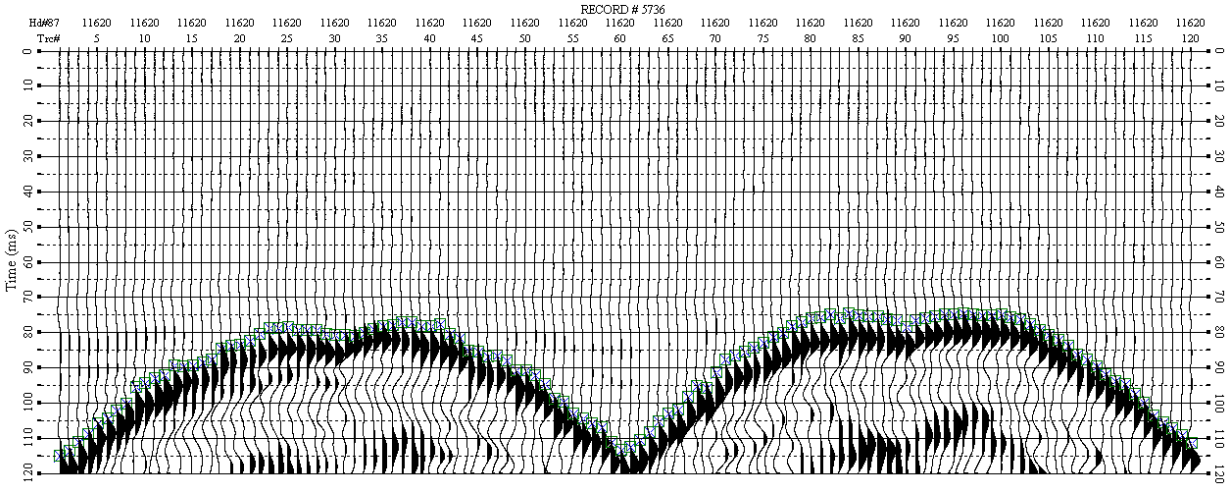

Figure 62. Estimation of direct-wave arrival times after reversing polarity of 3-D P-wave through-levee seismic data with source and receivers located at lowest altitude (closest to the toe), shot record 5736.

Shot gathers with source and receiver locations near the top of the levee possessed first-arrival patterns consistent with traveltime and velocity curves observed in the direct-wave arrivals interpreted from source and receiver stations near the toe of the levee, which, as mentioned earlier, arrived later in the wavetrain (Figure 63). Even with the source and receivers at the very top of the levee, direct-wave energy was not the first arrival on all traces. Refracted energy was again the source of the interference forcing the direct wave into a later position in the wavetrain. As with shot and receiver stations from near the bottom of the levee, it was easier to use the positive amplitude of the seismic wavelet and therefore polarity reversal was necessary (Figure 64). As a result, picking the zero crossing 180° out of phase from the actual onset of direct-wave energy, a constant 11 ms was calculated to be the difference between the actual direct through-levee arrival (negative amplitude) and the picked positive amplitudes. Therefore, after all the first arrivals were picked on polarity-reversed traces, 11 ms was subtracted from the interpreted first-arrival time.

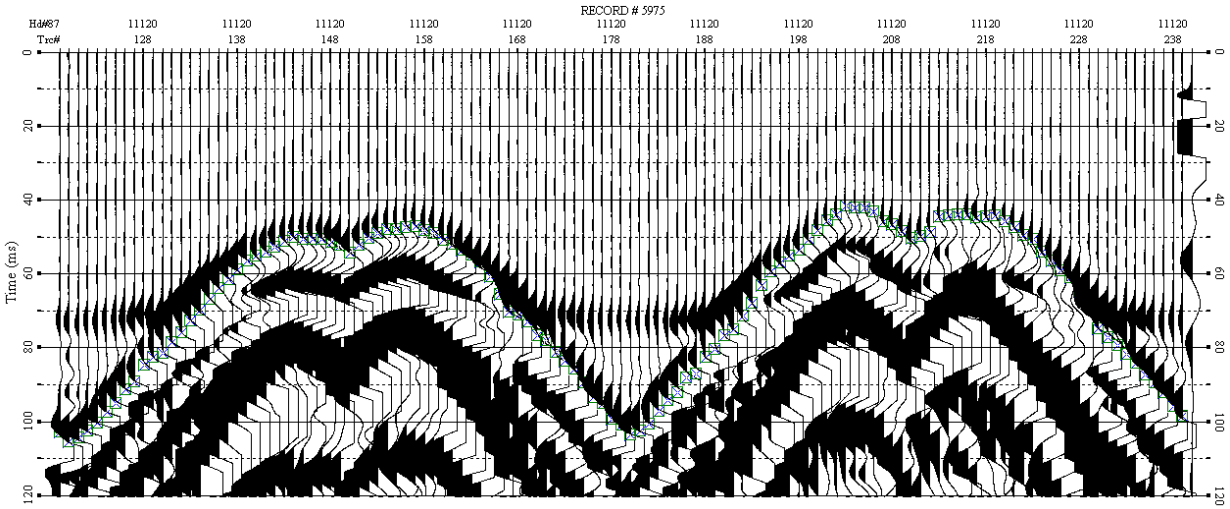

Figure 63. Estimation of direct-wave arrival times of 3-D P-wave through-levee seismic data with source and receivers located at highest altitude (near the top of the levee), shot record 5975.

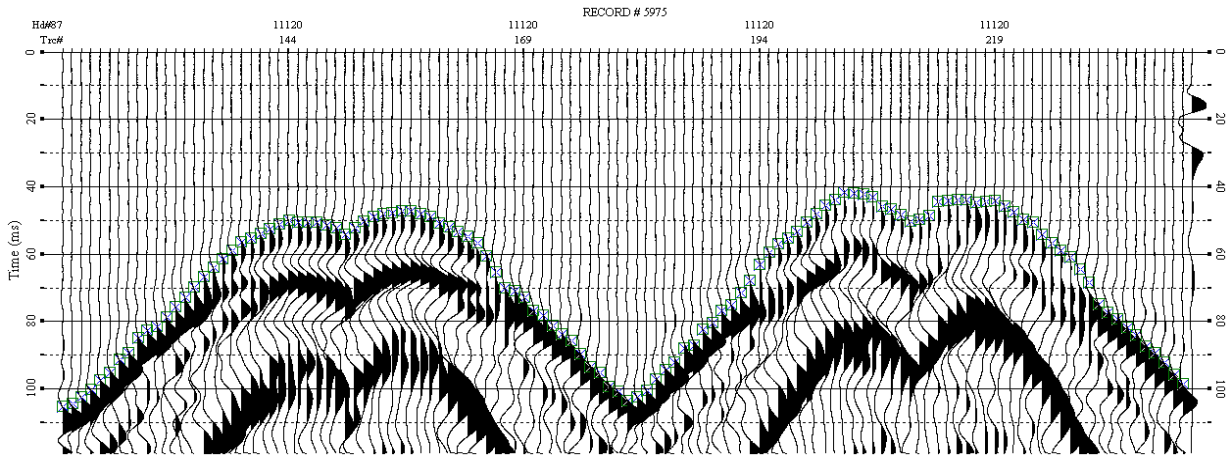

Figure 64. Estimation of direct-wave arrival times after reversing polarity of 3-D P-wave through-levee seismic data with source and receivers located at highest altitude (near the top of the levee), shot record 5975.

Inversion Results

All the data arrival times are plotted for quality control as a function of source-receiver separation (Figure 65a) and as a function of processing order supplied to the software (Figure 65b). Arrival times are clustered along a linear trend that represents the average velocity through the levee. Areas where the clusters of first arrivals deviate from the straight-line plot represent the range of velocities at a particular offset. Considering these scatter plots are not location dependent it is not possible to isolate areas with anomalous velocity zones, but areas with increased ranges of velocity for particular offsets and increased densities of first-arrival times at particular offsets are all related to the non-uniformity of the levee core.

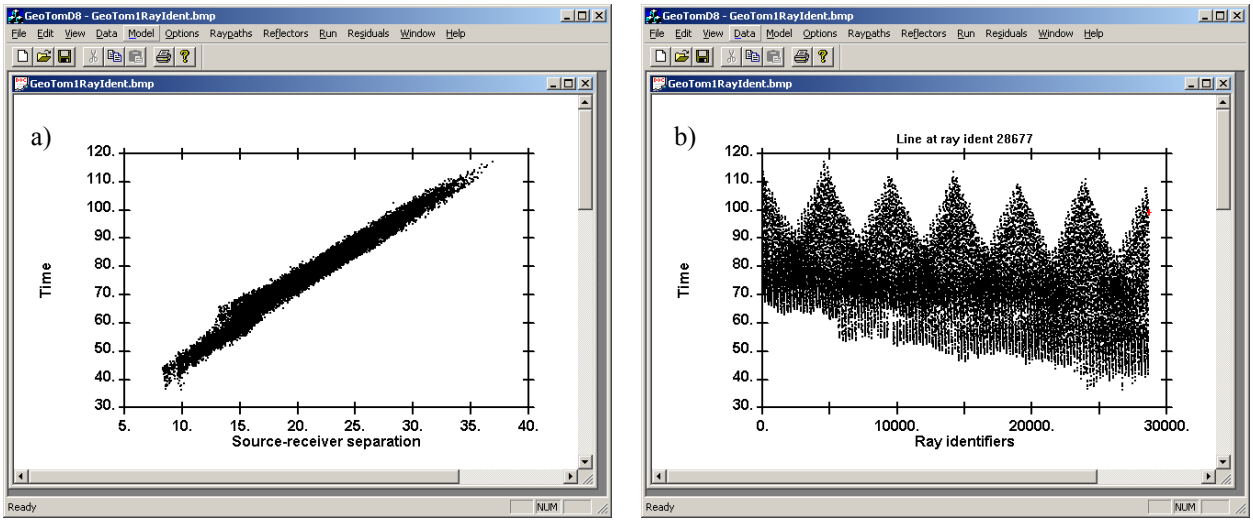

Figure 65. a) Plot of 3-D P-wave through-levee direct-wave arrival times versus source-receiver separation. b) Plot of 3-D P-wave through-levee direct-wave arrival times versus software order.

First-arrival time-offset pairs were inverted using *GeoTomCG* software with a residual RMS of 2.02 ms. The 3-D solution is presented using horizontal slices at elevation levels 32.29 m (Figure 66a), 33.05 m (Figure 66b), 33.81 m (Figure 66c), 34.57 m (Figure 66d), 35.32 m (Figure 66e), and 36.09 m (Figure 66f). A vertical slice along the levee volume was extracted (Figure 67) as noted by white circles (Figure 66f). The residuals from every raypath are plotted for quality control (Figure 68). An additional vertical slice was plotted that is consistent with the relative location of the 2-D MASW and refraction seismic lines (Figure 69).

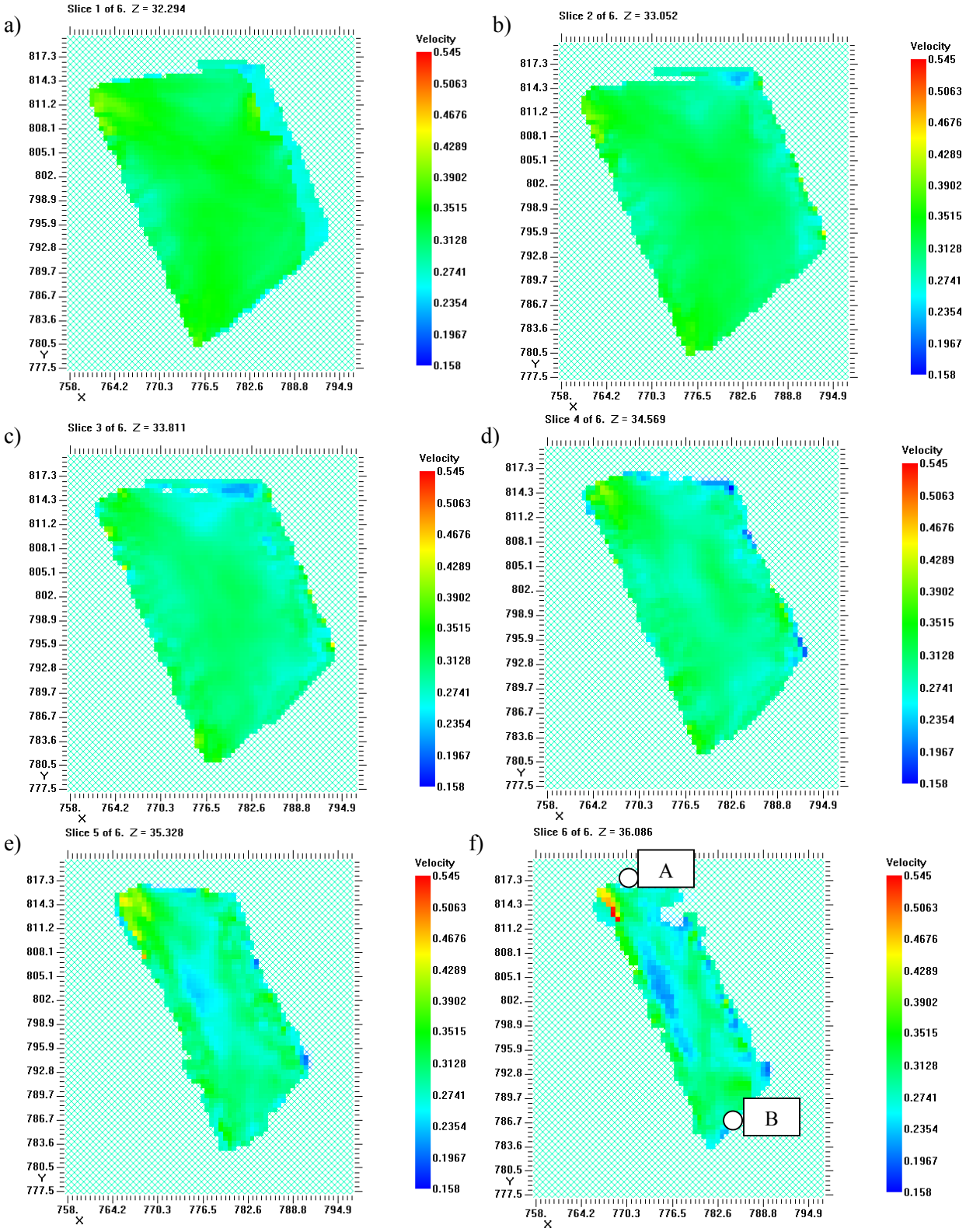

Figure 66. Horizontal slices extracted from the 3-D P-wave velocity volume obtained from inverting direct-wave arrivals. a) horizontal slice at elevation 32.29 m, b) horizontal slice at elevation 33.05 m, c) horizontal slice at elevation 33.81 m, d) horizontal slice at elevation 34.57 m, e) horizontal slice at elevation 35.32 m, and f) horizontal slice at elevation 36.09 m (A–B indicates position of vertical slice that was extracted).

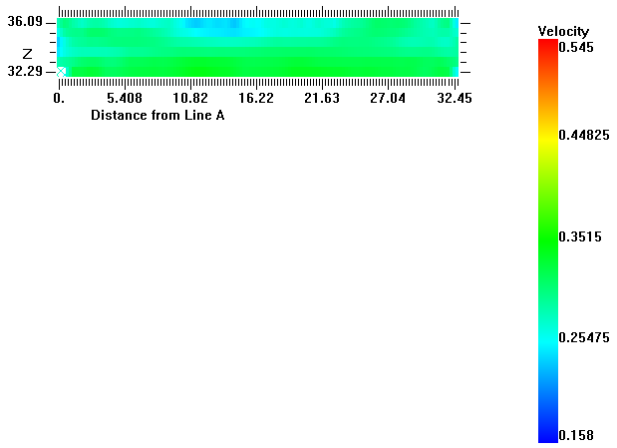

Figure 67. A vertical slice extracted from the 3-D P-wave velocity volume obtained from inverting direct-wave arrivals, coincident with the location of the 2-D P-wave seismic line.

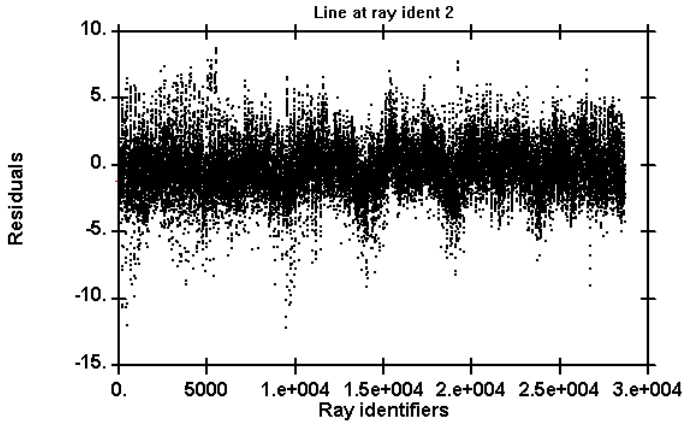

Figure 68. Residual error plot for all rays involved in the inversion. The sum of the residual errors is –4920 ms and the total RMS error is 2.02 ms.

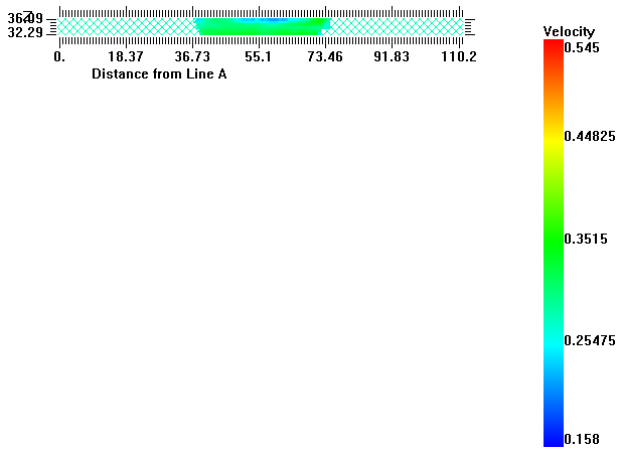

Figure 69. A vertical slice extracted from the 3-D P-wave velocity volume obtained from inverting direct-wave arrivals, compared with the extent of the 2-D P-wave seismic line.

S-wave 3-D Through-levee First-arrival Analysis

Identification of the Direct-wave Arrivals

In general the S-wave first arrivals should provide a picture of the subsurface that, in general, is consistent with that observed from P-wave first arrivals. Careful analysis and comparisons of the first-arrival wavelets proved beneficial for the P-wave through-levee tomography, so the same rigorous process was used for the S-wave data set. Adding to the complications resulting from refraction first arrivals on the P-wave data for S-wave data, the problems of mode conversions play a prominent role. Realistic velocities of shear-wave energy must be determined prior to trying to identify different arrivals on this kind of a shot gather. Because it is unlikely the direct S-wave will be the first arrival, problems similar to those encountered identifying direct energy on the P-wave through-levee shot gathers from the lower tier of receivers will be prevalent on all data.

For consistency and to minimize the number of variables in identifying direct shear energy, all analysis was completed on shot records where the source was located at station 610 (base of the slope, nearest the toe near the center of the grid). It is evident that there is a strong polarity, attenuation, or near-field problem that has left no consistency in the first-arriving wavelets along the top of the hyperbola that represents the closest receiver locations relative to the source (Figures 70 to 74). A lack of interpretable wavelets with consistent phase and amplitude characteristics at these close-offset receivers suggests a source problem (not generating sufficient shear energy with the appropriate polarity at close offsets) or a material characteristic (earth not conducive in the near-field to the production and propagation of shear-wave energy). This kind of a data characteristic would not be unexpected where a liquid or void was present with the appropriate dimensions and ratios. Another possibility is that the observed first-arrivals are refractions (from significantly faster underlying layers) instead of direct arrivals and closer offsets are less than the critical refracting offset distance.

If these longer-offset first arrivals are shear energy, they possess an apparent average velocity of about 300 m/s (1000 ft/s), which is much faster than the expected (200-300 ft/s). Velocities in this range are consistent with those observed on compressional-wave data sets. If these are near-receiver mode-converted waves, that would explain the apparent lack of arrivals at the nearest offset. These offsets would be only sensitive to energy polarized along the axis of the levee. Offsets further from the source will be at an angle relative to the axis and, due to orientation relative to the shear source, would be increasingly sensitive to compressional-wave energy with increasing angle from orthogonal relative to the source and levee axis.

Using the polarity sensitive nature of shear waves and the observations about energy recorded from non-orthogonal angles relative to the levee axis, arrivals immediate across the levee from the source are likely SH arrivals that have traveled through at least part of the levee. Using that assumption, the S-wave first-arrivals appear in the central part of each hyperbola, at about 80 ms, resulting in an average S-wave velocity of about 180 m/s (600 ft/s). This velocity is quite close to the MASW estimated shear velocity measured from the crest at depths from about 25 ft to 40 ft. Therefore, it is possible that the majority of the first-arriving shear-energy travel path was in that high-velocity zone.

Substantiating the suggestion that the greatest concentration of polarized shear arrivals are recorded at receivers in-line with the source relative to the levee axis can be accomplished by studying a record recorded with the source near the top of slope very near the crest and centered on the receiver grid (Figure 74). With the source location at station 310, the average velocity appears to be about 235 m/s (770 ft/s), which is still faster than the expected (200-300 ft/s), but not unreasonable for refracted energy traveling along the basal levee contact. As is clear with other through-levee data sets, wavelets arriving after the first arrival are strongly interfered with by the multitude of different types of energy and unique travelpaths that they follow between source and receiver. This also makes picking the true “direct arrival” from within the body of the wavetrain very speculative and inconsistent from record to record.

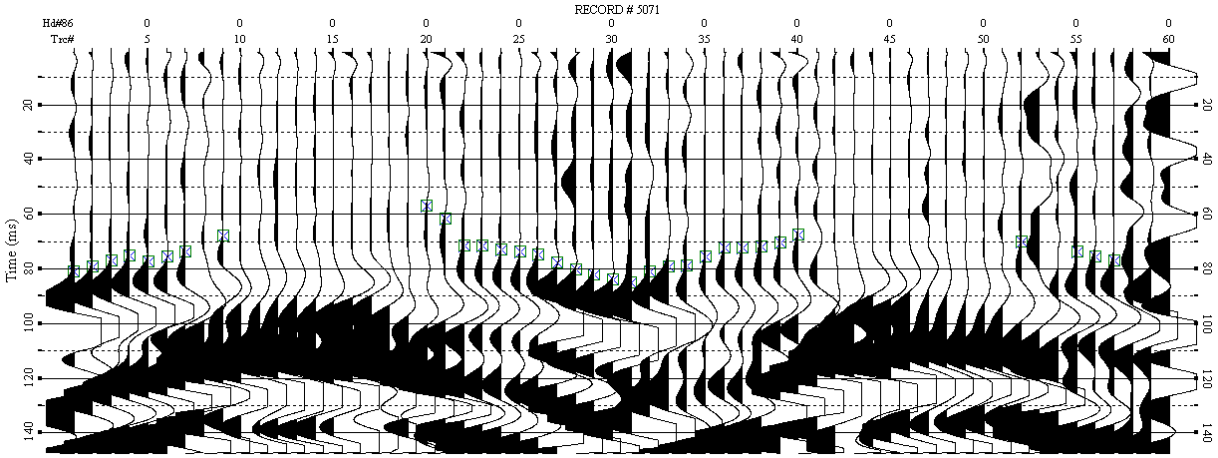

Figure 70. Estimation of first-arrival times on 3-D S-wave through-levee seismic data with source located at lowest altitude in the middle of the grid and receivers (from 0-60) located at the bottom two lines (closest to the toe) of the grid, shot record 5071.

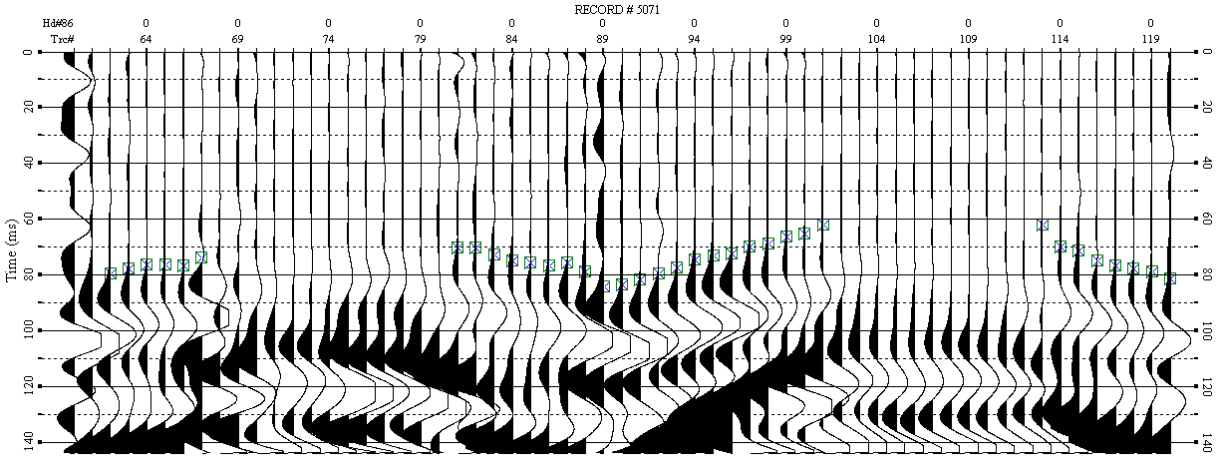

Figure 71. Estimation of first-arrival times on 3-D S-wave through-levee seismic data with source located at lowest altitude in the middle of the grid and receivers (from 61-120) located at two lines in the middle (closest to the toe) of the grid, shot record 5071.

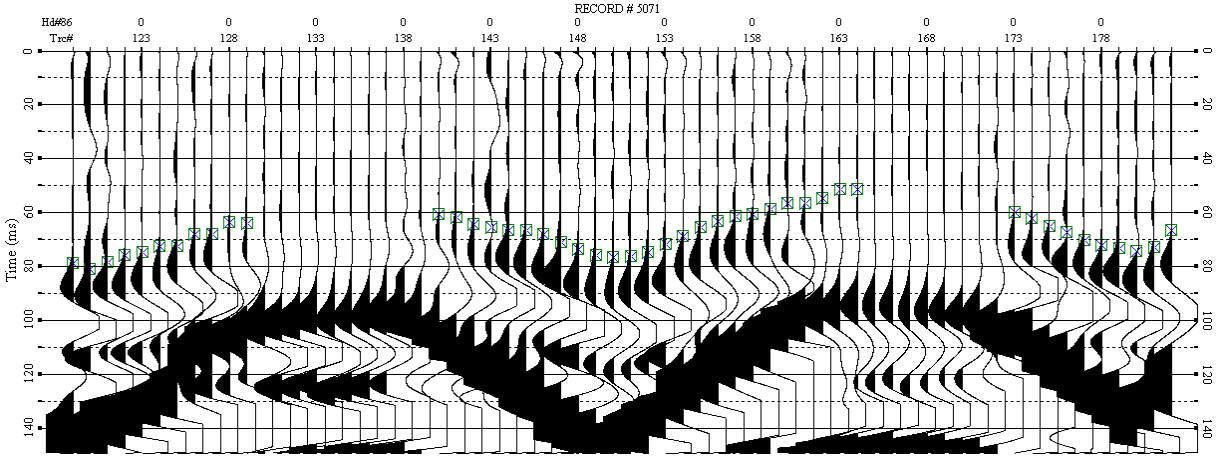

Figure 72. Estimation of first-arrival times on 3-D S-wave through-levee seismic data with source located at lowest altitude in the middle of the grid and receivers (from 121-180) located at two lines in the middle (closest to the top) of the grid, shot record 5071.

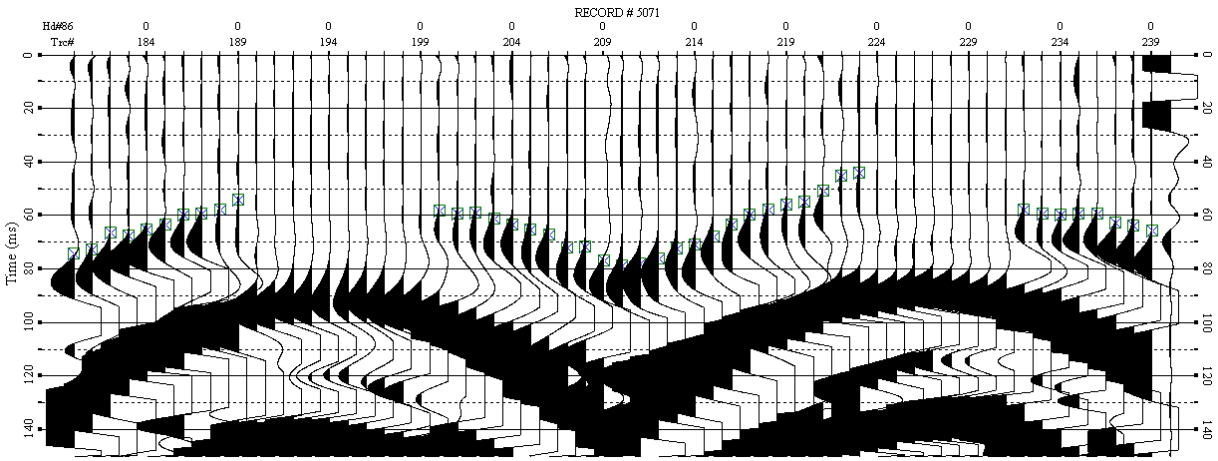

Figure 73. Estimation of first-arrival times on 3-D S-wave through-levee seismic data with source located at lowest altitude in the middle of the grid and receivers (from 180-240) located at the top two lines (closest to the top) of the grid, shot record 5071.

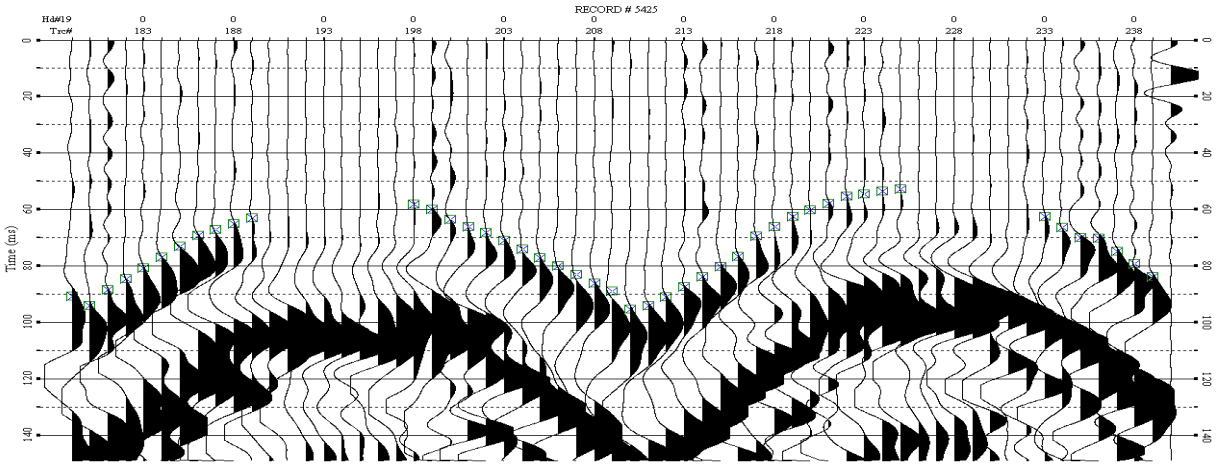

Figure 74. Estimation of first-arrival times on 3-D S-wave through-levee seismic data with source located at highest altitude in the middle of the grid and receivers (from 180-240) located at the top two lines (closest to the top) of the grid, shot record 5425.

P- and S-wave First-arrival Kinematic Comparison

A significant amount of effort was expelled trying to compare and relate direct arriving and first-arrival wavelets interpreted on P-wave data (p-wave source and geophones) with the first arrivals observed on the S-wave data. To minimize the number of variables for this multi-modal comparison, shot records studied all have the source located at station 610 (the bottom of the slope, near the toe and at the center of the grid) and the receiver locations are the same for all (Figures 75 and 76). First-arrival times on P-wave cross-levee tomography shots (Figures 75 and 76) are (within experimental error) identical to equivalent S-wave cross-levee tomography shots (Figures 73 and 74). This observation is consistent with one of the previous suggestions that the S-wave phones recorded converted energy or the angle away from orthogonal between source and receiver relative to the crest axis was sufficient that the S-wave source and S-wave oriented phones were generating and recording P-waves. The similarity between P- and S-wave first-arrival kinematic patterns is highly suggestive and enforces the current thinking that first arrivals on S-wave data should not be considered and analyzed as pure S-waves.

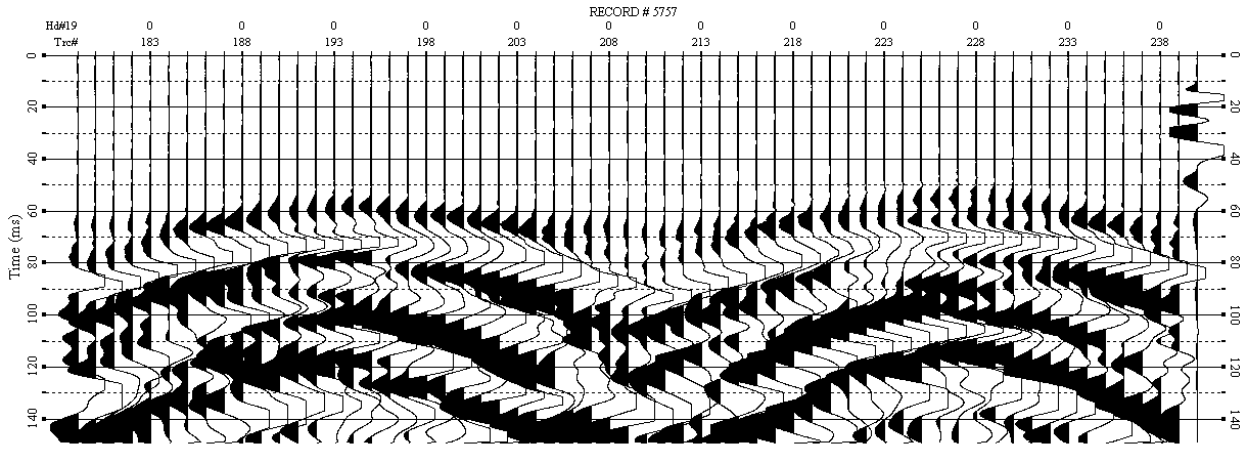

Figure 75. Estimation of first-arrival times on 3-D P-wave through-levee seismic data with source located at lowest altitude in the middle of the grid and receivers (from 180-240) located at the top two lines (closest to the top) of the grid, shot record 5757.

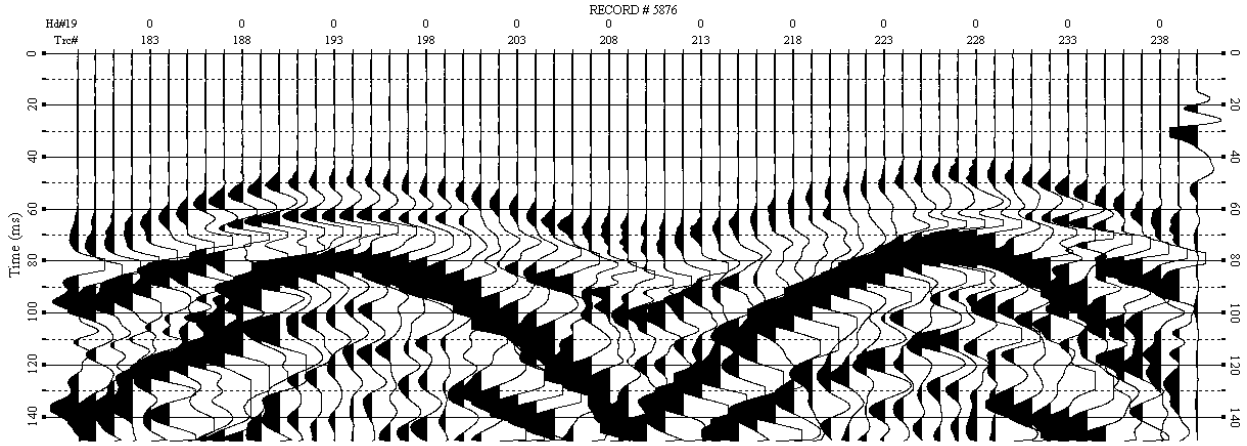

Figure 76. Estimation of first-arrival times on 3-D P-wave through-levee seismic data with source located at highest altitude in the middle of the grid and receivers (from 180-240) located at the top two lines (closest to the top) of the grid, shot record 5876.

S-wave Direct-raypath Search

Further study of S-wave data considered the possibility that other, non-first-arrival, energy arrival patterns could be the source of the observed S-wave first arrivals. The highest shot location (closest to the crest and at the center of the spread (station 310, Figure 77) was chosen as the spread geometry most likely to record shear-wave energy traveling directly from source to receiver; in effect, this geometry and these physical locations minimizes the possibility of recording refractions.

All the recorded wavelets examined had low dominant frequencies (15-20 Hz) and very limited bandwidth. These characteristics are consistent with the surface-wave energy observed on the recorded 2-D S-wave data at this same location (Figure 78). Picking consistent phase along a hyperbolic moveout pattern slow enough to be considered direct S-wave energy did not produce a velocity comparable with the distance divided by the direct arrival time. This inconsistency is suggestive of a propagation path that is not directly through the levee but either around the surface (such as a surface wave) or the result of multiple mode conversions and/or reflections/refractions from within the levee itself.

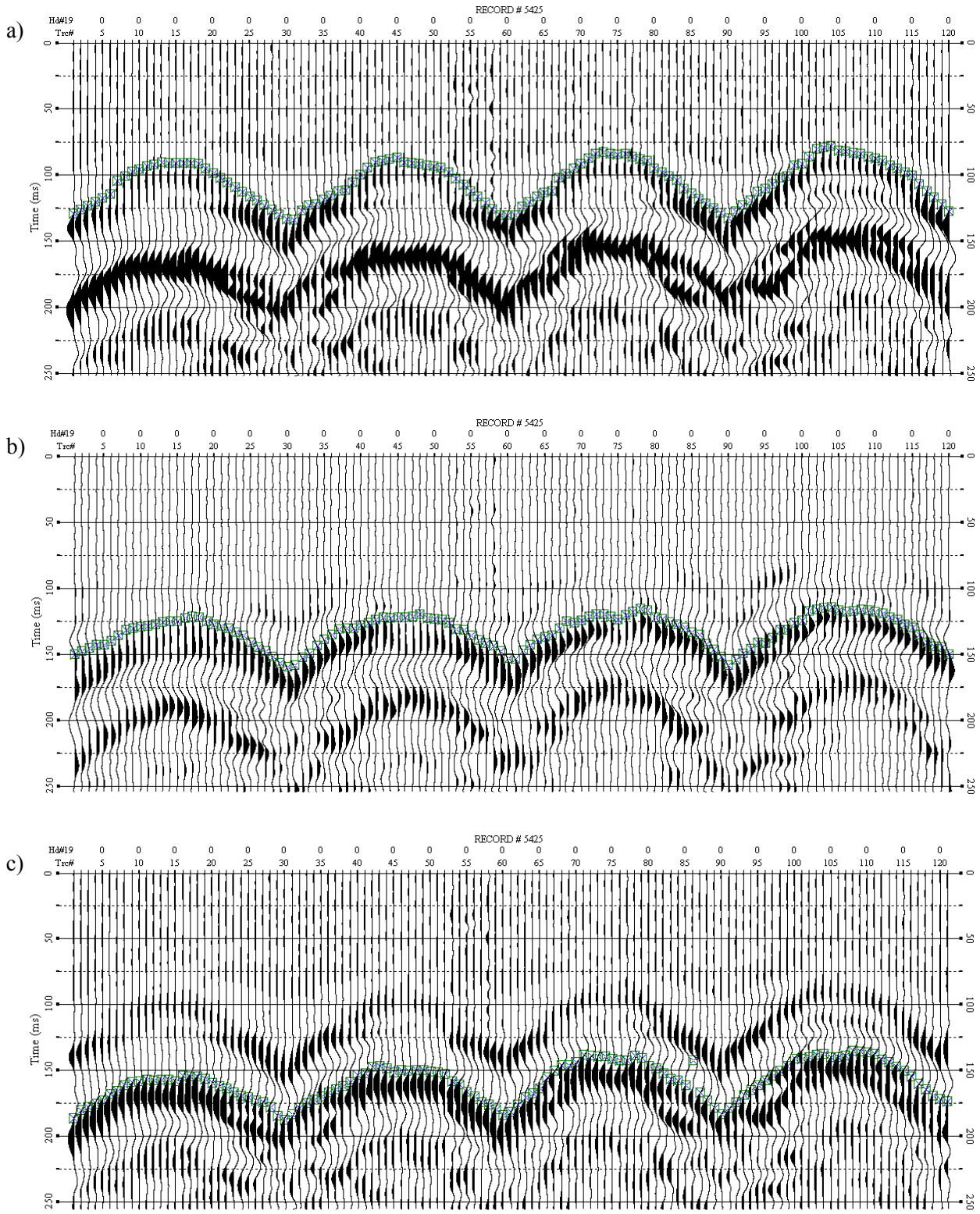

Figure 77. Possible S-wave refractions (direct-arrivals), which are not first arrivals. First-arrival events are hardly seen because of the lower gain. The average velocity of the first-arrivals of a) is about 600 ft/s (188 m/s); of b) is about 480 ft/s (143 m/s, reversed polarity traces); of c) is about 390 ft/s (119 m/s).

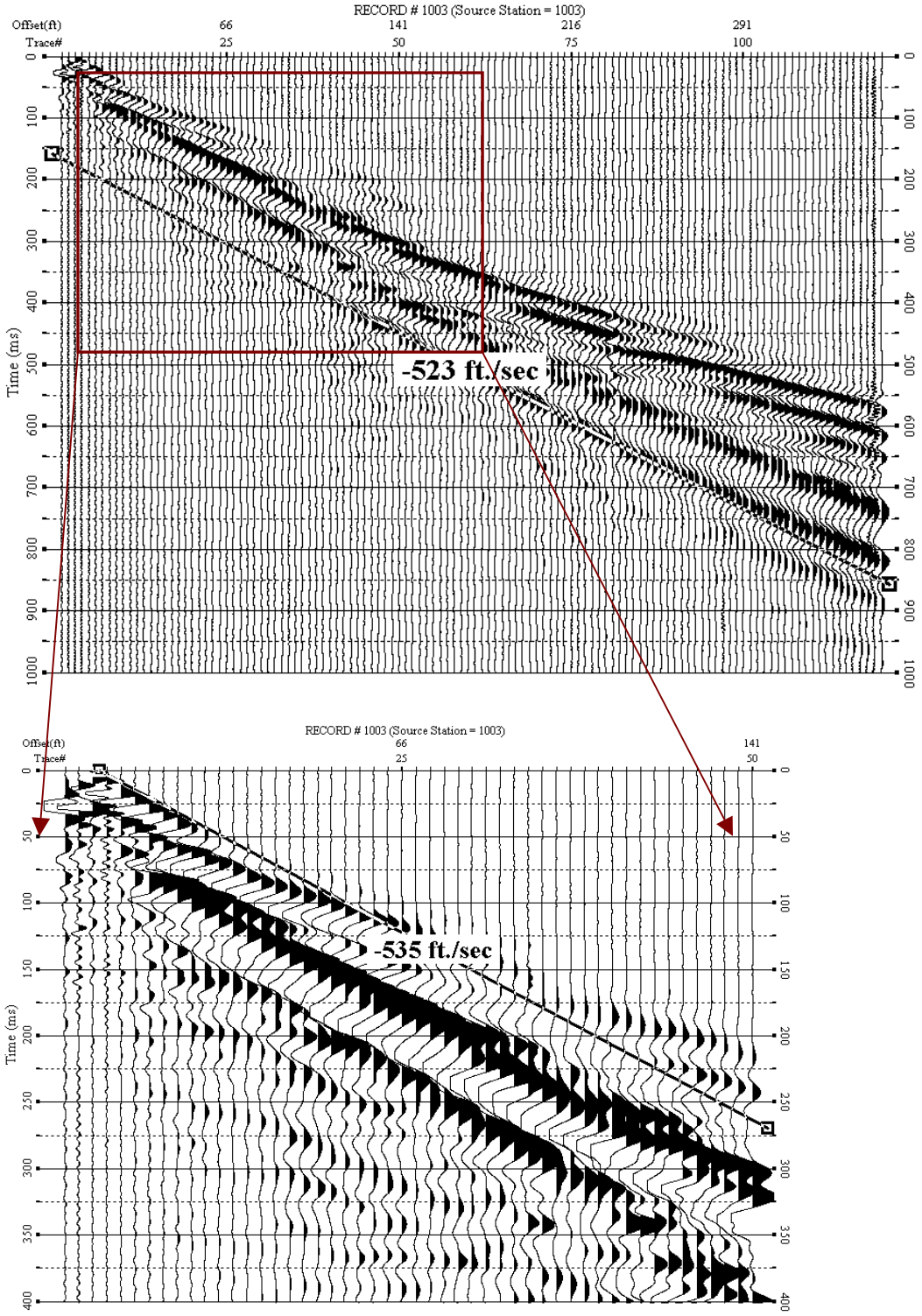

Figure 78. Seismic wavelet and apparent velocity observations on 2-D S-wave data record on top of the crest of the levee.

Love Wave

Unfavorable conditions present within the levee for the generation and detection of direct S-wave first-arrivals on 3-D through-levee data spurred a search for different ways to estimate Vs at the crest of these levees. Dispersion curve analysis of S-wave data produced very interesting results with a wide range of frequencies (6-30 Hz, Figure 79) detected in comparison to the previously analyzed P-wave surface-wave data (6-15 Hz, Figure 80). This wide range of dispersive frequencies observed in the S-wave surface-wave data was even more prominent when processing was limited to only the first 40 traces (Figure 81). With a phase velocity at 30 Hz of about 450 ft/s, the wavelength of the Love wave is equivalent to about 15 ft, providing a penetration depth of roughly 7.5 ft or half the wavelength. This observation demonstrates the potential of using Love waves to obtain shallow (upper 20 ft) Vs information. Unfortunately, algorithms and methods have not been sufficiently developed to allow confident and effective use of the dispersive attributes of Love waves to estimate seismic properties of earth materials.

After careful study of all data types and analysis methods, only the S-wave surface-wave (Love wave) possessed a sufficiently wide range of frequencies and sampling interval to provide Vs information from within the levees at a resolution that could potentially be used for long-term levee reconnaissance and differential characterization. A technique to invert Love waves is under development at several research institutes around the world. Even though it is currently not possible to invert the dispersive properties of Love waves, the dispersive properties can be used to identify zones within the subsurface that possess anomalous materials properties. A 2-D Love-wave dispersion display was generated from the top of the levee along the crest line (Figure 82). A gradient data set was calculated and filtered to emphasize potential anomalous zones (Figure 83). Clearly the characteristics of this filtered gradient data set are suggestive of real variability within the levee.

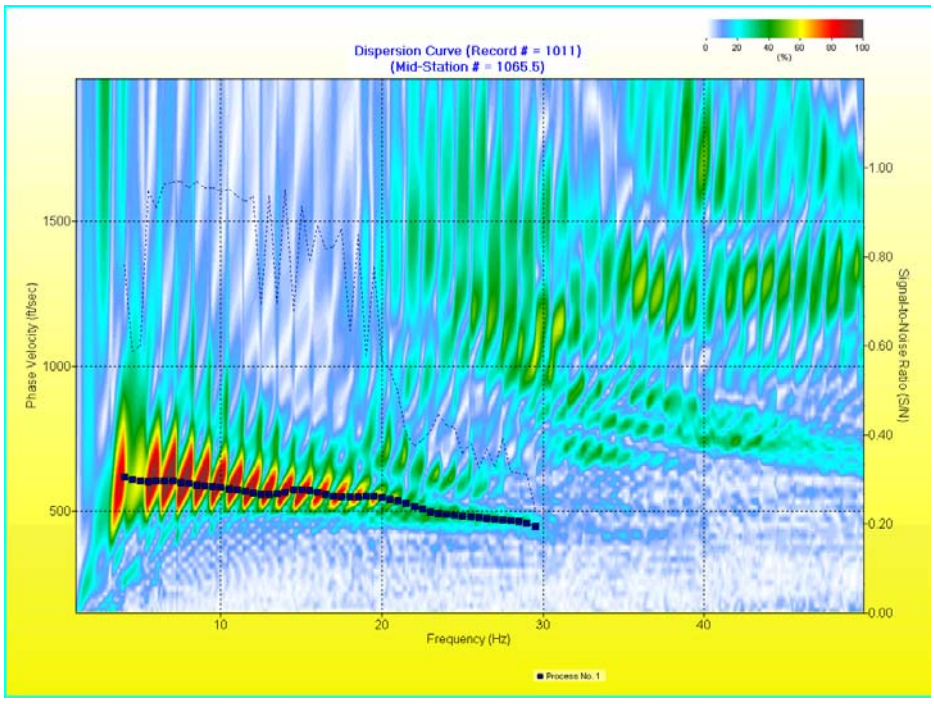

Figure 79. Dispersion-curve analysis of S-wave-data surface wave (Love wave).

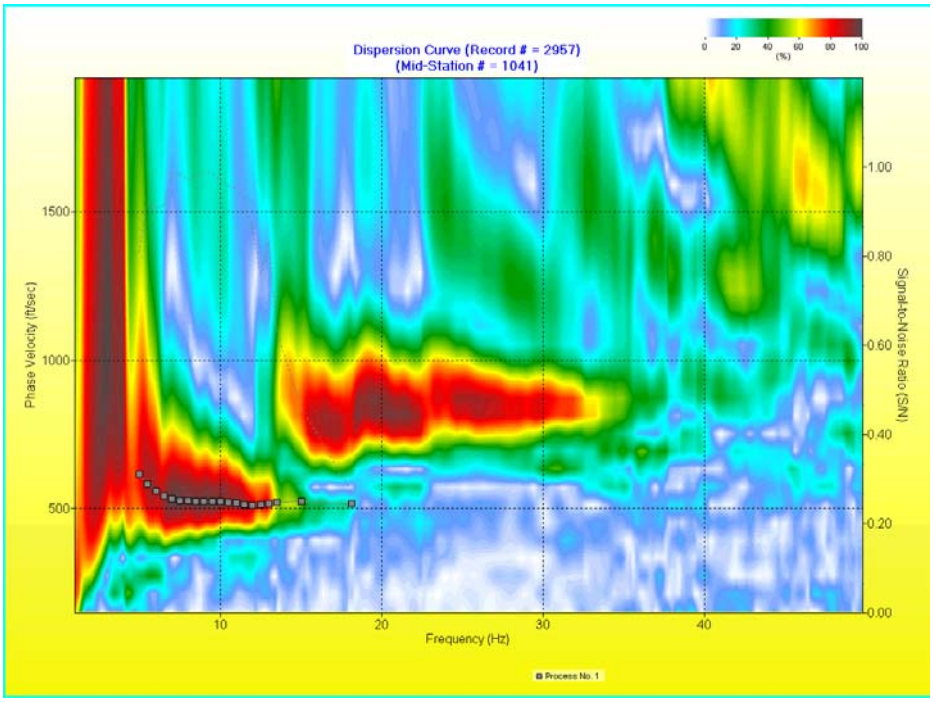

Figure 80. Dispersion-curve analysis of P-wave-data surface wave (Rayleigh wave).

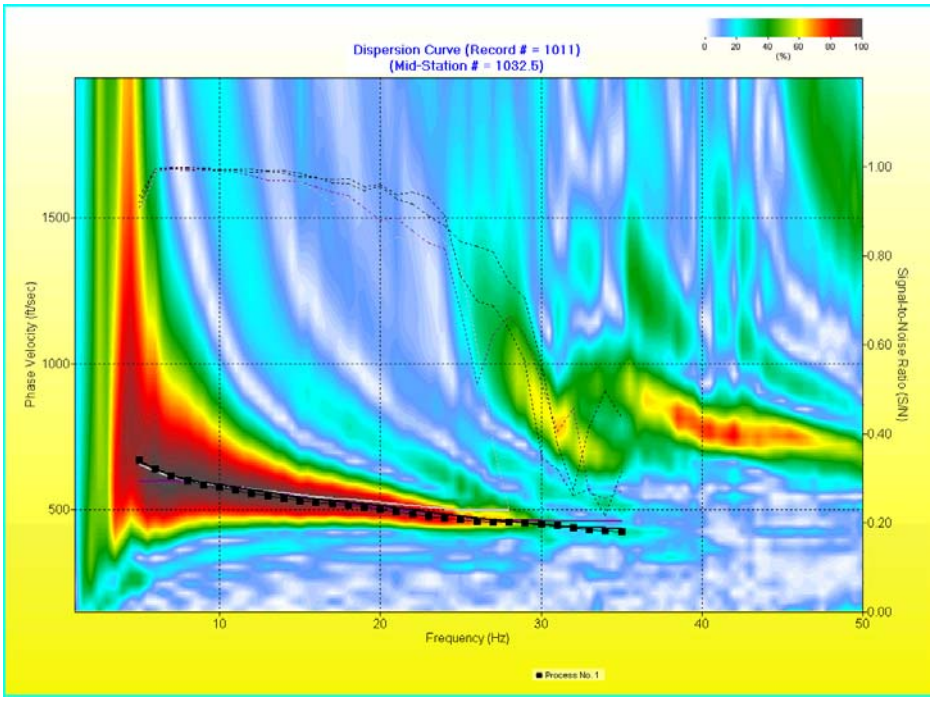

Figure 81. Dispersion curve analysis of first 40 traces of S-wave-data surface wave (Love wave).

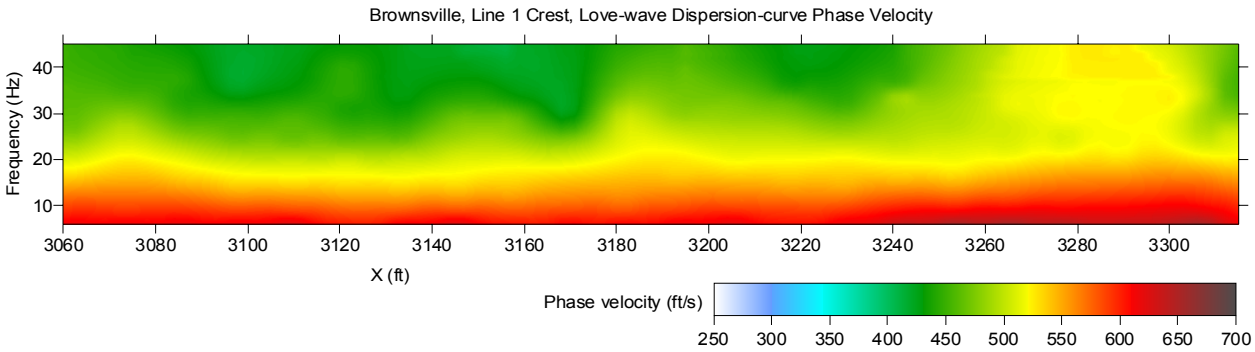

Figure 82. Love-wave dispersion-curve phase-velocity map estimated for line 1 by analyzing S-wave data.

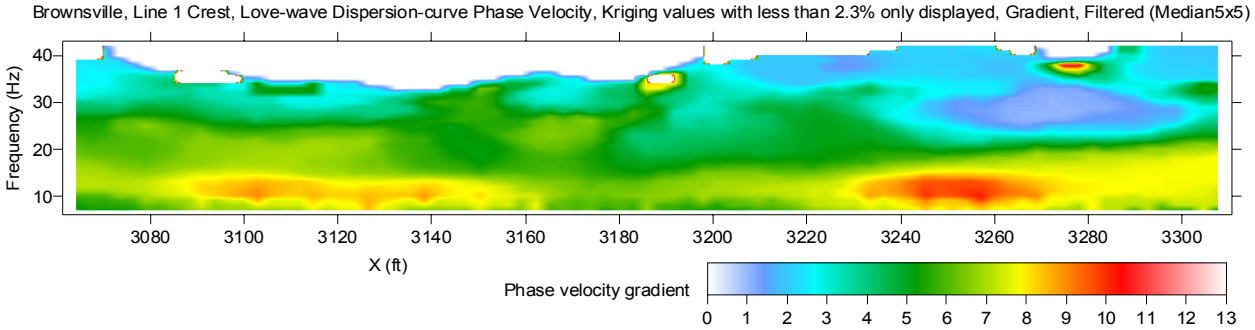

Figure 83. Love-wave dispersion-curve phase-velocity gradient map estimated for line 1 by analyzing S-wave data.

Site 2

Estimates of cross sectional Vs were obtained for both crest and toe using tomography and surface-wave inversion techniques. Vp information was extracted from P-wave data using first-arrival analysis (tomography) of seismic data collected along both toe and crest lines. Frequency-dwell data were analyzed for amplitude variations as a function of frequency, specifically looking for changes in phase that could be related to changes in material seismic velocity. A 120-channel through-levee travel-time study was undertaken for both P- and S-wave energy. This survey was much smaller in scope than the similar one undertaken for site 1. Data were acquired to allow the use of 3-D borehole tomography software to analyze first arrivals and generate a travel-time delay volume focused within the core of the levee.

Site 2 is unique with respect to its conductivity, surface fractures, and very shallow water table as evident by the oxbow lake just 100 ft north of the levee (Figure 3). Open fissures along the surface on the levee slopes at site 2 reinforced the suggestion that the core at this site was at least in part constructed of more expansive clay materials than likely present at other sites further north and that those clays were in a contracted state. Prior to the seismic study, a trench percolation test was performed to determine the velocity water would move through the core and therefore empirically appraise the permeability of the core. This site had several features and characteristics consistent with the suggestion that it would have the greatest failure potential in comparison to the other sites studied in this area.

Much of the data and many of the discussions pertinent and covered previously during site 1 reporting are also applicable to site 2. Unique data characteristics and observations that provide insight into the correlations between geology, construction, and geophysics will be discussed and displayed.

Tests and data analysis that provided no unique information or did not allow for a meaningful discussion applicable to the purpose of this study were not expanded on in-site observations.

P-wave First Arrivals

First-arrival picking was accomplished in a fashion completely consistent with that used for site 1. Similar problems were encountered and remedies were also quite similar, yet unique for the specifics of data from this site. Each shot gather was run through an algorithm designed to automatically pick the first-arriving impulse of source-generated seismic energy. Once these initial picks were made, each one was manually inspected to ensure consistency and accuracy.

First-arrival time-offset pairs were used to construct a 2-D refraction-tomography Vp solution for the cross section of the levee beneath the crest P-wave profile (Figure 84). This velocity cross section represents a vertical slice along the levee with colors indicative of different velocities. These velocities in many cases can be directly related to material properties. Horizontal uniformity of the velocity field is, in general, indicative of a relatively layered geology with no significant change in material type. With compaction will generally come higher velocities, therefore a gradationally increase in velocity with depth is a natural byproduct of vertical material accumulation via natural deposition or anthropologic construction activities.

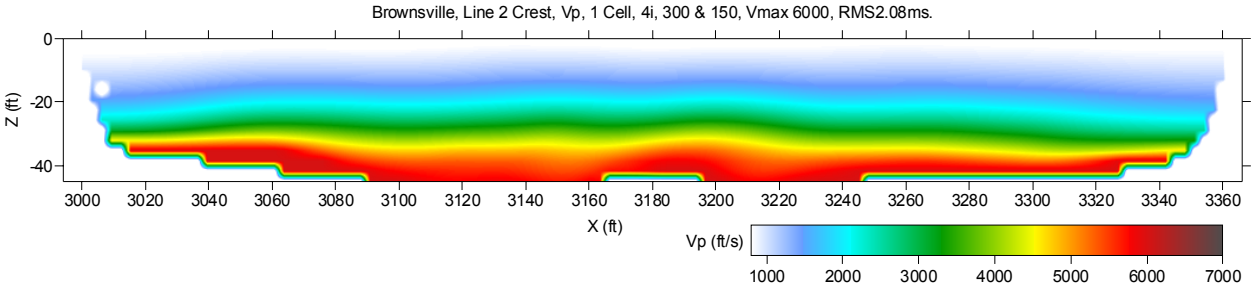

Figure 84. P-wave velocity model estimated for line 2 by analyzing P-wave-data first-arrival times using refraction-tomography software.

Vibrator Dwell Analysis at the Crest

Dwell or mono-frequency vibrator sweeps were recorded at the center and each end of the levee along the crest P-wave profile at site 2. At each shot location a separate seismic sweep was recorded for each of the following frequencies: 12, 15, 20, 25, 30, 50, 75, and 100 Hz. Each mono-frequency sweep was analyzed to determine if there was any dependence of apparent phase velocity of the seismic-wave packet (predominantly surface waves) across the 350-ft range of consecutive traces that make up this spread. Changes in phase velocity could be indicative of changes in material properties. For each constant frequency sweep, the apparent phase velocity was estimated across distances between 10 and 100 ft depending on uniformity of the seismic data using consecutive traces. Each station was assigned a velocity for each frequency (which can be correlated to depth using the half-wavelength criteria) and then all velocity information was plotted as a cross section according to depth and surface station. This 2-D representation of the phase-velocity distribution as a function of both depth and surface location was generated while the source was at the start of line 2 (station 991) (Figure 85). Apparent phase-velocity information was extracted from wiggle-trace plot (Figures 86 and 87, examples for 15 and 25 Hz).

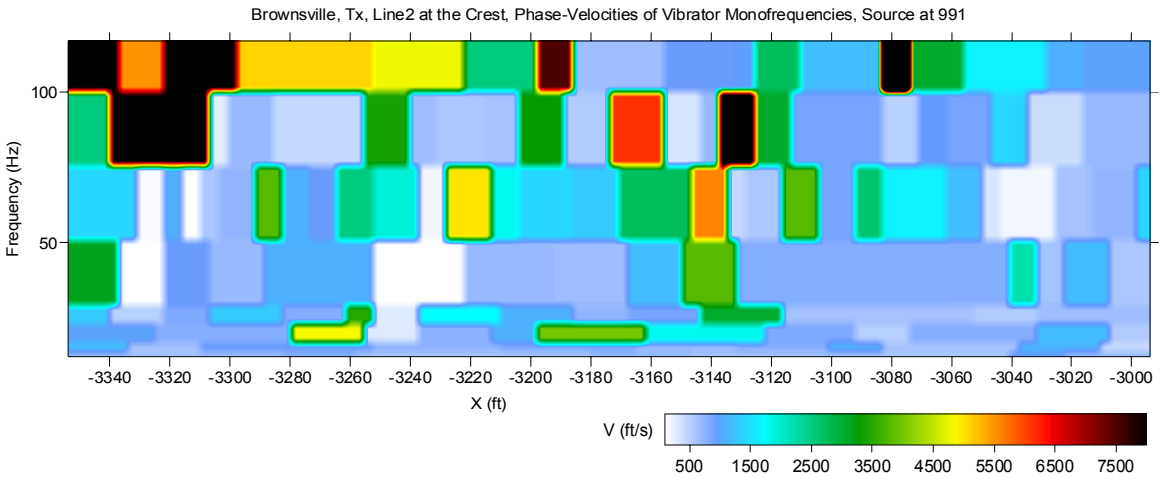

Figure 85. Rayleigh-wave apparent phase-velocity map estimated for line 2 by analyzing P-wave vibrator mono-frequency data.

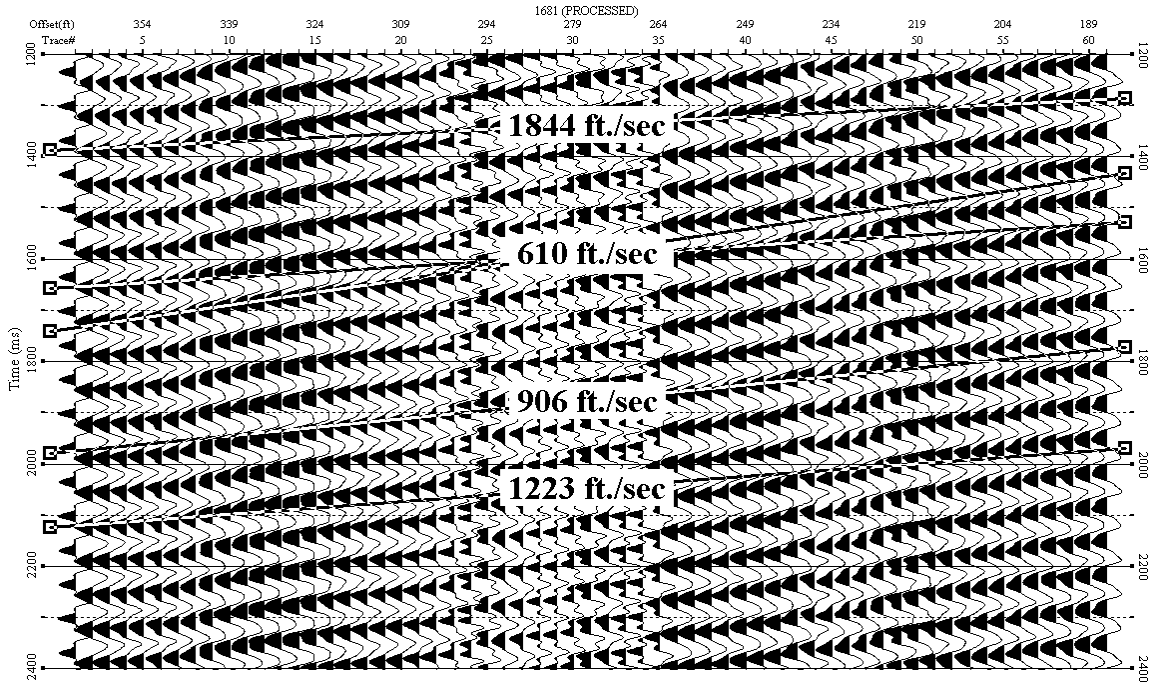

Figure 86. Apparent phase-velocity estimation of surface-wave propagation from 15 Hz mono-frequency vibrator data.

The same analysis was performed at the shot location from the other end of the line (station 1129). The very high frequency components (75 and 100 Hz) were not included with this analysis because penetration depths for these frequencies are only 2-3 ft below ground surface. These two directional opposing (source-to-receiver orientation) 2-D images (of measured phase velocity) did not provide similarities that could be confidently identified as anomalous zones within the levee where the seismic energy propagation characteristics were unique (Figure 88). A closer look at the low-frequency 2-D images did little to enhance the search of site-specific irregularities that might directly relate to material properties (Figure 89).

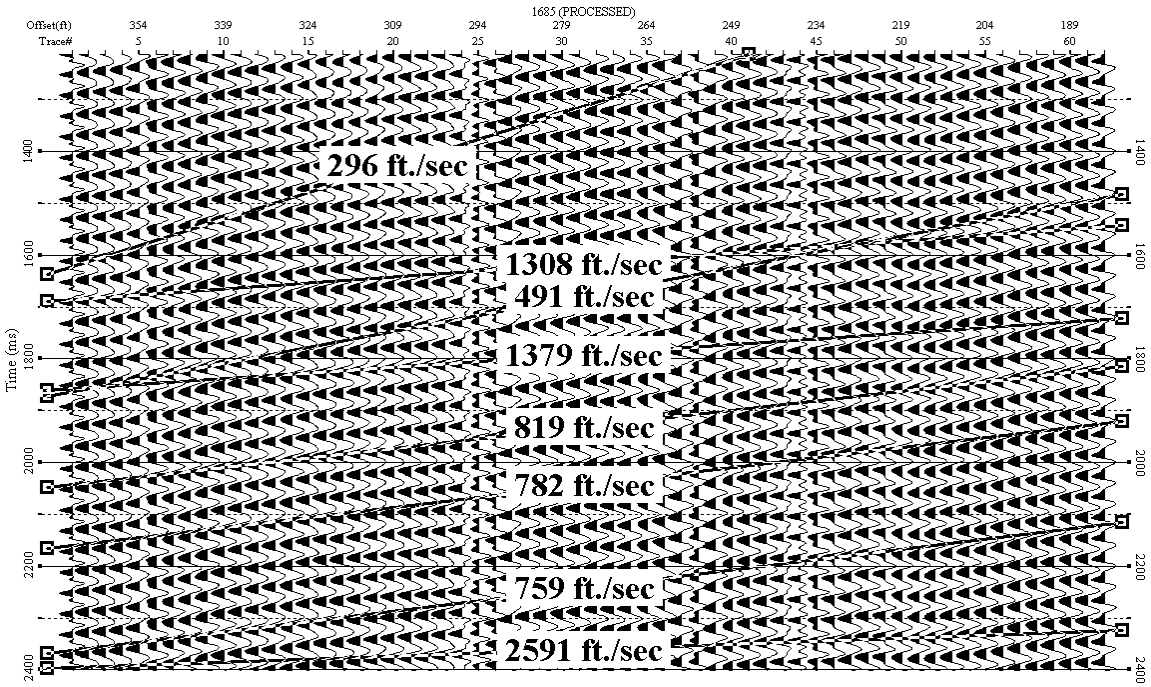

Figure 87. Apparent phase-velocity estimation of surface-wave propagation from 25 Hz mono-frequency vibrator data.

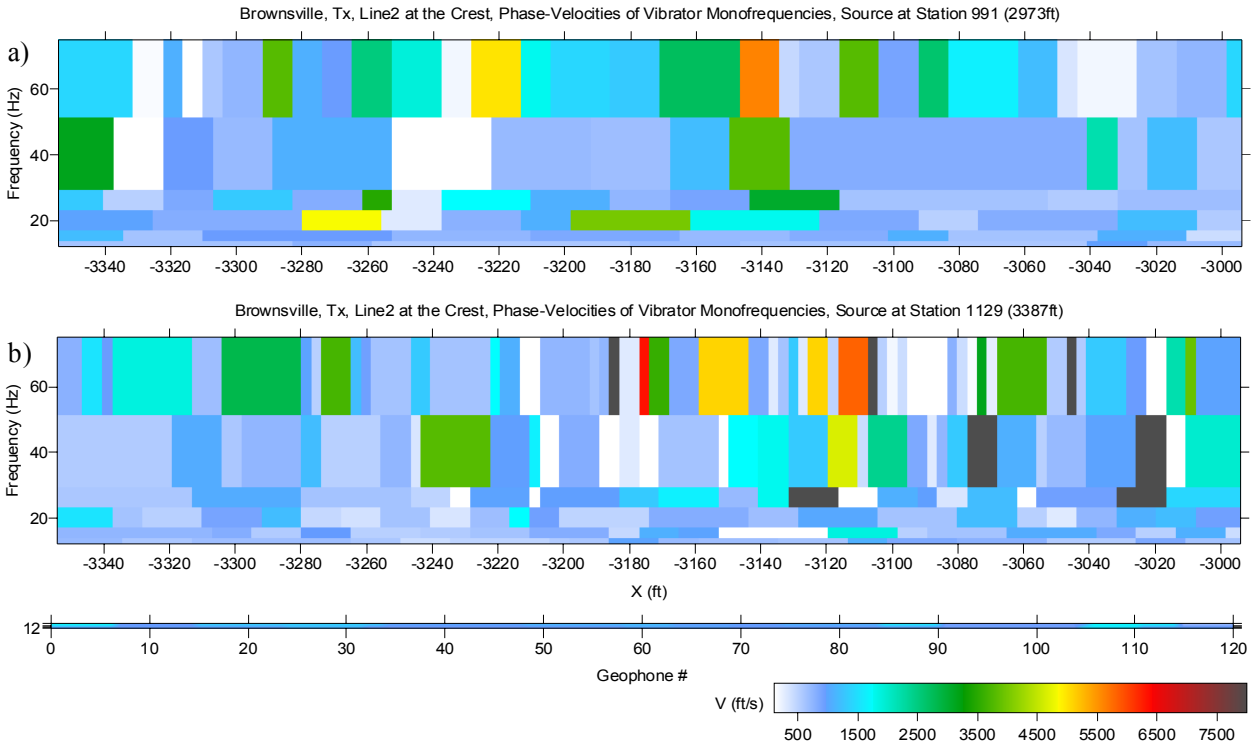

Figure 88. Rayleigh-wave apparent phase-velocity maps estimated for line 2 by analyzing P-wave vibrator mono-frequency data, a) vibrator is located at station 991 (X=2973 ft), b) vibrator is located at station 1129 (X=3387 ft).

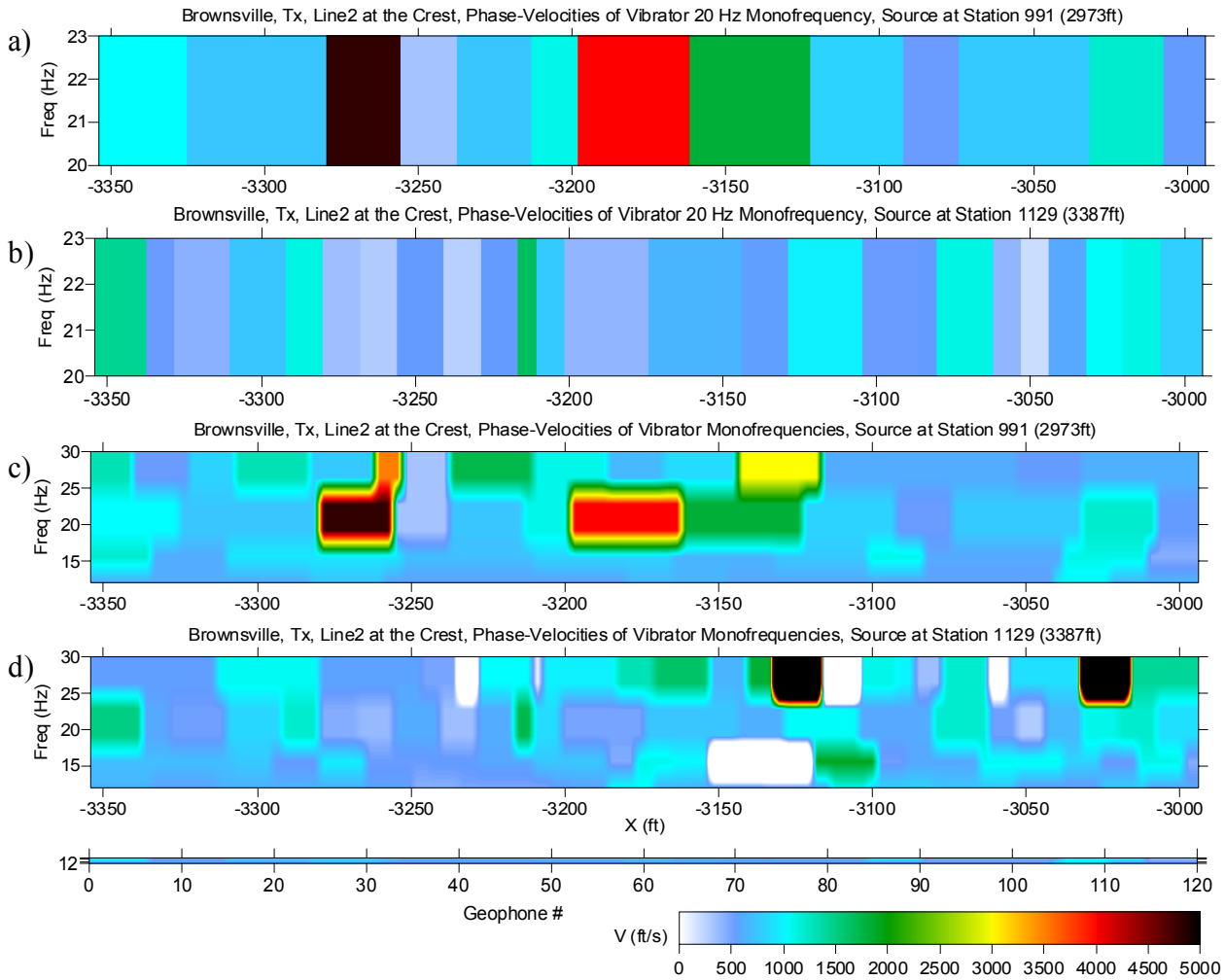

Figure 89. Rayleigh-wave apparent phase-velocity maps estimated for line 2 by analyzing P-wave vibrator mono-frequency data, a) and c) vibrator is located at station 991 (X=2973 ft), b) and d) vibrator is located at station 1129 (X=3387 ft).

Of particular interest, both in the field at the time of acquisition and later in the laboratory during data analysis, the 20 Hz mono-sweep generated when the source was at station 991 had an apparent phase-velocity change at the location previous trenched, used for the percolation test, and then later back-filled with native soils. This correlation between seismic observations and physical site activities justified a much closer look at these data and the product of their analysis (Figure 90). Disturbing the levee by trenching and then back-filling that trench likely caused changes in material compaction and distribution that manifested itself as changes in the apparent phase-velocity. This change is evident when comparing the trace-to-trace phase velocity inside the trench area relative to similar comparisons outside the trench area.

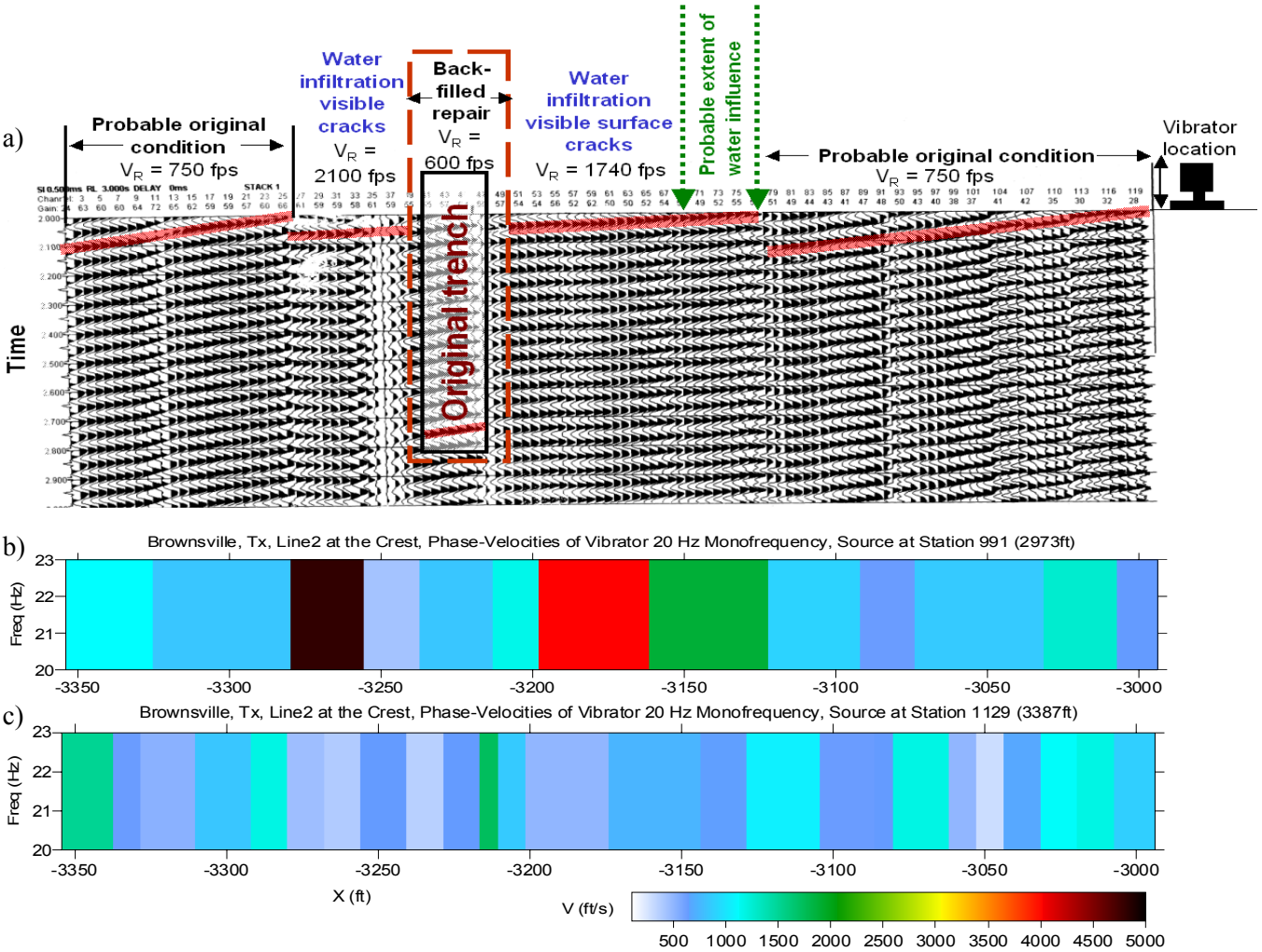

Figure 90. Rayleigh-wave apparent phase-velocity estimates for line 2 by analyzing p-wave vibrator 20 Hz mono-frequency data, a) seismic data from vibrator located at station 991 (X=2973 ft), b) 2-D phase-velocity map when vibrator is located at station 991 (X=2973 ft), c) 2-D phase-velocity map when vibrator is located at station 1129 (X=3387 ft).

Generalizing to the point where this type of anomaly can be categorized as diagnostic of this type of ground disturbance is not feasible because when the source station was moved to the opposite end of the spread (station 1129) this same feature was not observed coincident with the trench. Similar analysis was undertaken for the 25-Hz sweeps when the source was at stations 991 and 1129. Data sets from both shot stations showed unique changes in phase velocity across the spread, but neither produced a pattern that could be clearly distinguished and categorized as diagnostic of a particular change in levee materials or condition (Figures 91 and 92).

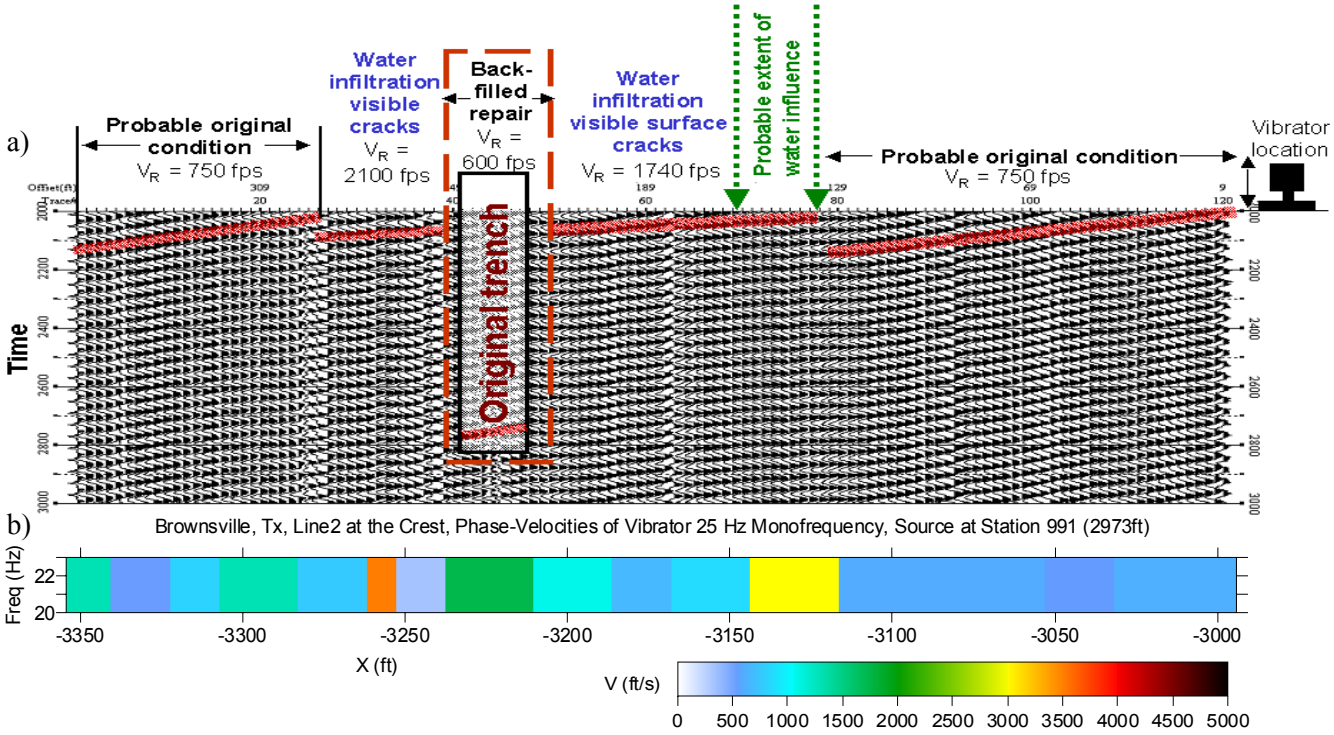

Figure 91. Rayleigh-wave apparent phase-velocity estimates for line 2 by analyzing P-wave vibrator 25 Hz mono-frequency data, a) seismic data from vibrator located at station 991 (X=2973 ft), b) 2-D phase-velocity map of the same data.

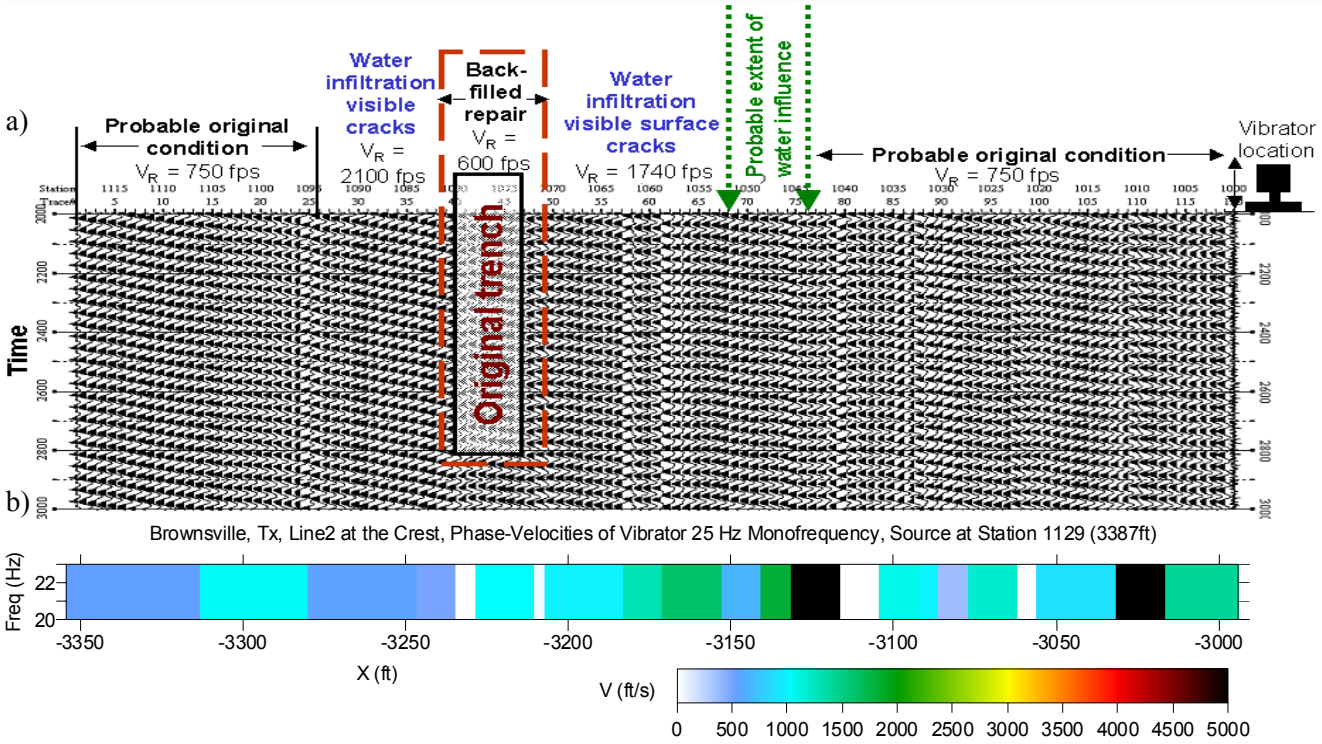

Figure 92. Rayleigh-wave apparent phase-velocity estimates for line 2 by analyzing P-wave vibrator 25 Hz mono-frequency data, a) seismic data from vibrator located at station 1129 (X=3387 ft), b) 2-D phase-velocity map of the same data.

S-wave First Arrivals

Shear-wave first arrivals were automatically picked on shot gathers in the same fashion described for site 1. Each automatic first-arrival pick went through a manual inspection process to ensure the program had made "best" possible selection. First-arrival interference with noise of any kind can result in cycle skipping or pre-emergent selections. Most automatic first-arrival missed picks can easily be seen as well as the reason for the miscue identified. This allows a more confident manual pick to be substituted for the automatic selection. Shear waves are particularly difficult to analyze due to mode conversions, proximity to the surface wave (velocity of surface wave ~0.9Vs), compressional dispersive guided waves, and narrow band nature of wavelet.

First-arrivals selected for S-wave shot gathers, acquired along the crest of the levee at site 2 were fed into a 2-D refraction-tomography algorithm with a standard initial model for this area. A well-constrained Vs solution (Figure 93) with good convergence was produced, having what is considered a reasonable Vp/Vs for unconsolidated, unsaturated sediments. The presence of the oxbow lake north of site 2 leads to the suggestion that this meander cut off feature likely extends in the subsurface beneath the levee. Therefore, it is not unexpected to see what appear to be undulations in the velocity field consistent with the cut and fill of an ancient meander path of the river.

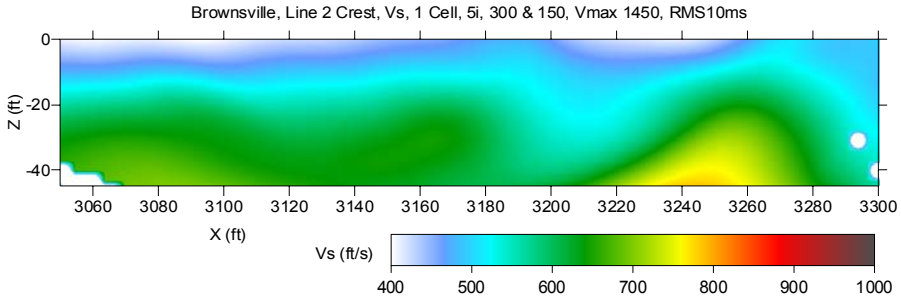

Figure 93. S-wave velocity model estimated for line 2 at the crest of the levee by analyzing S-wave-data first-arrival times using refraction-tomography software.

Shear-wave velocities within the depth range of the levee are between 400 ft/sec and 550 ft/sec. Considering the compressional-wave velocity in this same depth interval is 1000 ft/sec to 2000 ft/sec, the Vp/Vs is around 2.5 to 3 for the levee. This is a reasonable range for a compacted clay fill. The shallowest part of the levee (<10 ft) did not produce high confidence Vp or Vs values, making estimations of velocity ratios for those depths beyond these data.

Rayleigh Wave

Crest

Key to the extraction of shear-wave velocity information from surface waves is the presence of broadband fundamental-mode energy. Regardless of the source, receivers, or location, high-frequency fundamental-mode surface waves were just not recorded on these levees. It is our working hypothesis that the higher-frequency components of the surface wave were never produced due to near-surface (<2 ft) site conditions. An abundance of higher-mode energy was produced, but the current state-of-the-art in surface-wave analysis does not allow for incorporation of that type of energy into the inversion process. As the technology advances higher modes will allow key seismic characteristics of near-surface materials to be defined with reasonable confidence.

Although the fundamental mode of the surface wave lacked high frequencies (and thus did not provide shallow Vs information), the MASW method still provided an accurate overall estimation of the Vs between depths 25 ft and 85 ft at the crest of the levee (Figure 94). Interesting is the apparent discrepancy between the MASW data (which appears to be representative between 25 ft and 85 ft) and the

shear-wave velocity cross section generated using shear-wave tomography (Figure 93). Comparing the MASW Vs cross-section with the shear-wave tomography cross section along the same profile, a velocity discrepancy of about 15% to 20% is evident. Also notable is the exaggerated structure on the surface of bedrock interpretable on the Vs tomography cross section relative to the MASW cross section.

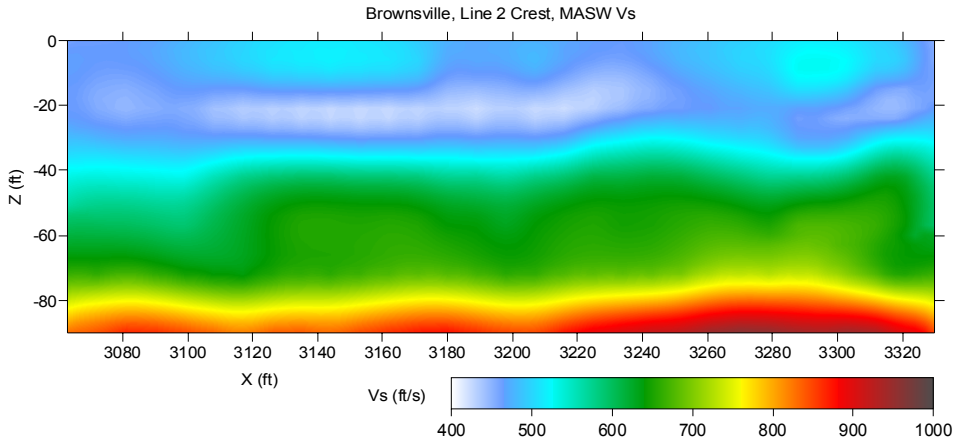

Figure 94. S-wave velocity model estimated for line 2 at the crest of the levee by analyzing P-wave-data surface-wave using MASW method.

Toe

Fundamental mode Rayleigh surface-wave energy possessed a sufficient broad range of frequency characteristics at the toe to avoid the high-frequency limitations observed on the crest data. The MASW method provided an accurate overall 2-D estimation of the Vs distribution at the toe of the levee (Figure 95a). Velocity and depth values matched reasonably well between MASW at the crest and MASW at the toe for the same absolute elevations (Figure 94). A subtle topographic west dip on the layer around 10 ft below ground surface on the toe data is not evident for the same layer when imaged from the crest.

Crest-Toe Comparison

All things considered the MASW-produced Vs images from the toe and the crest are reasonably similar (Figure 95). There is an up-going trend in the velocity contour from left to right at about -80 ft depth on both sections (for this report the levee crest is at elevation 0 at all sites). Greater detail observed in the toe image is probably due to the surface to boundary depth (that is, the boundary is about 20 ft closer to the surface at the toe in comparison to the crest), so there is less smearing and averaging of earth material by the surface wave along the toe line. A high-velocity lens-like anomaly location at range 3060 to 3120 ft on the toe MASW Vs, can not be interpreted on the crest MASW Vs image. One possibility is that it is a very local lens feature, evident on the higher-resolution data.

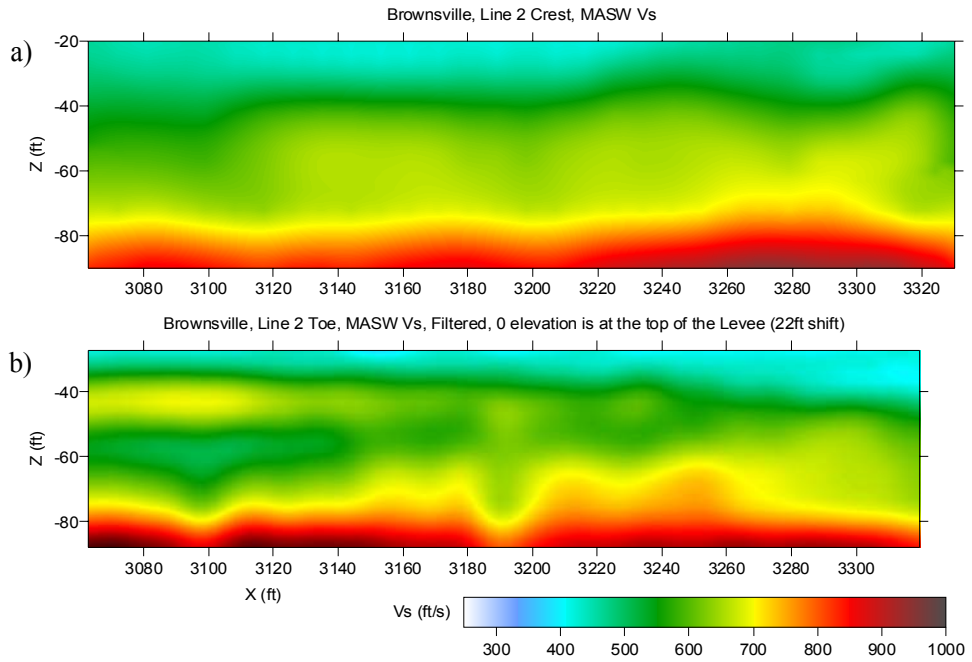

Figure 95. Line 2 S-wave velocity model estimates by analyzing P-wave-data surface-wave using MASW method, a) at the crest of the levee, b) at the toe of the levee.

Tomography

3-D Through-levee P-wave Direct Arrivals

First-arriving energy at site 2 was exclusively the result of refractions traveling in native materials below the basal contact of the levee (Figure 96). Differences in velocity with travel path, when calculated using the assumption of a straight ray path, are way outside what would be considered reasonable for any material fill of this nature. Clearly characteristics of the first arrivals as well as the next several tens of milliseconds of the wavetrain are consistent with that observed at site 1. However, unlike site 1, the direct-arriving energy is subdued by surface wave and guided waves. This interference was prevalent throughout these data.

Polarity reversing of shot gathers in a fashion identical to the process used to enhance direct arrivals on display of site 1 data was used on site 2 data but without the same benefits (Figure 97). A high-frequency arrival with a curvature consistent with that expected from the direct wave can be interpreted on the best through levee shot gathers from this site. However, their extremely low amplitude and lack of wavelet consistency made them impossible to both pick and confidently identify as the direct wave. Considering that when using the direct raypath distance the average velocity would be around 300 m/sec, it appears possible this arrival could be air-coupled wave. Therefore, it was only possible to pick with confidence the direct through-levee arrivals for site 1. On site 2 it was not possible to confidently separate direct-wave energy from secondary arrivals due to interference. One observation that can be made with reasonable confidence is the direct compressional-wave velocity through the levee at site 2 is slower than that observed at site 1.

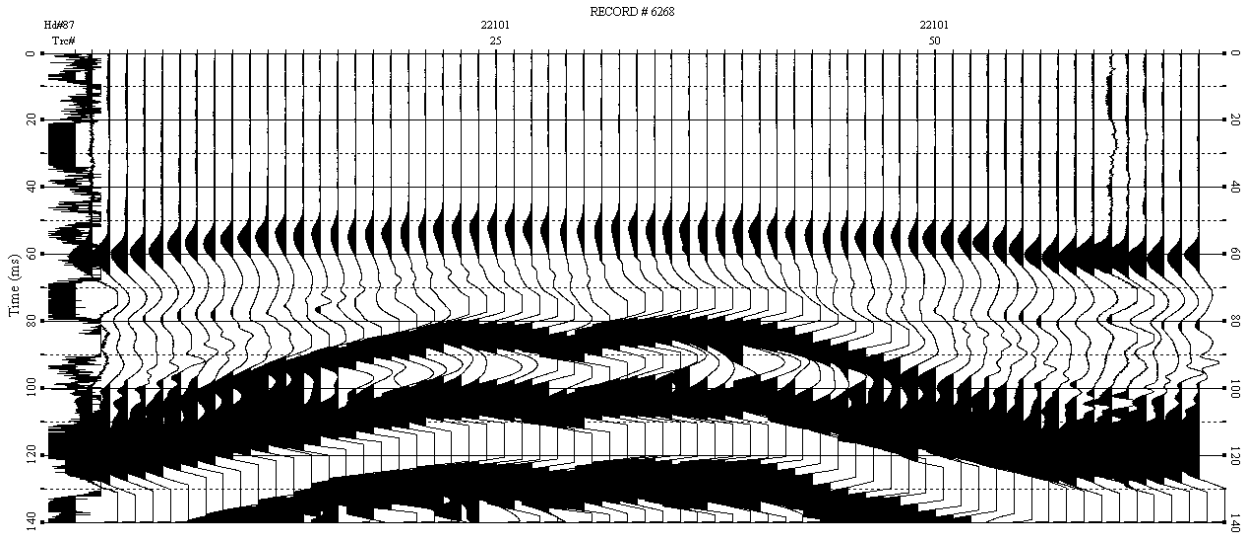

Figure 96. Estimation of first-arrival and secondary-arrival times on 3-D P-wave through-levee seismic data at site 2, shot record 6268.

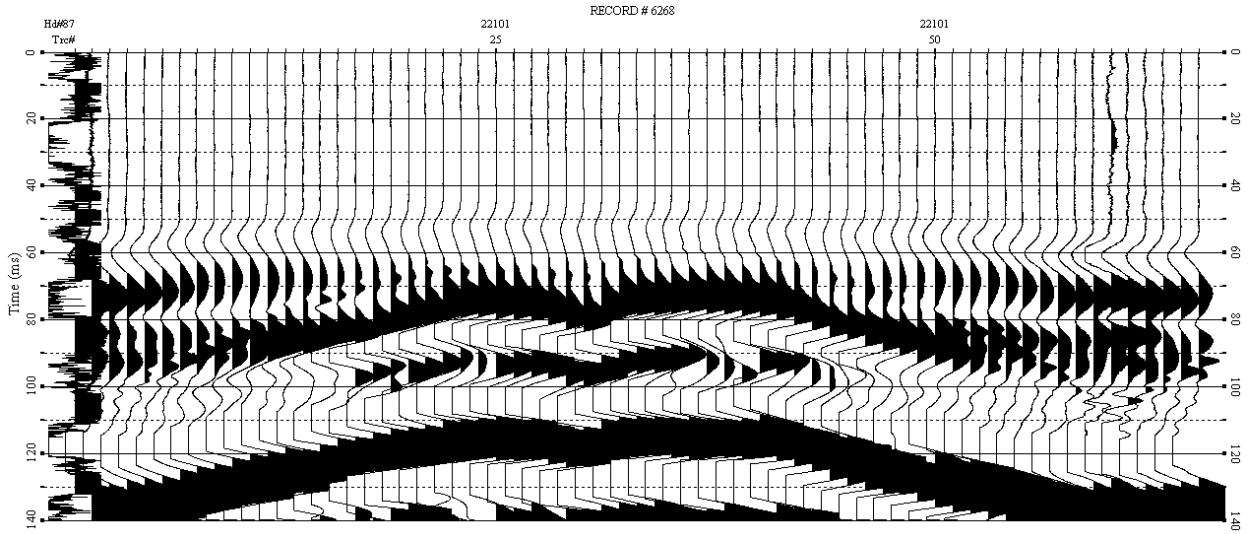

Figure 97. Estimation of first-arrival and secondary-arrival times after reversing polarity of 3-D P-wave through-levee seismic data at site 2, shot record 6268.

3-D Through-levee S-wave Direct Arrivals

Similar to site 1, it was not possible to identify S-wave direct through-levee arrivals on the S-wave data collected in the 3-D configuration. Many of the same anomalous arrival patterns were observed at this site consistent with site 1. Clearly, the orientation of source and receivers combined with the geometry of the levee adversely affected the recording of direct, polarized shear energy. With the exception of first arrivals on traces directly adjacent to the source relative to the levee axis, first-arriving energy was likely mode-converted compressional or Sv waves. This is based on the 3-D aspect of the receiver grid relative to the polarized source at wide angles, making receivers at greater offsets most sensitive to Sv and compressional-wave energy produced by the source.

Recorded wavelets within the first few cycles had relatively low dominant frequencies (15-20 Hz) and very limited bandwidth. These characteristics are consistent with surface-wave energy recorded on

2-D S-wave data at this same location. As with site 1, the inconsistency in first-arrival patterns is suggestive of a propagation path not directly through the levee but either around the surface (such as a surface wave) or the result of multiple mode conversions and/or reflections/refractions from within the levee itself.

Love Wave

Clearly the wave type with the apparent greatest potential for successfully and accurately measuring the shear-wave velocity field was the Love wave. The presence of a wide range of frequencies in the S surface wave (Love wave) is very suggestive of the potential depths of investigation possible with the Love wave. As with site 1, Love waves seem to have a great deal of potential interrogating the levee itself from the crest. This is true, of course, only if the same rules of thumb can be used with Love waves that appear to be applicable to Rayleigh waves. Critical to actualizing this potential is the development of a reliable, accurate, and meaningful technique for inverting Love waves to obtain a Vs model. For that reason only dispersion-curve analysis was performed on the Love-wave data in hopes of identifying areas that could represent anomalous zones within the levee. From 2-D Love-wave dispersion curves from the top of the levee (Figure 98) a gradient map was calculated and filtered to emphasize potential anomalous zones (Figure 99).

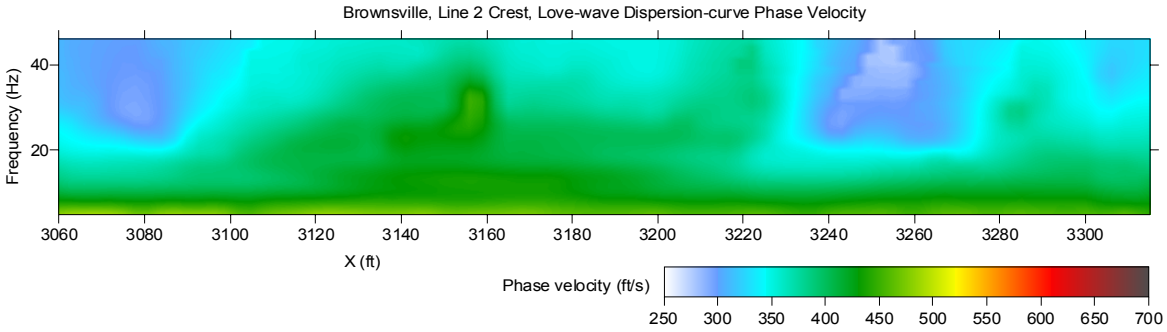

Figure 98. Love-wave dispersion-curve phase-velocity map estimated for line 2 by analyzing S-wave data.

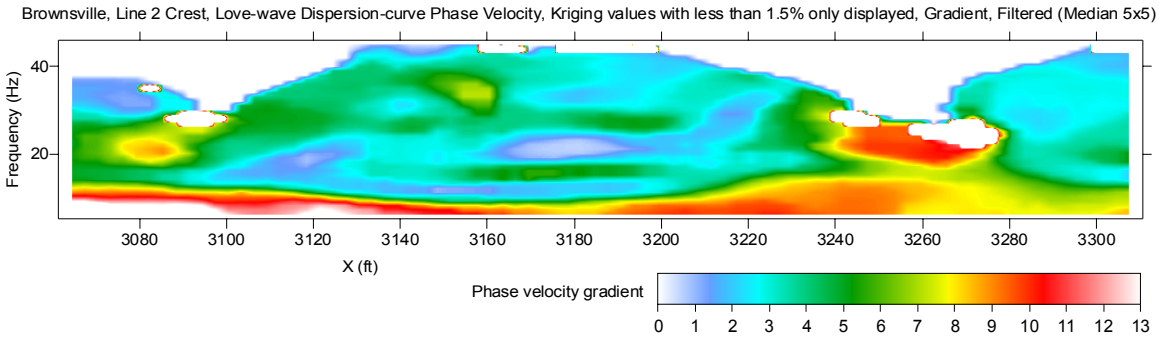

Figure 99. Love-wave dispersion-curve phase-velocity gradient map estimated for line 2 by analyzing S-wave data.

Sites 3, 4, and 5 were studied to provide background information important for establishing the seismic characteristics of different levee materials as determined from conductivity measurements and drilling.

Site 3

P-wave First Arrivals

Compressional-wave data along the crest and toe were collected at site 3 in a fashion consistent with sites 1 and 2. Maintaining a consistent acquisition and processing format allowed direct comparisons of the different levee sites and location at each levee site (toe and crest) without introducing error associated with equalization techniques. Signal-to-noise ratio on compressional-wave first arrivals was high enough to characterize most of the arrivals as instantaneous. Model convergence and a good 2-D refraction-tomography Vp solution was easily accomplished in part due to the high quality of the first arrivals on P-wave data shot gathers along the crest (Figure 100a) and toe (Figure 100b) of the levee.

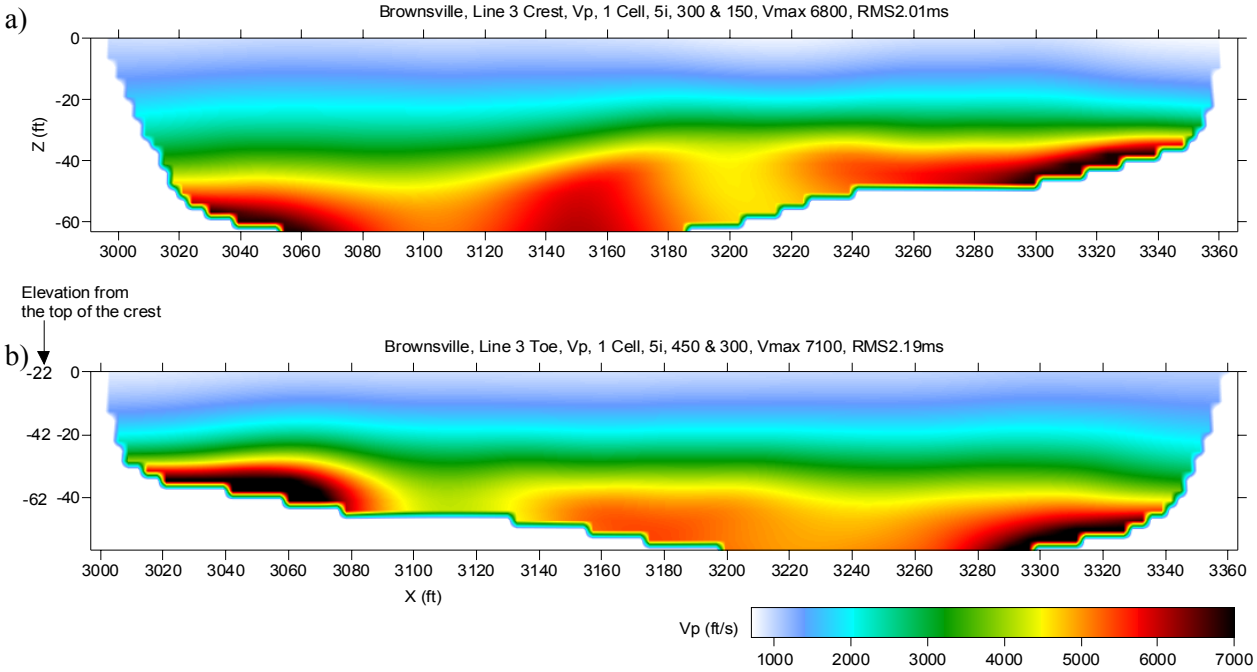

Figure 100. Line 3 P-wave velocity model estimates by analyzing P-wave-data first-arrival times using refraction-tomography software, a) at the crest of the levee, b) at the toe of the levee.

Crest-Toe Comparison

Ideally the compressional-wave data from toe and crest would result in near-identical velocity estimates from the native ground surface and deeper. However, several factors must be considered when making comparisons and contracting these data. First, the coupling and transmission characteristics of the levee will be significantly different than the toe. Second, with any inversion type processing, *a priori* information and non-uniqueness play a role in the final product. Finally, the velocity structure within the levee has the potential to alter the raypaths in the native materials, such that the toe and crest data sets actually have a less than expected overlap in sampled subsurface materials.

Similarity between the two data sets, which in principle sample the same materials, will be limited by differences in the near-surface properties. Simple differencing of these data sets will not provide beneficial results or gratifying conclusions. Changes in the material and therefore the raypaths between these two data sets most profoundly affect refraction tomography inversion, which is strongly

nonunique, meaning that there is a wide range of equally possible solutions. Therefore, a unique solution is not possible without abundant *a priori* information. This leaves two primary factors controlling the similarity between toe and crest data sets below the native ground surface—one is near-surface characteristics and the other is inversion non-uniqueness (Figure 100).

S-wave First Arrivals

Shear-wave data for line 3 possessed good quality first-arriving wavelets. At longer offsets the first arrivals are well pronounced, but their lack of unique character relative to the surface wave and merging with the guided wave raises some suspicion as to their likely propagation path and first-order mode. However, for purposes of our processing, the first arrivals were selected using the guide that direct and refracted body waves should be the first source-generated energy at the receiver. After first-arrivals were automatically selected and manually verified for all S-wave shot gathers collected along the crest of the levee, the arrival times and geometry information were fed into a 2-D refraction-tomography algorithm, which converged to a reasonable Vs solution (Figure 101).

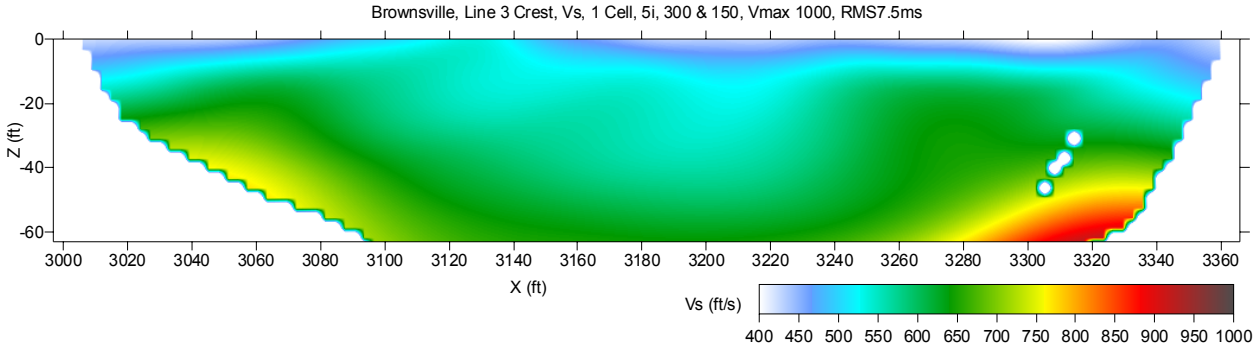

Figure 101. S-wave velocity model estimated for line 3 at the crest of the levee by analyzing S-wave-data first-arrival times using refraction-tomography software.

P-wave and S-wave V Solutions

As a quality control measure, the velocity solutions from tomography analysis for both types of body waves were visually compared to appraise similarity of gross features. Differences are relatively pronounced and suggestive of changes in material properties that uniquely affect the two body-wave velocity values. In this unconsolidated environment the compressional-wave velocity of a sand, for example, will change more significantly as saturation changes than will the shear-wave velocity. Therefore, a saturated sand lens within a clay could easy possess a transition in compressional-wave velocity from low to high and shear-wave velocity from high to low. With these kinds of inverse relationships, it is not unexpected for gradients of the same material to be significantly different for the two wave types.

Rayleigh Wave

Crest

At this levee site, as with sites 1 and 2, surface-wave data recorded from the top of the levee lacked the higher-frequency components necessary for interrogating the body of the levee. Clearly our inability to generate and/or propagate high-frequency surface wave is not isolated to a particular site and therefore the limitation must be based in either the source, near-surface material, levee geometry, or some combination of the three. Although the fundamental mode of the surface wave lacked high frequencies (and thus no shallow Vs information), the MASW method still provided an accurate overall estimation of the Vs, between depths 25 ft and 80 ft at the crest of the levee (Figure 102).

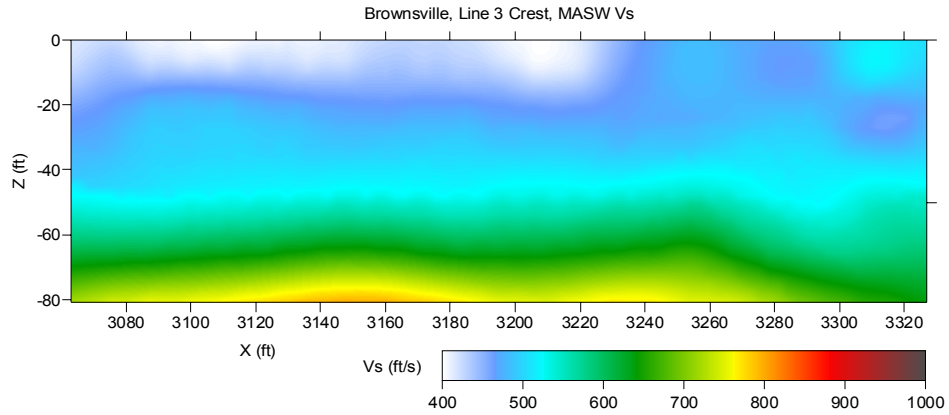

Figure 102. S-wave velocity model estimated for line 3 at the crest of the levee by analyzing P-wave-data surface-wave using the MASW method.

Crest-Toe Comparison

As a quality-control measure, comparison of the crest and toe data for each method was used to determine similarity. In contrast with the crest data, it was possible to estimate the fundamental-mode of the dispersion curve within a wide frequency range (Figure 103a). For MASW-determined Vs images at the toe and crest, the velocity ranges and general topography of velocity interfaces identified by rapid color change are very similar (Figure 103b,c). Compaction or removal of the shallow soil layer during construction likely changed the upper several feet beneath the present levee. Compounding that is the gravitational compaction that has taken place since placement of the levee materials. It is not surprising and is expected that the upper few feet at the toe is of slower velocity than its horizontal equivalent beneath the levee. With that understanding, comparisons demonstrate the consistency in the method and precision of the measurement process.

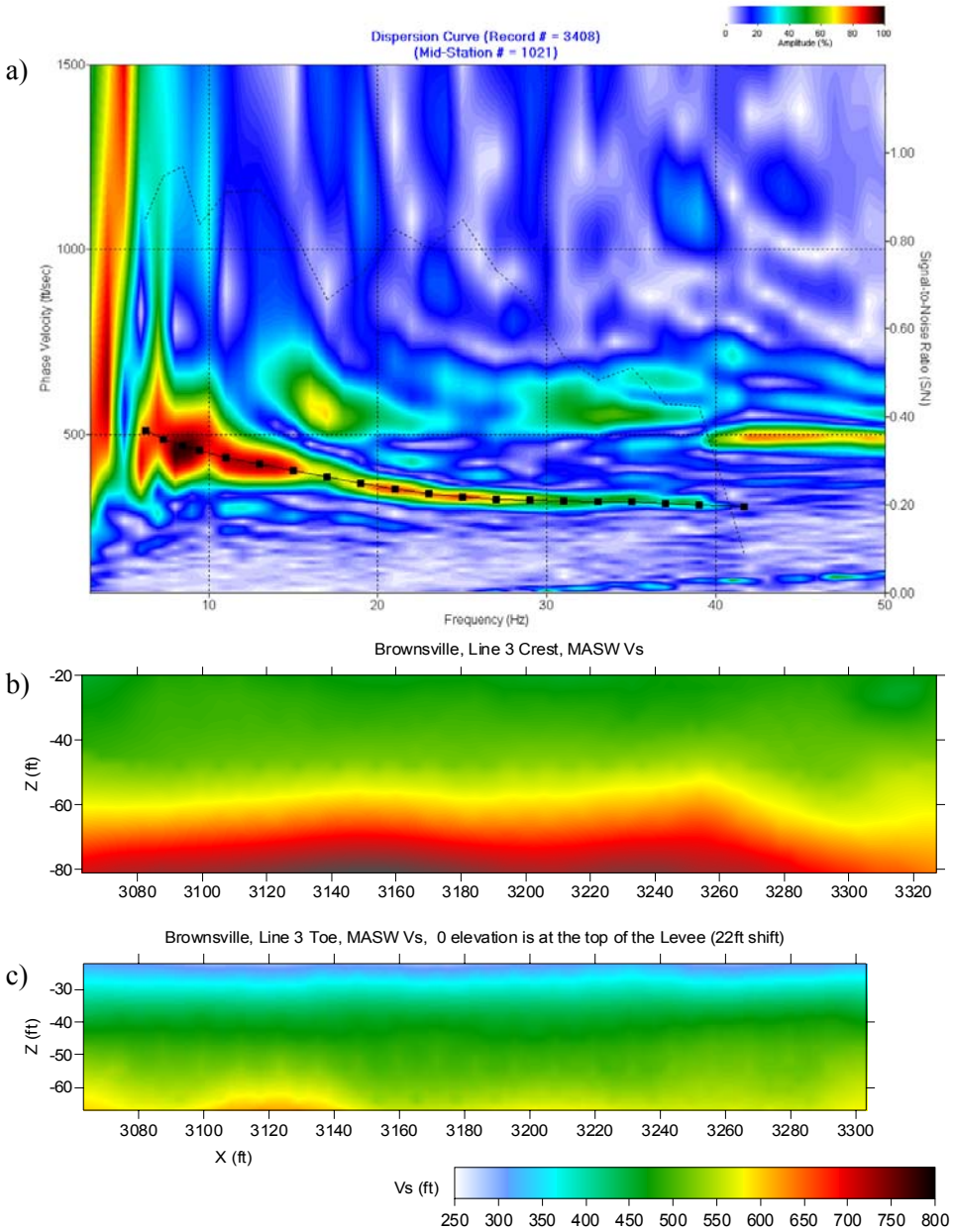

Figure 103. Line 3 S-wave velocity model estimates by analyzing P-wave-data surface-wave using the MASW method, a) Dispersion-curve analysis using the first 40 traces from shot record 3408, b) 2-D S-wave velocity model at the crest of the levee, c) 2-D S-wave velocity model at the toe of the levee.

Love Wave

A consistent theme at all sites seems to be the presence of a relatively wide range of frequencies within the surface-wave packet on S-wave data (Love wave). Assuming the same axiom that relates frequency to depth of penetration for Rayleigh waves is true for Love waves, then it can be stated with good confidence that Love waves were the only type of energy that provide Vs sampling within the levees. The technique for inverting Love waves is under development and therefore no depth estimations as a function of shear velocity can be assigned for these data. For that reason only dispersion-curve analysis was performed to locate anomalous zones. A 2-D Love-wave dispersion curve display was generated for the top of the levee (Figure 104). A gradient map was calculated and then filtered to emphasize potential anomalous zones (Figure 105).

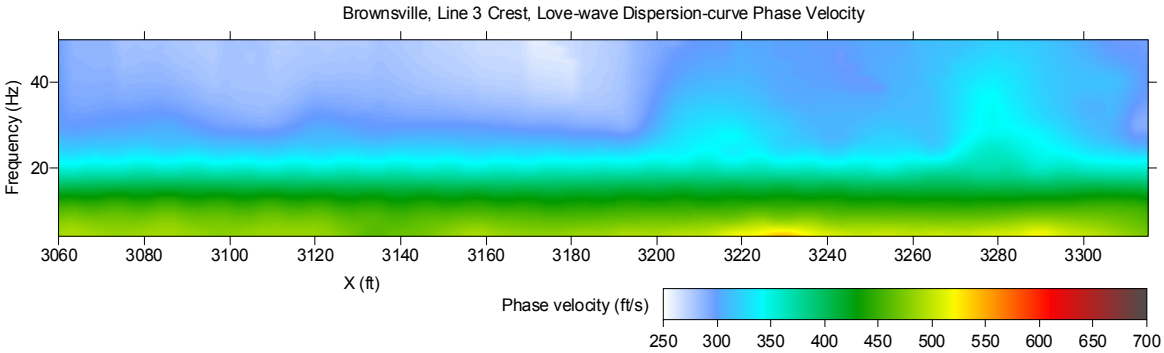

Figure 104. Love-wave dispersion-curve phase-velocity map estimated for line 3 by analyzing S-wave data.

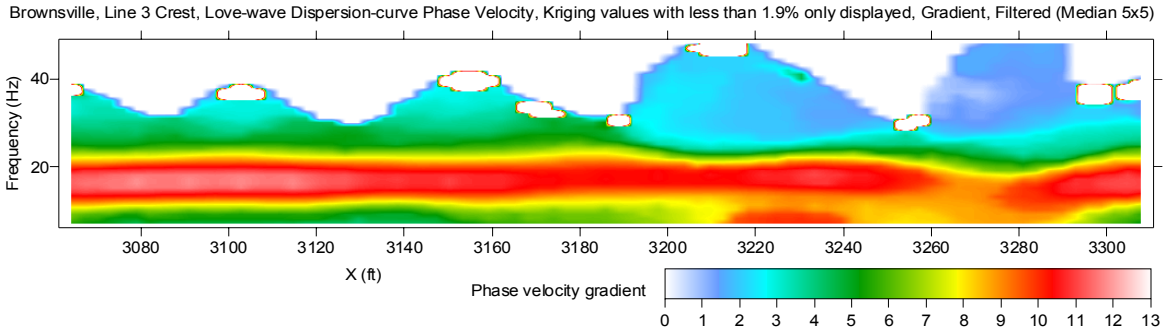

Figure 105. Love-wave dispersion-curve phase-velocity gradient map estimated for line 3 by analyzing S-wave data.

Site 4

P-wave First Arrivals

Compressional-wave data along the crest and toe were collected at site 4 in a fashion consistent with the previous three sites. Acquisition and processing methods and parameters were consistent for all sites to allow direct comparisons of the different levee sites and location at each levee site (toe and crest) without the need for equalization techniques. Signal-to-noise ratio on compressional-wave first arrivals was high enough to characterize most of the arrivals as instantaneous. Data quality was good with a strong apparent consistency in waveform and general velocity structure in comparison to data sets from other sites. Model convergence and a good 2-D refraction-tomography Vp solution was easily obtained in part due to the high quality of the first arrivals on P-wave data shot gathers along the crest (Figure 106).

S-wave First Arrivals

Shear-wave data is notorious for possessing narrower bandwidth and therefore more emergent first arrivals in comparison to equivalent compressional-wave data from a particular site. These characteristics were observed on shear-wave data from all sites occupied during this study. After both automatic and manual first-arrival picking was complete, a 2-D refraction-tomography Vs solution was obtained for the data acquired along the crest (Figure 107). At this stage of this research project only crest data were inverted to a velocity profile because the characteristics of the toe data were extremely similar to the other sites and consistent with the crest information below the zone identified previously as related to basal compaction of the levee during and post-construction.

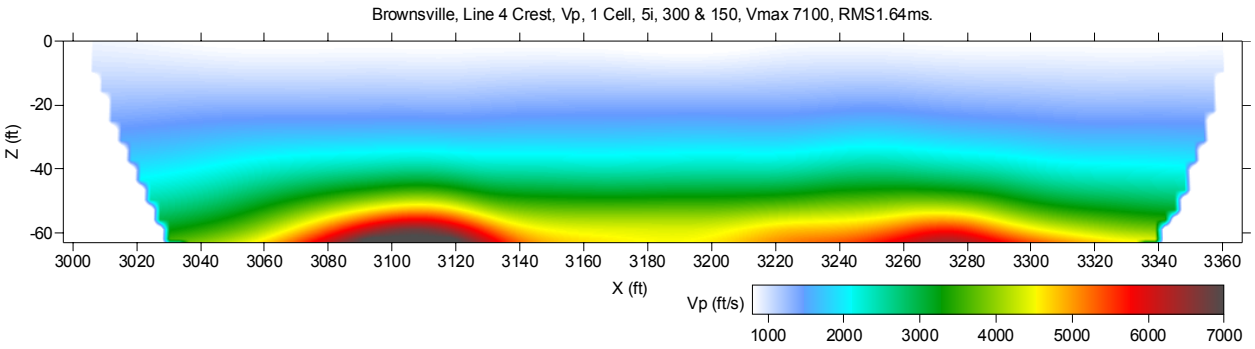

Figure 106. P-wave velocity model estimated for line 4 at the crest of the levee by analyzing S-wave-data first-arrival times using refraction-tomography software.

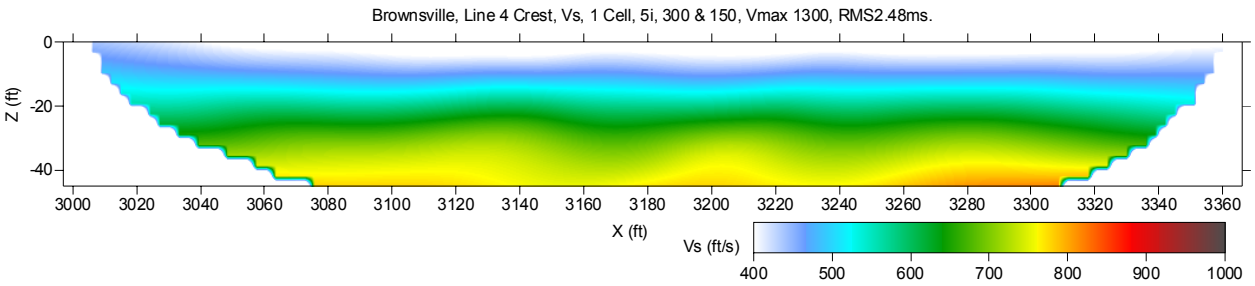

Figure 107. S-wave velocity model estimated for line 4 at the crest of the levee by analyzing S-wave-data first-arrival times using refraction-tomography software.

Rayleigh Wave

As with all the levee sites investigated during this study, Rayleigh-style surface waves did not possess the necessary broad spectrum of energy, likely as a result of either levee geometry or near-surface conditions. With the consistent lack of higher-frequency fundamental-mode surface-wave energy (and thus no Vs information within the levee itself), the MASW method was limited to providing estimations of the Vs from depths between 25 and 65 ft below the crest of the levee (Figure 108).

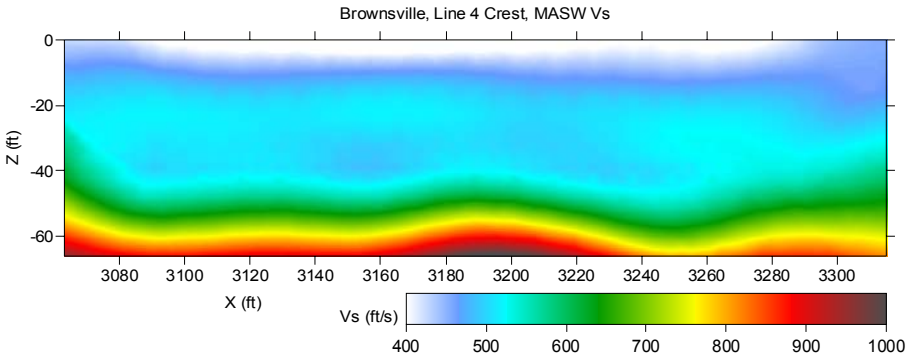

Figure 108. S-wave velocity model estimated for line 4 at the crest of the levee by analyzing P-wave-data surface-wave using the MASW method.

Love Wave

As with the other sites discussed so far, the presence of a relatively wide range of frequencies within the surface-wave packet on S-wave data (Love wave) is encouraging and may indicate information about the upper 15 ft at these sites might be rendered from seismic data after all. Assuming the same axiom that relates frequency to depth of penetration for Rayleigh waves is true for Love waves, then it can be stated with good confidence that Love waves appear to be the only type of seismic energy tested on this levee that have the potential to provide Vs sampling within the levees. The technique for inverting Love waves is under development and therefore no depth estimations as a function of shear velocity can be assigned for these data. For that reason only dispersion-curve analysis was performed to locate anomalous zones. A 2-D Love-wave dispersion curve was calculated from data collected along the top of the levee (Figure 109). A gradient map for these data was calculated and filtered to emphasize potential anomalous zones (Figure 110). Using a gradient map in this fashion assumes that significant lateral changes in velocity are not consistent with construction practices for levees.

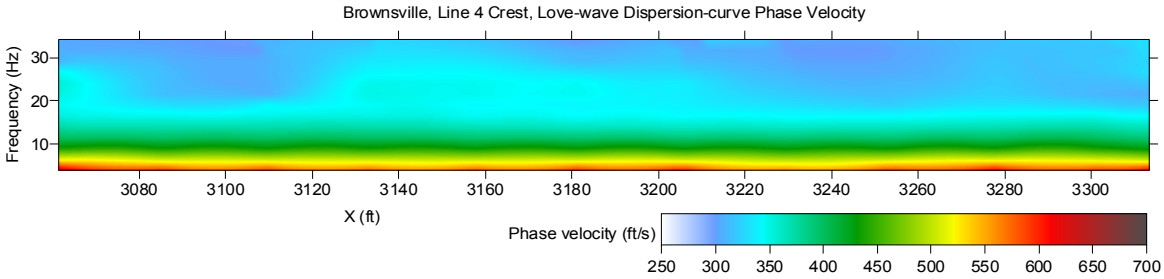

Figure 109. Love-wave dispersion-curve phase-velocity map estimated for line 4 by analyzing S-wave data.

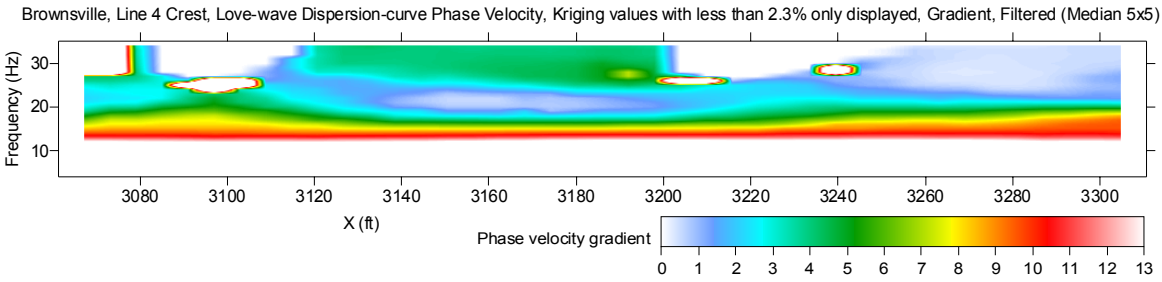

Figure 110. Love-wave dispersion-curve phase-velocity gradient map estimated for line 4 by analyzing S-wave data.

Site 5

P-wave First Arrivals

Compressional-wave data along the crest and toe were collected at site 5 in a fashion consistent with the previous four sites. Acquisition and processing methods and parameters were consistent for all sites to allow direct comparison of the different levee sites and locations at each levee site (toe and crest) without the need for equalization techniques. Signal-to-noise ratio on compressional-wave first arrivals was high enough to characterize most of the arrivals as instantaneous. Data quality was good with a strong apparent consistency in waveform and general velocity structure in comparison to data sets from other sites. Sites 4 and 5 were on younger levees (more recent construction methods and more uniform, less expansive clay composition) with a much more consistent velocity structure and therefore a more consistent first-arrival pattern. Model convergence and a good 2-D refraction-tomography Vp solution was easily obtained, in part due to the high quality of the first arrivals on P-wave data shot gathers acquired along the levee crest (Figure 111).

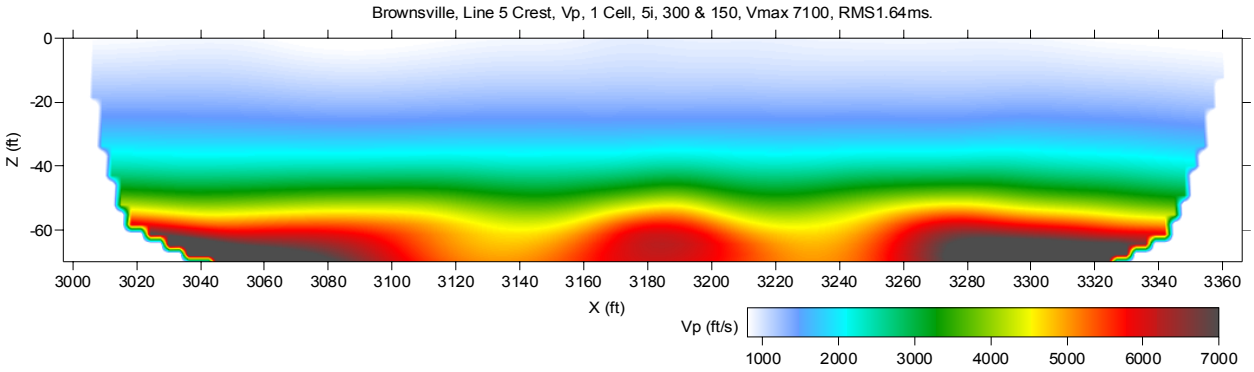

Figure 111. P-wave velocity model estimated for line 5 at the crest of the levee by analyzing S-wave-data first-arrival times using refraction-tomography software.

S-wave First Arrivals

Regardless of the much stiffer material properties measured in borehole samples of the levee at site 5, the shear-wave data possess a narrower bandwidth and therefore more emergent first arrivals than their equivalent compressional-wave data. As previously noted, these characteristics can be observed on shear-wave data from all sites occupied during this study. After completion of both automatic and manual first-arrival picking, a 2-D refraction-tomography Vs solution was obtained for the data acquired along the crest (Figure 112). At this stage of this research project, only crest data were inverted to a velocity profile because the characteristics of the toe data were extremely similar to the other sites and consistent with the crest information below the zone identified previously as related to basal compaction of the levee during and post-construction.

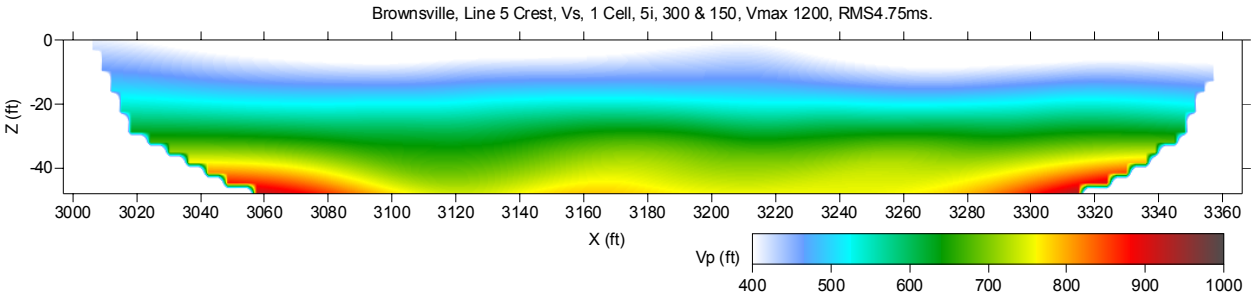

Figure 112. S-wave velocity model estimated for line 5 at the crest of the levee by analyzing S-wave-data first-arrival times using refraction-tomography software.

Rayleigh Wave

As with all the other levee sites investigated as part of this study, Rayleigh-style surface waves at site 5 did not possess the necessary frequency range to fully sample the depth range of primary interest. This ineffectiveness was likely the result of either levee geometry or near-surface conditions. With the consistent lack of higher-frequency fundamental-mode surface-wave energy (and thus no Vs information within the levee itself), the MASW method was limited to providing estimations of the Vs from depths between 25 ft and 65 ft below the crest of the levee (Figure 113).

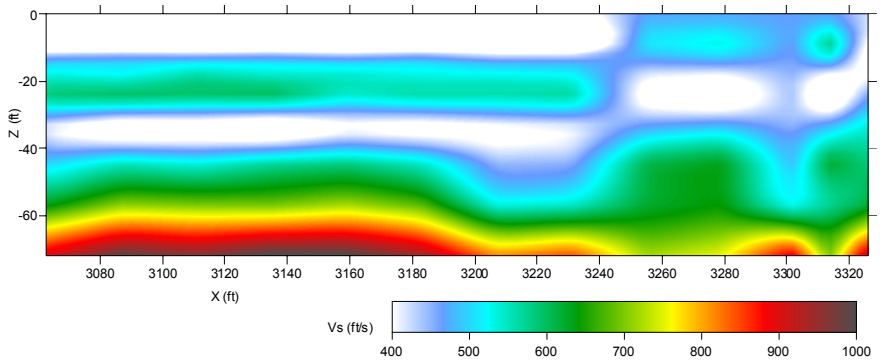

Figure 113. S-wave velocity model estimated for line 5 at the crest of the levee by analyzing P-wave-data surface-wave using MASW method.

Love Wave

A relatively wide range of frequencies within the surface-wave packet on S-wave data (Love wave) provided significant encouragement in evaluating various seismic energy modes for characterizing the upper 15 ft at sites like these around this area. Assuming the same axiom that relates frequency to depth of penetration for Rayleigh waves is true for Love waves, it can be stated with good confidence that Love waves appear to be the only type of seismic energy tested on this levee system that has the potential to measure Vs distribution within the levees. The technique for inverting Love waves is under development and therefore no depth estimations as a function of shear velocity can be assigned for these data. For that reason only dispersion-curve analysis was performed to locate anomalous zones. A 2-D Love-wave dispersion curve was calculated from data collected along the top of the levee (Figure 114). A gradient map for these data was calculated and filtered to emphasize potential anomalous zones (Figure 115). Using a gradient map in this fashion assumes that significant lateral changes in velocity are not consistent with construction practices for levees.

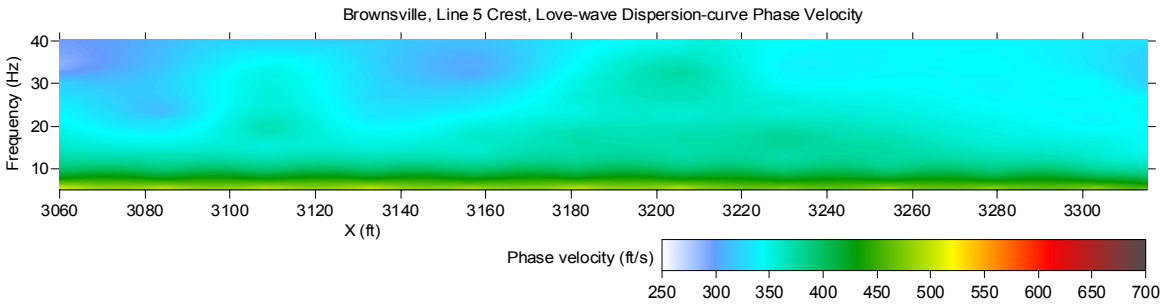

Figure 114. Love-wave dispersion-curve phase-velocity map estimated for line 5 by analyzing S-wave data.

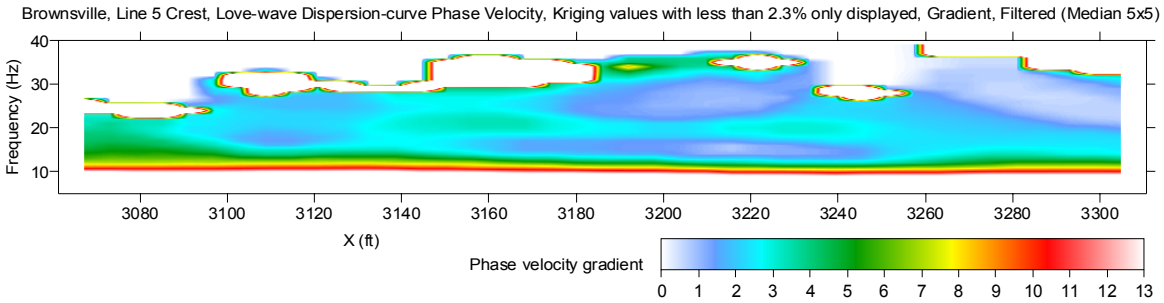

Figure 115. Love-wave dispersion-curve phase-velocity gradient map estimated for line 5 by analyzing S-wave data.

Other Processing

JARS P-wave Tomography

The JARS method was developed to overcome the wide range of equally possible solutions for the inverse refraction-tomography problem. It uses an abundant amount of *a priori* information from the MASW method as a reference for selecting one of the many possible refraction-tomography solutions as an initial model. The JARS method was proposed as a superior first-arrival methodology for application to the crest of the levees. However, with the lack of higher-frequency fundamental-mode surface-wave energy, the method was severely limited by the lack of Vs information in the top 20-25 ft—the actual levee core—thereby eliminating any improvement in the initial refraction model within the key depth range of interest.

At the Toe of the Levee (sites 2 and 3)

At the toe of the levees the JARS method was applied with a great deal of success because MASW at the toe provided a wide enough range of Vs values throughout the upper 50 ft to define an initial model (Figure 116a). This success was due in large part to the richness of the high-frequency fundamental-mode surface-wave energy recorded in the relatively undisturbed material beneath the toe lines (Figure 103a). Using the MASW results, a JARS Vp solution for the toe at site 2 with good convergence was formulated (Figure 116b). The MASW Vs results at the toe for site 3 did not possess sufficient depth coverage to fully develop the initial model at that site (Figure 102). Fortunately, the MASW Vs results for the crest at site 3 had the deeper information missing on the toe Vs field and by appending the Vs results from the crest onto the toe cross section (Figure 103b), a sufficiently encompassing range of *a priori* information was available to appropriately feed the JARS method (Figure 117a). Using a Vs model constructed in that fashion provided for a good JARS Vp solution for the toe at site 3 (Figure 117b). Incorporating this JARS Vp solution as the initial model for the standard P-wave refraction tomography inversion solution (Figure 100b) demonstrates that both solutions are possible to the inverse refraction tomography problem (their RMS error is very small: 2.19 and 2.17 ms) and a consistent overall nature. This comparison exemplifies how uniquely different equally possible refraction solutions may be from each other for a single site using the same input data. Still, because the JARS method

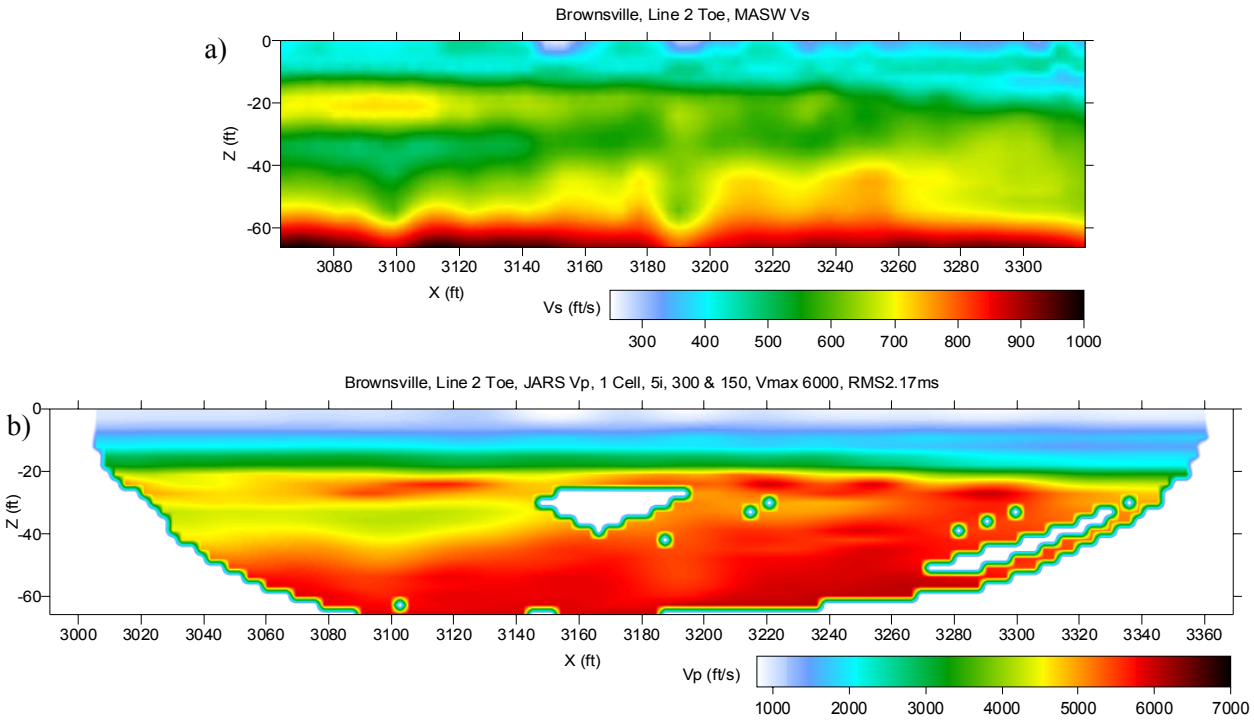

Figure 116. Application of JARS method at the toe of line 2, a) S-wave velocity model estimated at the toe of the levee by analyzing P-wave-data surface-wave using the MASW method, b) JARS P-wave velocity model estimated by analyzing P-wave-data first-arrival times and using a reference P-wave velocity model derived from the S-wave velocity model.

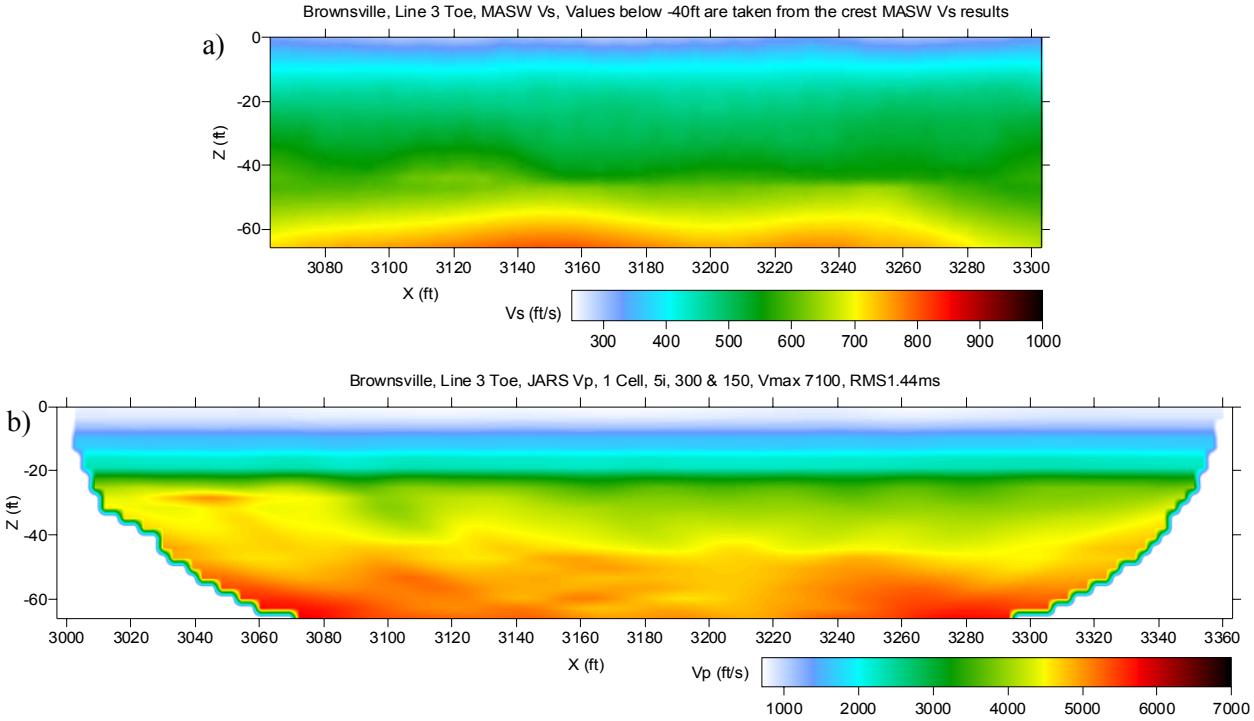

Figure 117. Application of JARS method at the toe of line 3, a) S-wave velocity model estimated at the toe of the levee by analyzing P-wave-data surface-wave using the MASW method, b) JARS P-wave velocity model estimated by analyzing P-wave-data first-arrival times and using a reference P-wave velocity model derived from the S-wave velocity model.

chooses a solution based on *a priori* information obtained from MASW, while the standard refraction-tomography solution does not use any *a priori* information in selecting a solution, it is reasonable to suggest the JARS solution is likely closer to the truth. Furthermore, the JARS solution looks more realistic from geologic perspective for this site.

At the Crest of the Levee (site 1)

Even though MASW did not successfully produce a velocity image of the upper 20 ft beneath the crest profile, an attempt to apply the JARS method at the crest of the levee was made using the reliable Vs data from the MASW analysis with extrapolation into the no-data zone. This extrapolation of deeper Vs information into the no-data zone within the levee was accomplished using Kriging (a very reliable geostatistical method). Because the Vs model generated by the MASW method is only used as an initial model, this extrapolation, even though not an accurate representation of the levee materials, does provide a starting point for the iterative inversion process used by the JARS method. Using the expanded Vs data set, a JARS solution was obtained for line 1 (Figure 118). As with any iterative inversion technique, many possible solutions exist for a data set; the one provided here represents the most likely considering all *a priori* data. Even though this solution honors all *a priori* data and has an RMS error of only 1.55 ms (meaning the data and model are an excellent fit), and therefore represents a possible solution, it does not appear realistic considering the known internal structural characteristics of the levees in this area. This excellent fit to the data—but a resultant unrealistic solution—suggests our attempt to interpolate into shallow areas without measured values was not only unreliable, but the estimates were sufficiently far from the "truth" that even with multiple iterations beyond the initial model, this starting point was sufficiently distant from the true values so that the real solution was outside the bounds of the method.

Refraction tomography is a well proven and effective way to estimate compressional-wave velocity structure of the earth from first-arriving seismic energy. However, like any inversion method, the results are only as reliable as the input data and the volume and redundancy of that data. Key to any

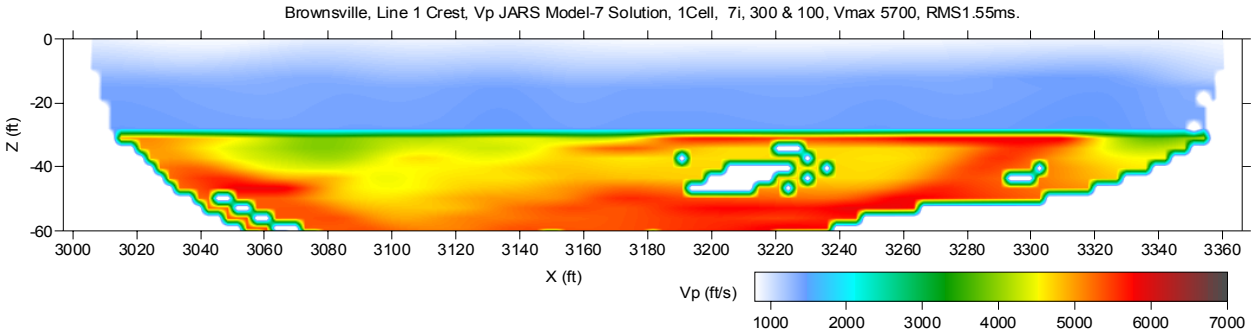

Figure 118. Application of JARS method at line 1 levee crest estimating a P-wave velocity model by analyzing P-wave-data first-arrival times and using reference P-wave velocity model derived from S-wave velocity model.

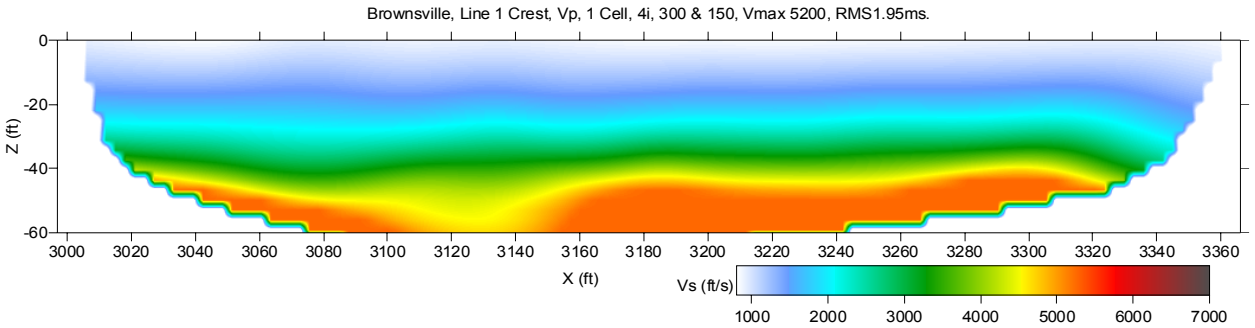

Figure 119. P-wave velocity model estimated at line 1 levee crest by analyzing P-wave-data first-arrival times using refraction-tomography software.

inversion is the initial model. To demonstrate the wide range of possible refraction-tomography solutions with these data the JARS Vp solution (Figure 118) can be compared to the standard refraction-tomography solution for the crest at site 1 (Figure 119). Although both are possible, neither of these solutions is considered to be likely due to a lack of abundant *a priori* information.

Discussion of Data and Processing at Each Site: Trip 2

Site 1

P-wave First Arrival

Data from the second trip possess notably different seismic characteristics than those observed on data acquired about a year previously during the first trip. Spectra were broader and waveforms were much more impulsive, supporting a higher signal-to-noise ratio (Figure 120, compare to Figure 44, p. 30). This difference can only be attributed to the near-surface materials. Acquisition and processing methods, equipment, and parameters were as near identical as possible for both surveys. After inquiring, the most likely reason for this difference is saturation of near-surface sediments. During the fall months a significantly larger volume of rain fell than in the same time period throughout most of the previous decade. These data were acquired in part to confirm that the change in near-surface velocities observed at site 2 were consistent for the area and not specific to site 2.

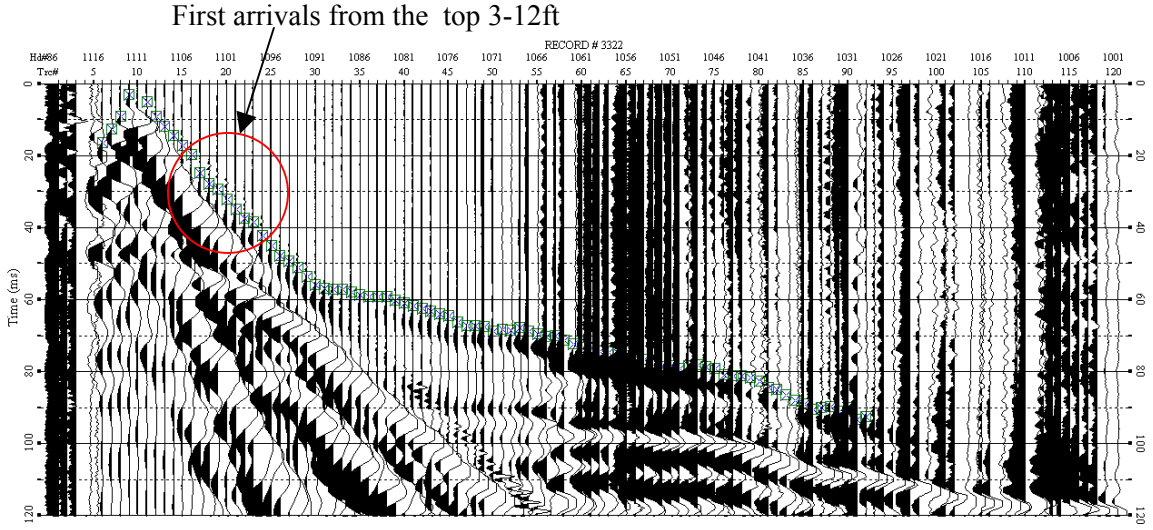

Figure 120. Estimation of first-arrivals times on a P-wave seismic data with source located at station 1111 (horizontal coordinate at 3333 ft) at site 1 in 2004.

Refraction-tomography Vp analysis from the 2003 and 2004 seismic data sets resulted in Vp images that were extremely similar with respect to the overall velocity structure and associated variability in materials as evidenced by changes in velocity (Figure 121). Considering the clear difference in seismic character, a better estimate of possible changes in the Vp properties between the 2003 and 2004 surveys was necessary. Therefore, a velocity-increment map with respect to the 2003 Vp measurement was calculated to more closely identify changes in velocity between the two survey dates (Figure 121c). A velocity increase between 3 and 8% is evident for most of the top 5-8 ft and about 3% at a 30-ft depth, with the exception of the 3130-3180 ft offset range where the velocity decreases around 8-10%.

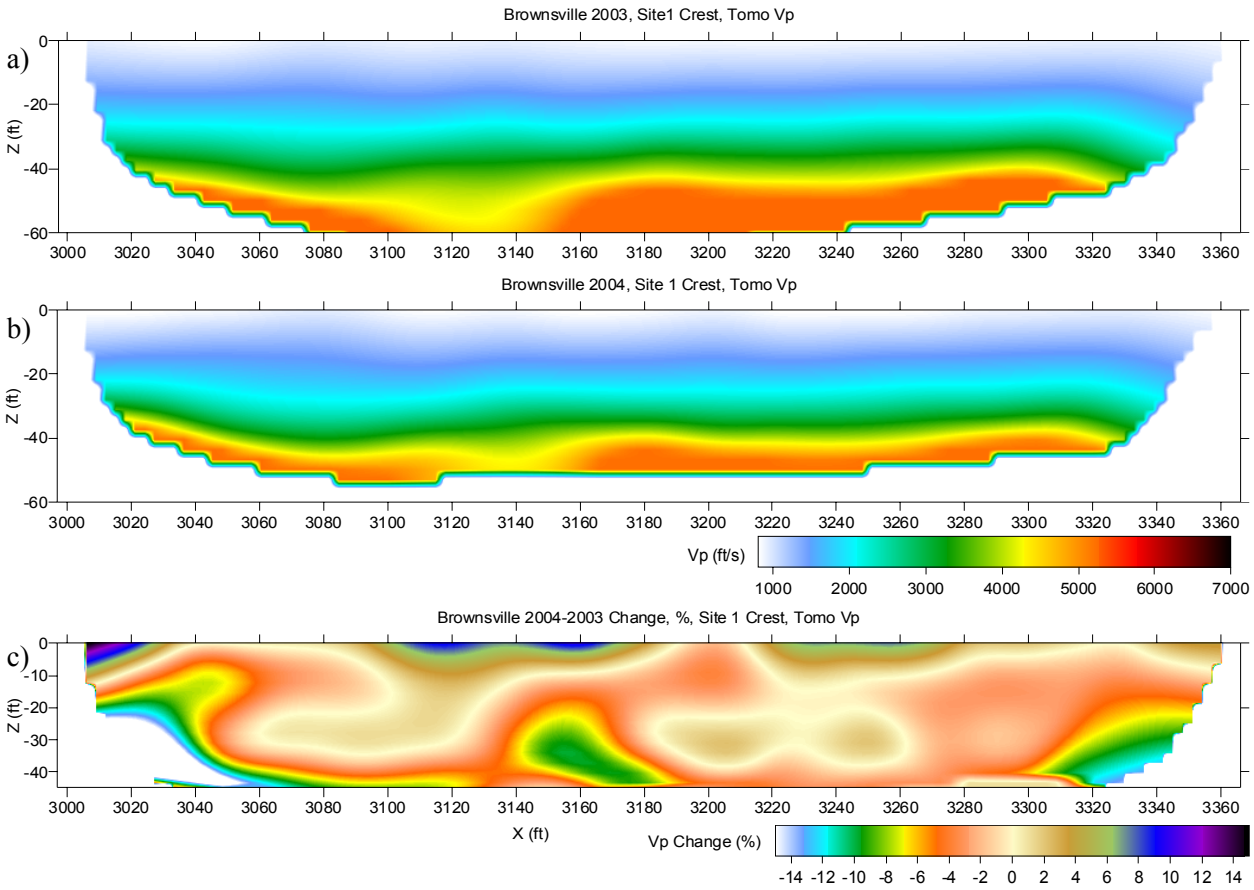

Figure 121. P-wave velocity models estimated at the crest of the levee at site 1 analyzing P-wave-data first-arrival times using refraction-tomography software, a) P-wave velocity model obtained from the seismic data acquired in 2003, b) P-wave velocity model obtained from the seismic data acquired in 2004, c) difference between the P-wave velocity models obtained in 2003 and 2004.

Rayleigh Wave

With the change in near-surface seismic characteristics came a marked improvement in the bandwidth of the surface-wave data as well. This improvement was most clearly seen in the increased high-frequency components of the fundamental-mode Rayleigh-wave energy. The availability of a wide range of both low- and high-frequency fundamental-mode energy in the dispersion curves from the 2004 seismic data provided a greatly improved and detailed Vs image of the levee (Figure 122a). The difference is extremely evident when compared directly to the Vs image from the 2003 seismic data (Figure 122b).

This success of MASW at site 1 in calculating the Vs using surface waves provides a great deal of optimism that the near-surface conditions were the limiting factor during 2003 and not the geometry of the levee. With this observation comes the realization that it might still be possible to use MASW as a tool for estimating Vs within levees susceptible to changes in stiffness due to long-term or seasonal changes in core-moisture content. Reconnaissance surveys designed to identify areas with reduced shear velocity, and therefore reduced rigidity, could be susceptible to internal erosion during high-water events.

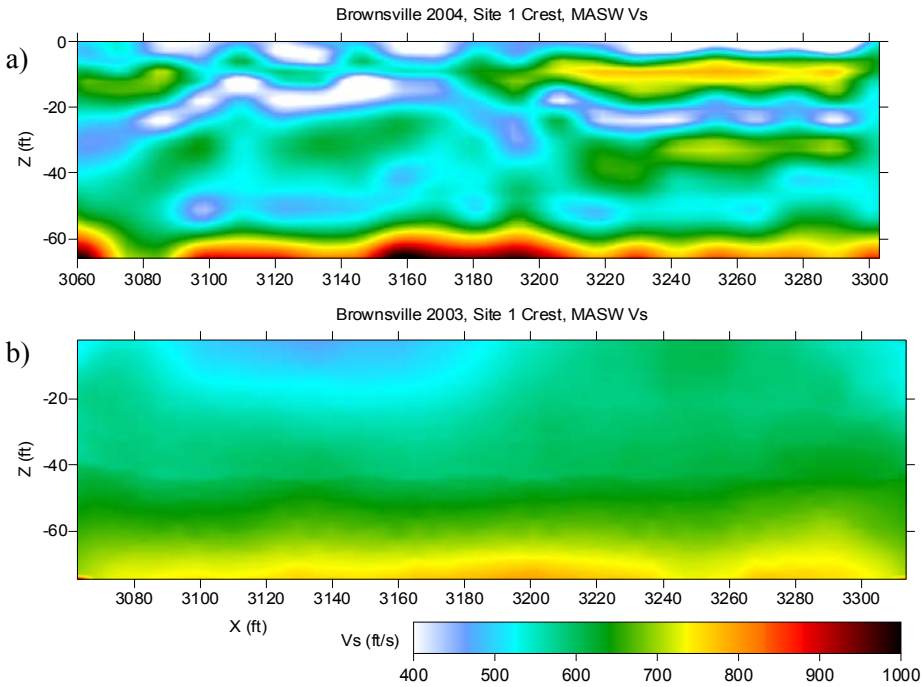

Figure 122. S-wave velocity models estimated at the crest of the levee at site 1 by analyzing P-wave-data surface-wave using MASW method acquired in, a) S-wave velocity model obtained from the seismic data acquired in 2004, b) S-wave velocity model obtained from the seismic data acquired in 2003.

Site 2

P-wave First Arrival

The lion's share of seismic testing during the 2004 component of the study was undertaken at site 2. Site 2 was the location of the ponding experiment designed to evaluate the potential of the levee to absorb water during a high-water event, allowing internal erosion of the core, such that failure could result. Seven surveys throughout the multi-day test were acquired, each with compressional and shear recorded along two profiles, one along the south edge of the crest nearest the pond and one along the north side. First-arrivals were picked on all seismic data automatically and then manually edited prior to population of the database. A 2-D refraction tomography Vp solution was obtained for all seven time slices both on the south line (Figure 123a-123g) and on the north line (Figure 124a-124g). Refraction-tomography Vp images of the south and north lines do not appear to suggest compressional-wave velocity is terribly sensitive to material changes that occurred in this segment due to infiltration of water. Based on these data alone, it is also possible that the skin layer covering the core acted to repel any water from making its way into the levee, and therefore no changes in Vp simply means no moisture penetrated the skin layer.

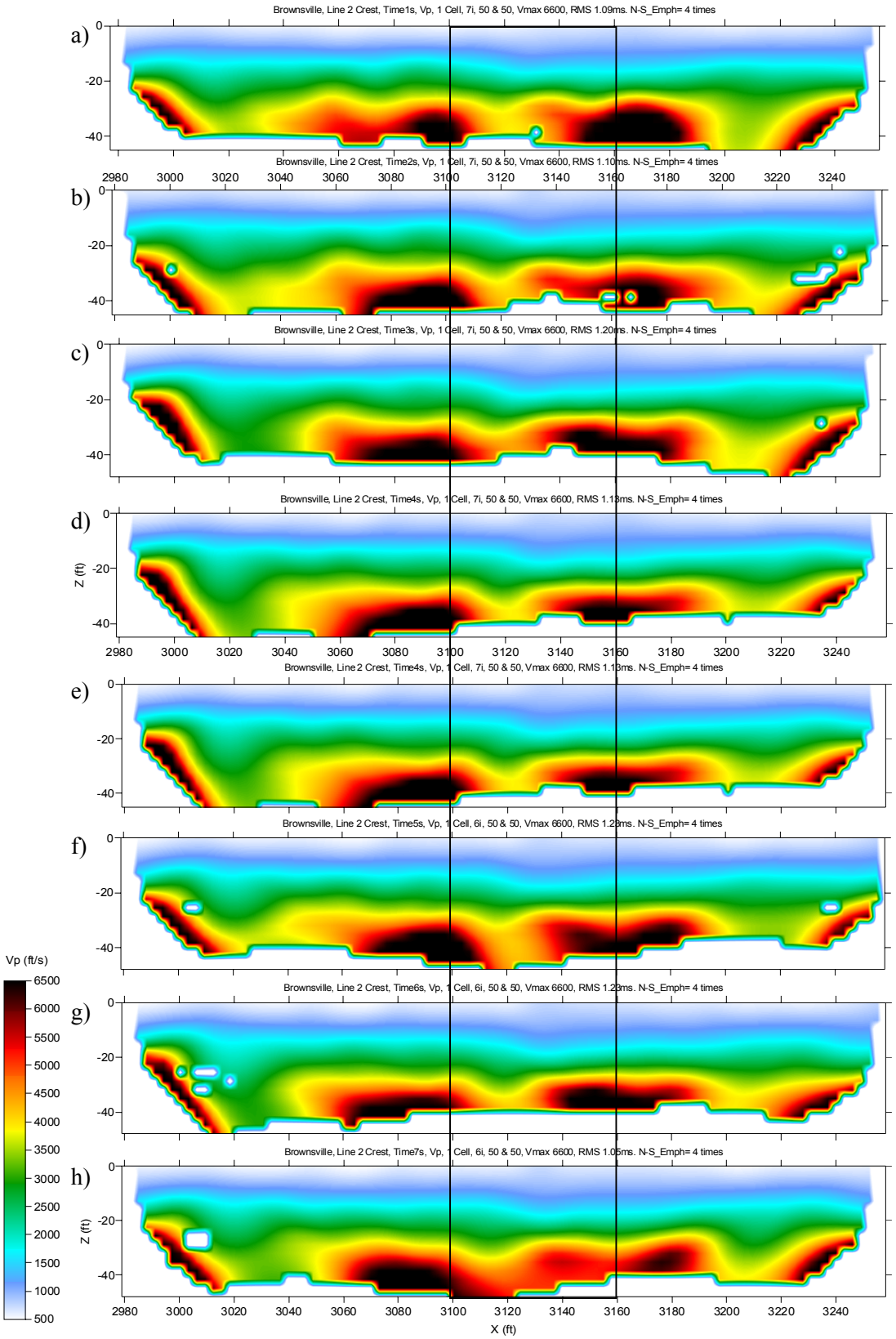

Figure 123. Refraction-tomography p-wave velocity models estimated at the south edge of the crest on site 2 by analyzing first-arrival times estimated from P-wave data a) base survey, and at the following times after beginning of ponding: b) 24 hours, c) 36 hours, 4) 48 hours, e) 60 hours, f) 72 hours, and g) 84 hours.

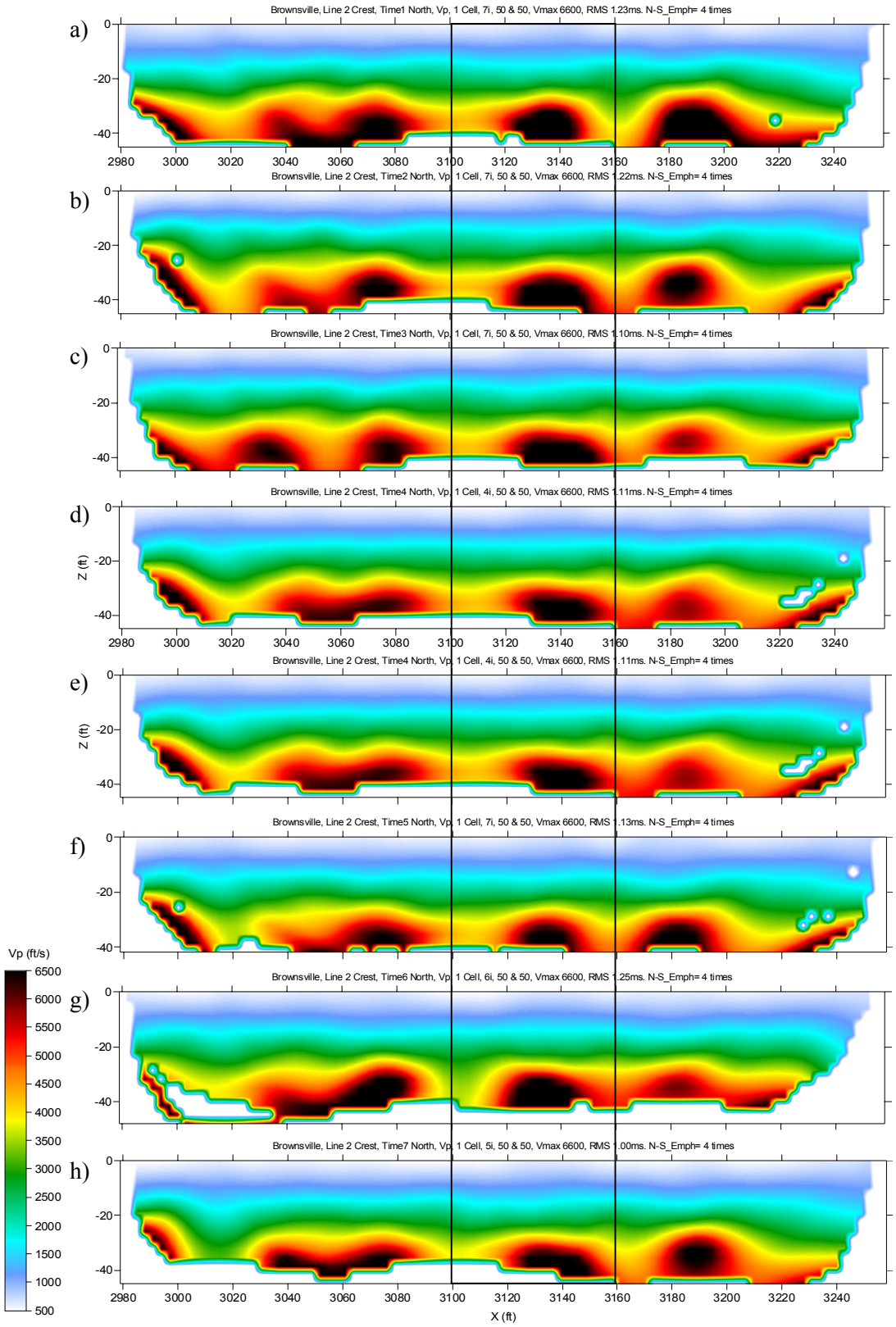

Figure 124. Refraction-tomography P-wave velocity models estimated at the north edge of the crest on site 2 by analyzing first-arrival times estimated from P-wave data a) base survey, and at the following times after beginning of ponding: b) 24 hours, c) 36 hours, 4) 48 hours, e) 60 hours, f) 72 hours, and g) 84 hours.

To better estimate possible changes in the Vp properties, velocity-increment maps with respect to the base-line Vp measurement were calculated (Figure 125). An increase in velocity is evident for the top 5 ft along the crest adjacent to the ponding experiment (3060-3160 ft) for time slices 2-4. Because the water had not reached the crest yet at the time of those surveys, it is most likely this increase in velocity is due to the multiple pass with the hammer and plate compacting the near-surface sediments. It was not until time slice 5 that the pool height reached maximum and changes in material properties in the upper 5 ft were possible as a result of the presence of water. Further Vp increases at time slices 5-7 at locations 3120-3140 ft could well be due to the presence of water against the sides of the levee.

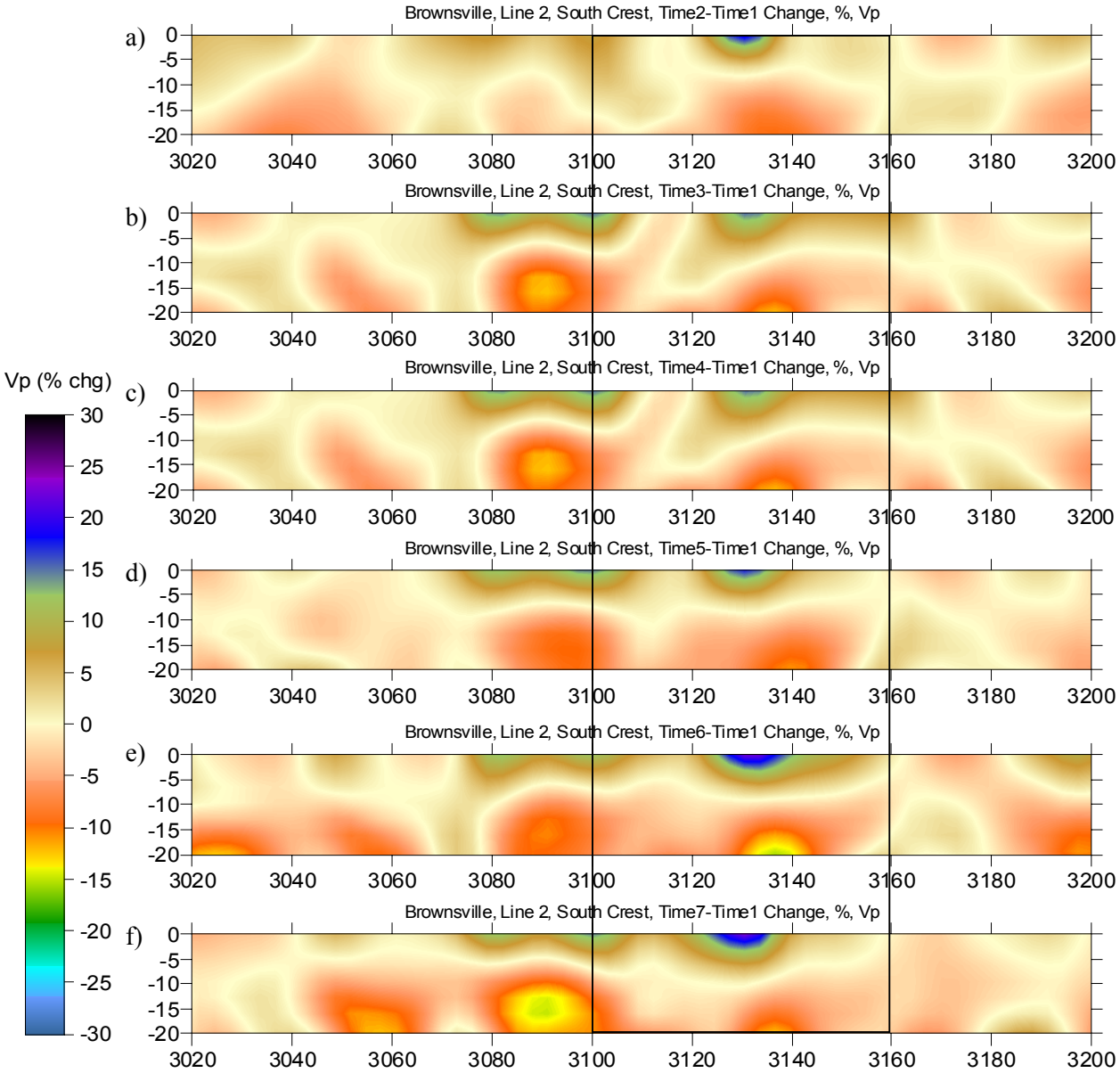

Figure 125. Refraction-tomography P-wave velocity-model increments with respect to the base survey estimated at the south edge of the crest on site 2 at the following times after beginning of ponding: b) 24 hours, c) 36 hours, 4) 48 hours, e) 60 hours, f) 72 hours, and g) 84 hours.

S-wave First-arrival Analysis

A shear-wave shot gather possessed greater signal-to-noise and more impulsive first arrivals than those observed on previous surveys at this site. For each compressional-wave survey (seven in all) an equivalent shear-wave survey was acquired. With the success of MASW to calculate the Vs for the near surface, especially the upper 10 ft or so of the levee, the shear-wave data have not been fully processed. However, with the much improved quality of the Rayleigh-wave and shear-wave data sets, Vs calculated from refraction-tomography using shear-wave data will be an excellent way to evaluate the accuracy of both methods in this setting. With the data being collected in transverse mode, both polarities of shear energy were recorded, which should provide the opportunity to improve signal-to-noise by canceling a significant amount of the source-generated and mode-converted compressional-wave energy.

Rayleigh Wave

Compressional-wave shot gathers from the seismic data acquired along the levee crest were analyzed for dispersive surface-wave energy using the MASW method. In contrast with the 2003 data set (Figure 53, p. 35), it was possible to pick a wide range of frequencies and phase velocities from fundamental-mode dispersion curves (Figure 126).

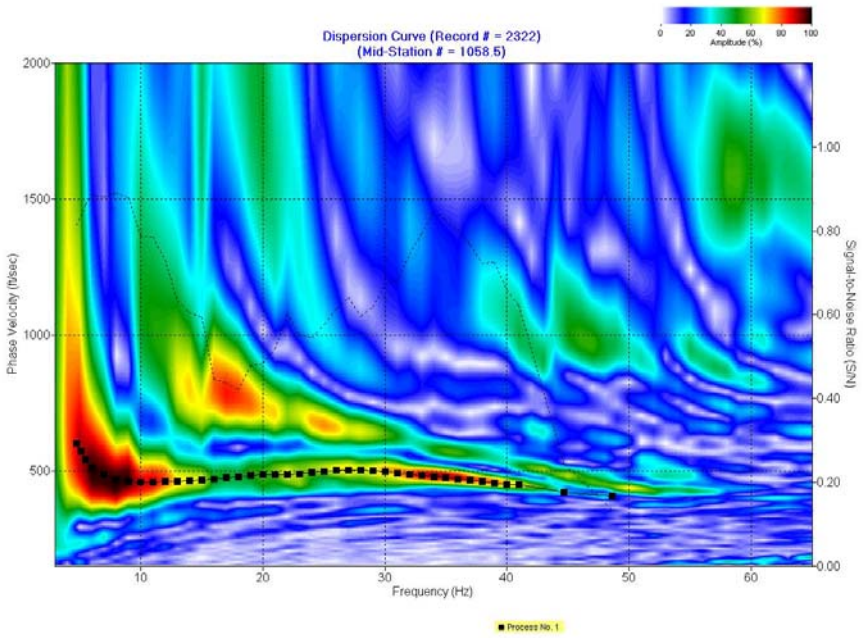

Figure 126. Dispersion-curve analysis of P-wave-data surface-wave using the first 40 traces from shot record 2322.

MASW Vs data calculated along the south seismic line for all seven time slices are of excellent quality and provide a consistent and logical progression of velocity change within the levee (Figure 127a-127g). As well, MASW Vs data were calculated for data from the north seismic line at each of the seven time slices (Figure 128b-128g). An interesting lack of lower-frequency surface-wave energy was observed in seismic data from the north side of the levee crest for the first or baseline survey prior to ponding on the south. This lack of low-frequency energy is still unexplainable, but it did prohibit the generation of a Vs profile for the baseline or time zero slice (would have been Figure 128a).

Love Wave

As with the shear-wave refraction tomography, no analysis was done to evaluate the Love wave energy on shear-wave data collected along the crest during the ponding experiment. The data are available and will be analyzed once technology exists to exploit the dispersive characteristics of the Love wave and invert for Vs.

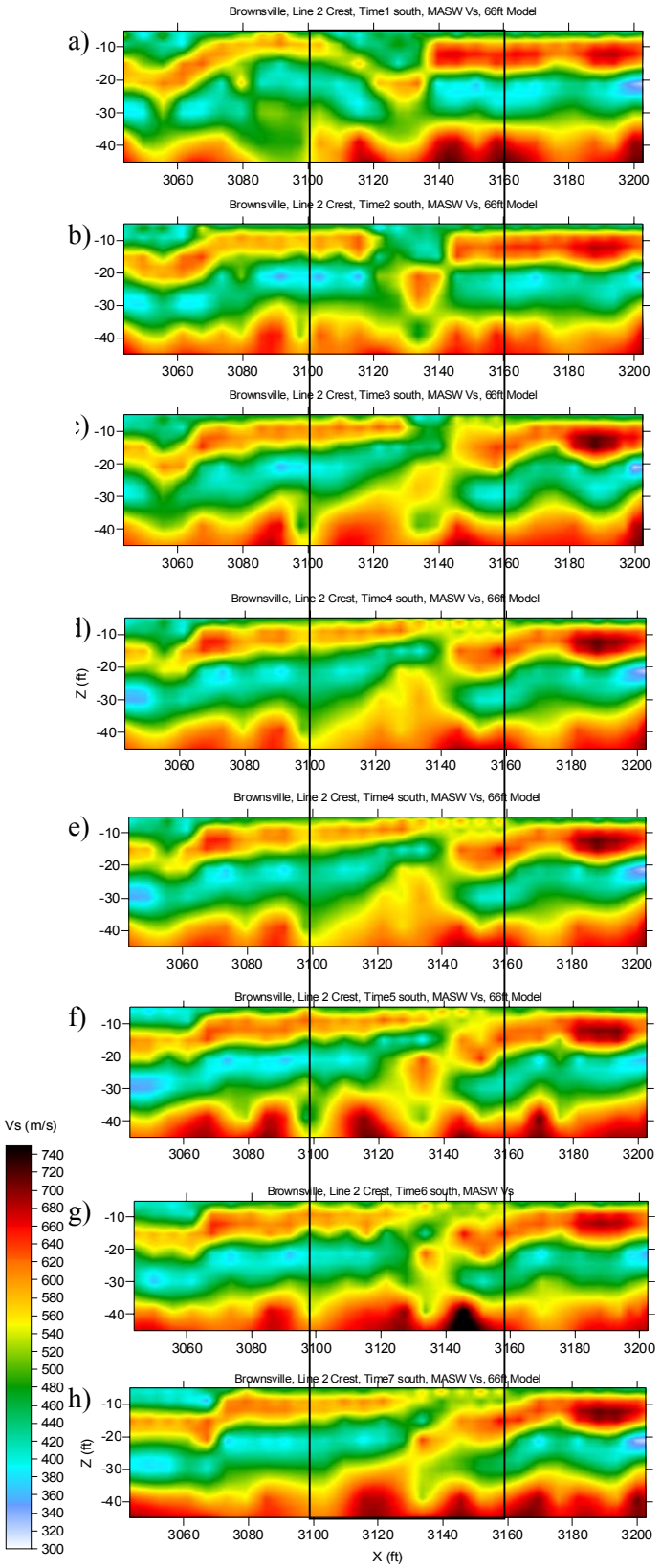

Figure 127. MASW S-wave velocity models estimated at the south edge of the crest on site 2 by analyzing surface wave from P-wave data a) base survey, and at the following times after beginning of ponding: b) 24 hours, c) 36 hours, 4) 48 hours, e) 60 hours, f) 72 hours, and g) 84 hours.

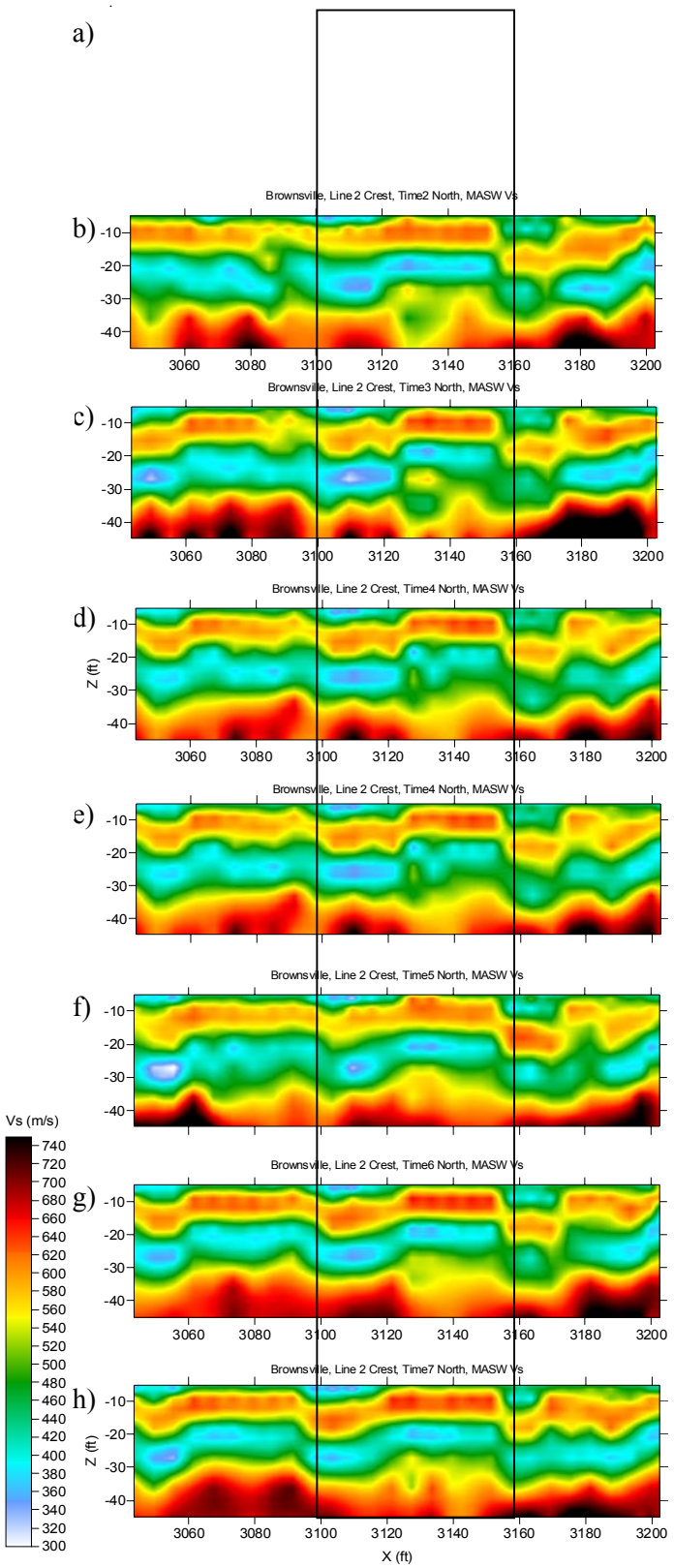

Figure 128. MASW S-wave velocity models estimated at the north edge of the crest on site 2 by analyzing surface wave from P-wave data a) base survey, and at the following times after beginning of ponding: b) 24 hours, c) 36 hours, 4) 48 hours, e) 60 hours, f) 72 hours, and g) 84 hours.

Site 4

P-wave First Arrival

Compressional-wave data were recorded at site 4 to allow comparison and evaluation of any relative changes in velocity that could be related to changes in the near surface, possibly related to increased precipitation as speculated to be the cause of reduced water infiltration into the levee during the ponding experiments and the observed increase in seismic velocity. Data were acquired in a fashion as consistent with the 2003 trip as possible, with data processing matched for both data sets to avoid any parameters or operations that might be unique to either data set. Based on field analysis, a slight increase in velocity consistent with that observed at sites 1 and 2 was also observed at site 4.

Rayleigh Wave

Improvements in the bandwidth in the surface-wave energy were sufficient to allow calculation of the fundamental-mode dispersion curve for energy within the levee. With the availability of a wide range of both low- and high-frequency fundamental-mode energy, the dispersion curves from the 2004 seismic data provided a greatly improved and detailed Vs image of the levee. The difference is evident when compared directly to the Vs image from the 2003 seismic data.

This success of MASW at site 4 calculating the Vs using surface waves compounds the optimism that near-surface conditions were the limiting factor during 2003 and not the geometry of the levee. As noted previously, with this observation comes the realization that it is likely that MASW could be used as a tool for estimating Vs within levees susceptible to changes in stiffness due to long-term or seasonal changes in core-moisture content.

6—RESULTS/DISCUSSION

These investigations targeted seismic velocities, both absolute and relative (changes). Seismic velocities of levee materials were estimated and compared both site to site and within specific sites. A unique study of surface-wave phase velocity was conducted observing phase variations in the expected (for consistent material characteristics) uniform wavetrain at and near resonance (resonance in this case is controlled by levee height and surface-wave velocity of the materials: wavelength). This surface-wave study was conducted in hopes of identifying anomalous zones where changes in phase velocity might be indicative of reduced or increased material strength. Seismic velocities were measured based on travel time between adjacent sets of receivers.

Compressional-wave velocities were for the most part within a “reasonable” range for this setting; however, shear-wave velocities were estimated to be significantly higher than expected based on both levee materials and equivalent compressional-wave velocities. Shear velocities were consistently measured with a Vp/Vs ratio around 2, which is generally more characteristic of consolidated rocks. Ratios for unconsolidated fill materials such as these are generally expected to fall in the 3 to 5 range. This higher than expected ratio could result from measuring mode-converted shear rather than the primary direct shear arrival. It is also possible this higher than expected shear velocity could be real and related to these earth materials and the mechanical compaction used to construct these levees.

Estimates of shear velocity using both refraction tomography and slope intercept methods provided shear velocities that were unrealistically high and with offset dependent arrival patterns extremely consistent with the faster compressional-wave arrivals. Calculating shear-wave velocity from inverted surface waves was strongly dependent on bandwidth and percentage of higher-mode energy recorded. During the first survey ground conditions were not conducive to producing and/or recording broadband surface waves. Therefore, no confident shear-wave velocity sections were produced. On the

second trip near-surface conditions had sufficiently changed to allow sufficient broadband surface wave that a 2-D shear wave profile could be produced for the levee core.

Velocity anomalies within the levee were detected at each of the three Retamal levee sites. Distribution and range of values for these anomalies are consistent with variations in material types used during construction and the construction processes itself. It is not clear that velocity information alone will be sufficient to identify areas with a high density of cracks, which could be present as a result of the dewatering during drought of the expansive clays used in some places during core construction. However, it does seem likely that reduction in the material stiffness of the levee core could be used to identify failure risk areas with a relatively high resolution. Discontinuities in the levees associated with cracks seem to interfere with the otherwise uniform propagation of surface waves through the levee. These disturbances, once fully understood, could provide relatively accurate locations of weak zones within the core material.

Problems and pitfalls associated with using seismic techniques to estimate velocities intended to help characterize levee competence do exist and require significant attention to detail and understanding of the seismic wavefield arrival patterns (t-x) and significance of the spectral properties of each mode. In particular, mode converted shear-wave energy can lead to completely incorrect conclusion. Interpreting the propagation irregularities in surface-wave energy is not clearly understood and therefore not yet ready for use as a routine tool in interrogating levees. It must also be kept in mind that the geometry of the levee and the proximity of its basal contact with native earth can result in refracted first arrivals dominating the majority of close-offset traces where direct waves are normally expected.

Infiltration of water into the levee skin was identified on seismic data during the ponding experiment conducted during the second site visit at site 2 (oxbow lake site). Notable changes in both compressional and shear velocity can be associated with the infiltration of water dammed against the south levee face. Compressional-wave data suggest percolation of water into the native river valley sediments beneath the levee. Shear-wave velocity change was rapid, occurring at the very beginning of the simulation, and was isolated to one area within the pond. The isolated nature of the infiltration on the shear data could be related to a fracture/crack system opened as a result of the years of drought and dewatering of the core. An alternate possibility is a possible material inconsistency resulting from construction practices and locally mined core material.

7—CONCLUSIONS

Rapid, precise seismic methods for identifying areas worthy of further investigation could be developed for specific levee geometries and construction materials. Monitoring is by far the most confident and accurate application for seismic techniques on levees. Consideration must be given for changes in skin conditions due to seasonal variations in moisture. At the five sites studied on the Retamal and Main levees, LRGV compressional-wave velocity estimations were most accurate for all conditions using refraction tomography. Shear-wave velocity survey data were contaminated with mode-converted energy and therefore difficult to use to estimate material characteristics. Changes in near-surface conditions between the first and second survey resulted in an increase in recorded surface-wave bandwidth and, therefore, reasonably confident shear-wave velocity estimations within the levee. This change in surface conditions did not seem to change the arrival patterns observed on data recorded to capture first-order shear-wave first arrivals.

Considering the observations from the ponding experiment and five-site study, it is clear that the seismic tool can be used during flood events to detect more permeable areas where infiltration is active and the potential exists for failure. The most effective use of this tool would be as a monitoring system, where a baseline survey is acquired for all suspect areas; then, during a flood event, repeat surveys are run

using differencing techniques to detect weak points pre-failure. Complications from mode conversions and near-surface dependent propagation characteristics will limit the use of this tool in some settings until more advanced processing capabilities have been developed. Clearly, more information is present in the seismic wavefield than we currently have the capability to meaningfully extract. Optimized future use of this tool will depend to some degree on acquisition of baseline data sets that will allow full wavefield processing once the methods have been fully developed. Current research in these areas is active and incrementally moving forward with providing solution to many problems encountered in this study.

8—REFERENCES

Batzle, M., D. Han, and J. Castagna, 1999, Fluids and frequency dependent seismic velocity of rocks [Exp. Abs.]: Soc. Explor. Geophys., p. 5-8.

Berryman, J.G., P.A. Berge, and B.P. Bonner, 1999, Role of λ-diagrams in estimating prorosity and saturation from seismic velocities [Exp. Abs.]: Soc. Explor. Geophys., p. 176-179.

Chiu, S.K.L., E.R. Kanasewich, and S. Phadke, 1986, Three-dimensional determination of structure and velocity by seismic tomography: *Geophysics*, v. 51, p. 1559-1571.

Clement, W.P., S. Cardimona, A.L. Endres, and K. Kadinsky-Cade, 1997, Site characterization at the Groundwater Remediation Field Laboratory: *Leading Edge*, v. 16, p. 1617-1621.

Cottin, J.F., P. Deletie, H. Jacquet-Francillon, J. Lakshmanan, Y. Lemoine, and M. Sanchez, 1986, Curved ray seismic tomography–Application to the Grand Etang Dam (Reunion Island): *First Break*, v. 4, no. 7, p. 25-30.

Gaffran, Peter, 1999, WAC Bennett Dam Sinkhole Investigation Geophysics Report, Report MEP401, November.

Glover, R.H., 1959, Techniques used in interpreting seismic data in Kansas: In *Symposium on Geophysics in Kansas*, ed. W.W. Hambleton. Kansas Geological Survey Bulletin 137, p. 225-240.

Goforth, T., and C. Hayward, 1992, Seismic reflection investigations of a bedrock surface buried under alluvium: *Geophysics*, v. 57, p. 1217-1227.

Guo, T., and L. Liu, 1999, Non-intrusive evaluation of submarine tunnel foundation using dynamic high-frequency surface wave prospecting: Proceedings of the Symposium on the Application of Geophysics to Engineering and Environmental Problems (SAGEEP 1999), Oakland, Calif., March 14-18, p. 67-74.

Haeni, F.P., 1978, Computer modeling of ground-water availability in the Pootatuck River valley, Newtown, Connecticut, with a section on quality of water by Elinor H. Handman: U.S. Geological Survey Water Resources Investigations Open-file Report 83-4221.

Haeni, F.P., 1986, Application of continuous seismic reflection methods to hydrologic studies: *Ground Water*, v. 24, p. 23-31.

Hunter, J.A., S.E. Pullan, R.A. Burns, R.M. Gagne, and R.L. Good, 1984, Shallow seismic reflection mapping of the overburden-bedrock interface with the engineering seismograph–Some simple techniques: *Geophysics*, v.49, p.1381-1385.

Ivanov, J.M., C.B. Park, R.D. Miller, and J. Xia, 2000, Mapping Poisson's ratio of unconsolidated materials from a joint analysis of surface-wave and refraction events: Proceedings of the Symposium on the Application of Geophysics to Engineering and Environmental Problems (SAGEEP 2000), Arlington, Va., February 20-24.

Ivanov, J., 2002, JASR – Joint analysis of surface waves and refractions. Ph.D. dissertation, University of Kansas.

Ivanov, J., R.D. Miller, J. Xia, and D.W. Steeples, 2005, The inverse problem of refraction traveltimes, part II: Quantifying refraction nonuniqueness using a three-layer model: *Pure and Applied Geophysics*, v. 162, n. 3, p. 461-477.

Jongerius, P., and K. Helbig, 1988, Onshore high-resolution seismic profiling applied to sedimentology: *Geophysics*, v. 53, p. 1276-1283.

Kilty, K.T., and A.L. Lange, 1990, Acoustic tomography in shallow geophysical exploration using a transform reconstruction: Soc. Explor. Geophys. Investigations in Geophysics no. 5, S.H. Ward, ed., *Volume 3: Geotechnical*, p. 23-35.

Knapp, R.W., and D.W. Steeples, 1986, High-resolution common-depth-point, seismic-reflection profiling: Field acquisition parameter design: *Geophysics*, v. 51, p. 283-294.

Lankston, R.W., 1990, High-resolution refraction seismic data acquisition and interpretation: Soc. Explor. Geophys. Investigations in Geophysics no. 5, Stan H. Ward, ed., *Volume 1: Review and Tutorial,* p. 45-73.

Lanz, E., H.R. Maurer, and A.G. Green, 1998, Refraction tomography over a buried waste disposal site, *Geophysics*, v. 63, p. 1414-1433.

Lytle, R.J., and K.A. Dines, 1980, Iterative ray tracing between boreholes for underground image reconstruction: *Inst. Electr. Electron. Eng. Trans. Geosci. Remote Sensing*, v. GE-18, p. 234-240.

Michaels, P., 1999, Use of engineering geophysics in the design of highway passing lanes: Proceedings of the Symposium on the Application of Geophysics to Engineering and Environmental Problems (SAGEEP 1999), Oakland, Calif., March 14-18, p. 179-187.

Miller, R.D., D.W. Steeples, and M. Brannan, 1989, Mapping a bedrock surface under dry alluvium with shallow seismic reflections: *Geophysics,* v. 54, p. 1528-1534.
Miller, R.D., D.W. Steeples, and P.B. Myers, 1990, Shallow seismic-reflection survey across the Meers fault, Oklahoma: *GSA Bulletin*, v. 102, p. 18-25.
Miller, R.D., and D.W. Steeples, 1991, Detecting voids in a 0.6-m coal seam, 7 m deep, using seismic reflection: *Geoexploration,* Elsevier Science Publishers B.V., Amsterdam, The Netherlands, v. 28, p. 109-119.
Miller, R.D., N.L. Anderson, H.R. Feldman, and E.K. Franseen, 1995, Vertical resolution of a seismic survey in stratigraphic sequences less than 100 m deep in Southeastern Kansas: *Geophysics*, v. 60, p. 423-430.
Miller R.D., and J. Xia, 1999, Using MASW to map bedrock in Olathe, Kansas: Kansas Geological Survey Open-file Report 99-9.
Miller, R.D., J. Xia, C.B. Park, and J.M. Ivanov, 1999, Multichannel analysis of surface waves to map bedrock: *Leading Edge*, v. 18, n. 12, p. 1392-1396.
Miller, R.D., T.S. Anderson, J.C. Davis, D.W. Steeples, and M.L. Moran, 2001, 3-D characterization of seismic properties at the Smart Weapons Test Range, YPG: Proceedings of the Military Sensing Symposium on Battlefield Seismic and Acoustic Sensing, October 23-25, Laurel, Maryland, Published on CD.
Mooney, H.M., 1981, Handbook of engineering geophysics: Bison Instruments, Inc.
Nazarian, S., K.H. Stokoe II, and W.R. Hudson, 1983, Use of spectral analysis of surface waves method for determination of moduli and thicknesses of pavement systems: Transportation Research Record No. 930, p. 38-45.
Palmer, D., 1981, An introduction to the generalized reciprocal method of seismic refraction interpretation: *Geophysics*, v. 46, p. 1508-1518.
Park, C.B., R.D. Miller, D.W. Steeples, and R.A. Black, 1996, Swept impact seismic technique (SIST): *Geophysics*, v. 61, p. 1789-1803.
Park, C.B., R.D. Miller, and J. Xia, 1999, Multichannel analysis of surface waves (MASW): *Geophysics*, v. 64, p.800-808.
Peterson, J.E., B.N.P. Paulsson, and T.A. McEvilly, 1985, Applications of algebraic reconstruction techniques to cross-hole data: *Geophysics*, v. 53, p. 1284-1294.
Pullan, S.E., and J.A. Hunter, 1990, Delineation of buried bedrock valleys using the optimum offset shallow seismic reflection technique: Soc. Explor. Geophys. Investigations in Geophysics no. 5, S.H. Ward, ed., *Volume 3: Geotechnical*, p. 75-87.
Redpath, B.B., 1973, Seismic refraction exploration for engineering site investigations, NTIS AD-768710.
Sander, J.E., 1978, The blind zone in seismic ground-water exploration: *Ground Water*, v. 165, p. 394-397.
Schepers, R., 1975, A seismic reflection method for solving engineering problems: *Journal of Geophysics*, v. 41, p. 267-284.
Schneider, W.A., Jr., K.A. Ranzinger, A.H. Balch, and C. Kruse, 1992, A dynamic programming approach to first arrival traveltime computation in media with arbitrarily distributed velocities: *Geophysics*, v. 57, p. 39-50.
Scott, J.H., 1973, Seismic refraction modeling by computer, Geophysics, v. 38, p. 271-284.
Scott, J.H., 1977, SIPT–A seismic refraction inverse modeling program for timeshare terminal computer systems: U.S. Geological Survey Open-file Report 77-365.
Shtivelman, V., U. Frieslander, E. Zilberman, and R. Amit, 1998, Mapping shallow faults at the Evrona playa site using high-resolution reflection method: *Geophysics*, v. 63, p. 1257-1264.
Soske, J.L., 1954, The blind zone problem in engineering geophysics: *Geophysics*, v. 24, p. 359-365.
Steeples, D.W., and R.D. Miller, 1990, Seismic reflection methods applied to engineering, environmental, and groundwater problems: Soc. Explor. Geophys. Investigations in Geophysics no. 5, S.H. Ward, ed., *Volume 1: Review and Tutorial,* p. 1-30.
Steeples, D.W., C.M. Schmeissner, and B.K. Macy, 1995, The evolution of shallow seismic methods: *Journal of Environmental and Engineering Geophysics*, v. 0, n. 1, p. 15-24 (invited paper).
Steinhart, J.S., and R.P. Meyer, 1961, Explosion studies of continental structure: Carnegie Institution of Washington Publication 622.
Stokoe II, K.H., S.G. Wright, J.A. Bay, and J.M. Roësset, 1994, Characterization of geotechnical sites by SASW method: in *Geophysical Characterization of Sites*, ISSMFE Technical Committee #10, ed. R.D. Woods, Oxford Publishers, New Delhi.
Xia, J., R.D. Miller, and C.B. Park, 1999, Estimation of near-surface velocity by inversion of Rayleigh waves: *Geophysics*, v. 64, p. 691-700.
Xia, J., R.D. Miller, C.B. Park, J.A. Hunter, J.B. Harris, and J. Ivanov, 2002, Comparing shear-wave velocity profiles from multichannel analysis of surface wave with borehole measurements: *Soil Dynamics and Earthquake Engineering*, v. 22, n. 3, p. 181-190.
Yilmaz, O., 1987, Seismic data processing; S.M. Doherty, ed.; *in* Series: Investigations in Geophysics, no. 2, E.B. Neitzel, series ed.: Soc. Explor. Geophys.